UNIVERSITÀ DEGLI STUDI DI PARMA

Dottorato di Ricerca in Scienze del Farmaco, delle Biomolecole e dei Prodotti per la Salute

Ciclo XXIX

Interactors and allosteric effectors of serine racemase

Coordinatore:

Chiar.mo Prof. Marco Mor

Tutor:

Chiar.mo Prof. Stefano Bruno

Dottorando: Marilena Margiotta

CONTENT

3. Disrupted in Schizophrenia-1 as interactor of serine racemase

4. Glyceraldehyde 3-phosphate dehydrogenase and NADH as effectors of human serine racemase

5. Glyceraldehyde 3-phosphate dehydrogenase as target of irreversible inhibitors

Summary

Serine racemase is a pyridoxal phosphate-dependent enzyme responsible for the synthesis of D-serine in the central nervous system. D-serine is a co-agonist of the glutamate NMDA receptors, thus playing an important role in glutamatergic neurotransmission. Serine racemase has been recently recognized as a drug target for the control of D-serine levels, which are associated to a number of pathological conditions. This thesis work is focused on the characterization of the interaction of serine racemase with allosteric effectors and interactors, particularly divalent cations (Chapter 2), DISC1 (Chapter 3), NADH and glyceraldehyde 3-phosphate dehydrogenase (Chapter 4). Divalent cations, Mg^{2+} and Ca^{2+}, stabilize the enzyme and increase the activity of serine racemase, but with different affinity. Together with ATP, they modulate the quaternary equilibrium of the protein. NADH partially inhibits serine racemase through the N-substituted 1, 4-dihydronicotinic ring, which was predicted to bind at a site adjacent to the ATP binding site. NADH binds with a binding constant much higher than its intracellular concentrations, but some of its derivatives exhibited a much higher affinity, thus suggesting a novel class of inhibitors. DISC1, a recently discovered interactor of serine racemase, was expressed in insect cells using the baculovirus expression system, at the Institute of biomedical research of Strasbourg, (Institut Génétique Biologie Moléculaire Cellulaire). A preliminary characterization confirmed that it binds and stabilizes serine racemase. Human GAPDH, contrary to what was suggested in a recent publication, did not seem to interact with human serine racemase and an alternative explanation for the observed effect was suggested. GAPDH was also used in a side work to characterize novel covalent inhibitors to be used as antiprotozoal or anti-cancer drugs: 3-bromo isoxazolines and 2-phenoxy-1, 4-naphthoquinone derivatives. Chapter 5 is dedicated to this side project.

Chapter 1

General introduction

1. Serine racemase

Serine racemase (SR, EC 5.1.1.18) is the 5'- pyridoxal phosphate (PLP)-dependent enzyme responsible for the racemization of serine and for the irreversible β-elimination of both L-serine and D-serine to pyruvate and ammonia (Scheme1).

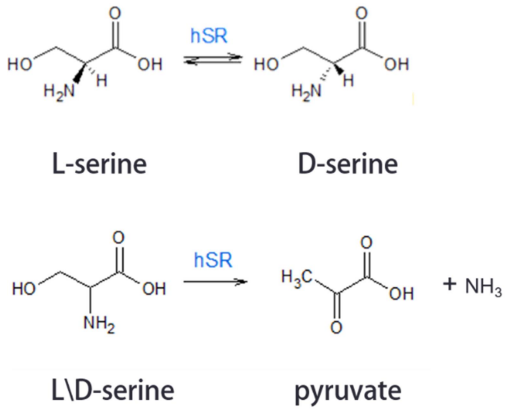

***Scheme 1**. Reactions catalysed by serine racemase.*

D-serine is the physiological co-agonist of the NMDA receptors for glutamate and serine racemase is its only source in the brain. NMDA receptors are involved in excitatory neurotransmission and participate in numerous physiological processes, including learning, memory and synaptic plasticity. Their overstimulation causes excitotoxicity and subsequent neurodegeneration associated to ischemia, head trauma, Huntington's, Parkinson's, Alzheimer's diseases and epilepsy. An NMDA system hypofunction has been associated to schizophrenia and mood disorders.

Serine racemase belongs to the fold type II group of pyridoxal 5'-phosphate enzymes, as confirmed by the crystal structures currently available (Table 1.1). The

first crystal structure to be solved was that of the homologous *Schizosaccharomyces pombe* protein [4], followed by the human and rat homologs [6].

Ligand	*Saccharomyces pombe*	*Rattus norvegicus*	*Homo sapiens*	*Zea mays*	*Enterococcus faecalis*
PLP + Mg^{2+}\ Mn^{2+}	1V71	3HMK		5CVC	(4ECL)
PLP + Mg^{2+} + AMP-PCP	1WTC				
PLP + Mg^{2+} + serine	2ZR8				
Lysinoalanyl residue	2ZPU				
PLP + Mg^{2+}\ Mn^{2+} +malonate		3L6R	3L6B		

***Table 1.1**. Protein data Bank codes for serine racemase crystal structures in the presence of different ligands (updated in 2016).*

All serine racemase homologs for which a crystal structure is available exhibit a high sequence similarity. The alignment of *Schizosaccharomyces pombe, Rattus norvegicus, Homo sapiens* and *Zea mays* are shown in Figure 1.1. Human and rat orthologs show 90% sequence similarity and 35.1% and 37.4% identity to the *S. pombe* sequence, respectively [7]. *Zea mays* serine racemase exhibits a 40% identity with the rat homologs [8]. Serine racemase exhibit a much lower degree of sequence similarity with other PLP-dependent fold-type II enzymes, particularly serine dehydratases: 38% sequence identity for threonine dehydratase from *Salmonella typhimurium* [9], 30% for threonine dehydratase from *E. coli* [10], 24% for serine

dehydratase from rat [11], 19% for threonine synthase from *Thermus thermophilus* HB8 [12].

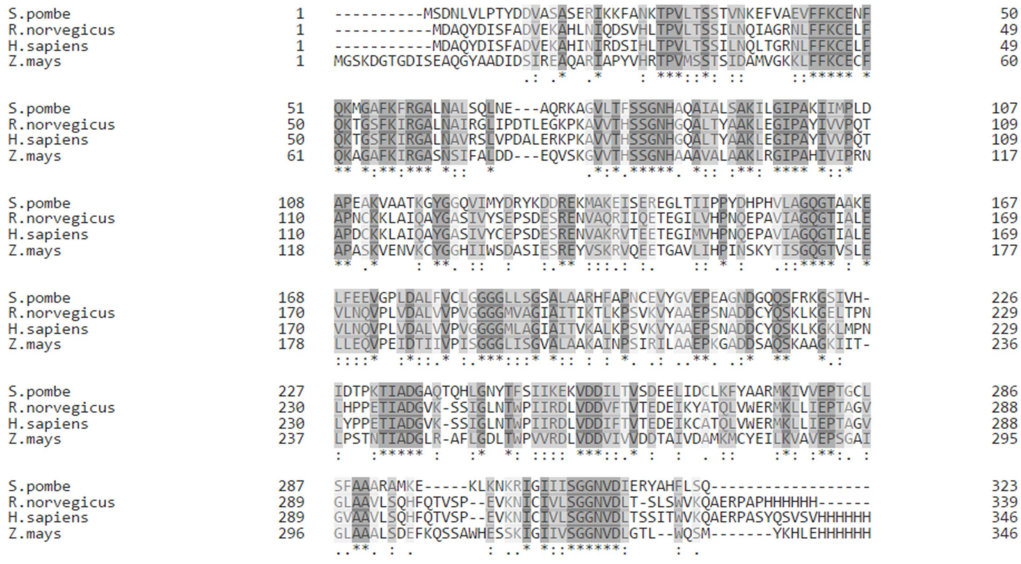

Figure 1.1. *Multiple sequence alignment of serine racemase from S. pombe, R. norvegicus, H. sapiens, and Z. mays using clustal omega program.*

From the structural point of view, as all fold type II PLP-dependent enzymes, serine racemase exhibits a large domain and a flexible small domain (Figure 1.2). The large domain consists of residues 1–68 (human homologue numbering) and 157–340, whereas the small domain spans residues 78 to 155. A flexible loop region connecting both domains includes residues 68–77 and 145–149 [6]. The large domain includes the binding site for the PLP cofactor, with the active site located at the interface between the two domains (Fig. 1.2). Two subunits are associated into a symmetric homodimer.

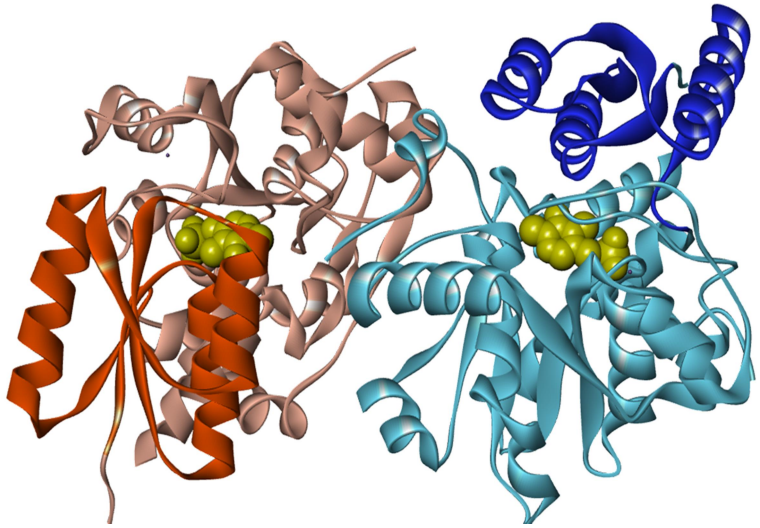

Figure 1.2. *Structure of the homodimer of hSR. The PLP cofactor is represented in yellow. The two domains are represented in blue and red, with the small domains highlighted in a darker shade (PDB entry 3L6B).*

1.1 Catalytic mechanism of serene racemase

Serine racemase catalyses the racemization of L-serine to D-serine and their β-elimination to pyruvate. The racemization is highly specific towards serine, and, with a much lower activity, to aspartate [13]. On the contrary, the dehydration reaction can be accomplished on a variety of amino acids and their derivatives. The mechanism of racemization was first studied on bacterial enzymes and, then, on the mammalian homologs, first purified from rat brain and functionally characterized in 1999 [14]. The reaction consists of several steps: the PLP cofactor is linked covalently to Lys-56, forming a Schiff base; the amino acid, either L- or D-serine, attacks the C4 of the Schiff base of the internal aldimine with an unprotonated α-amino group to form the external aldimine and release of Lys56. When L-serine is the substrate, the free amino group of residue Lys56 itself extracts the proton and forms a quinonoid species. At this point, the orientation of Ser84 (human homologue numbering) enables the hydroxyl group to donate its proton to the Cα atom of the intermediate,

resulting in the formation of D-serine. The elimination reaction involves the protonation of the quinoid intermediate on the β-hydroxyl group, which is subsequently eliminated as water to form the α-amino acrylate Schiff base. This species is released and quickly degrades to form pyruvate and ammonia. Mutagenesis studies reported by Yoshimura and Goto [15] showed the essential role of Ser-84 for the isomerization of serine and the consumption of D-serine (Fig. 1.3).

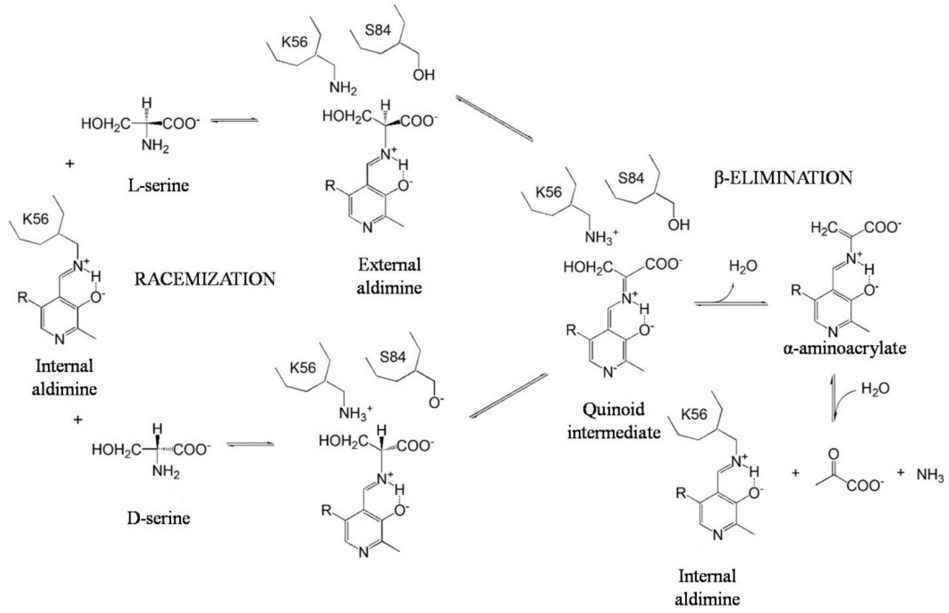

***Figure 1.3**. Mechanism of serine racemase catalysis (adapted from [1])*

1.2 Localization of serine racemase

Serine racemase is localized prevalently in the hippocampus, the amygdala, the retina and various cortical regions, predominantly in the cytosol of neurons. Initial studies reported that astrocytes were the only source of D-serine, but recent studies with more specific and sensitive antibodies have excluded this possibility [16]. Ehmsen et al., using transgenic mice with the serine racemase coding region replaced with enhanced GFP, revealed neuronal expression of serine racemase and

only traces in astrocytes in the cortex and hippocampus [17]. Recent findings reported by Wolosker et al., seem to confirm that most of D-serine that regulate NMDA receptors originates and is released by neurons through the neuronal alanine-serine-cysteine transporter-1 (Asc-1) [5].

On the other hand, L-serine synthesis occurs prevalently in astrocytes because of the exclusive astrocytic localization of 3-phosphoglycerate dehydrogenase (Phgdh), which catalyzes the first step in L-serine biosynthesis [18]. L-serine is then exported from astrocytes to neurons via the Asc-1 transporter and converted into D-serine by serine racemase. This metabolic cross talk between neurons and astrocytes was hypothesized by Wolosker in 2011 and was named the "serine shuttle" (Fig. 1.4) [3].

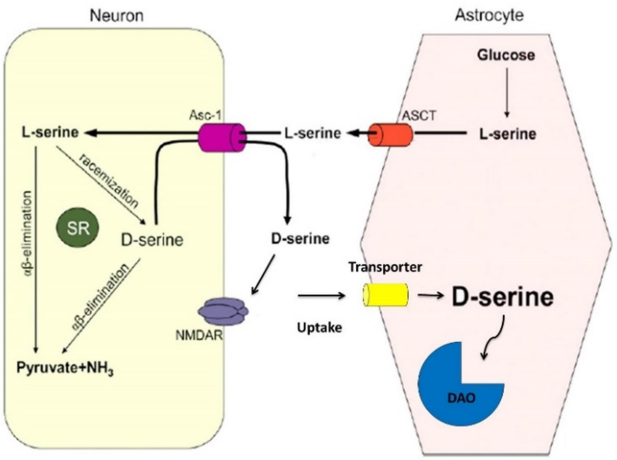

Figure 1.4. *Cross –talk between neurons and astrocytes. Glucose is converted into L-serine, which exits the astrocytes through the neutral amino acid exchanger Asc-1 and is uptaken by neurons. Serine racemase converts L-serine into D-serine, which is subsequently released from neurons through Asc-1. D-serine signaling may terminate through neuronal or astrocytic uptake and oxidation by DAO (scheme modified from [3] and [5]).*

2. Regulation of serine racemase by small molecule ligands

Regulation of serine racemase is still unclear, although different molecules have been characterized for their regulatory activity. PLP, magnesium [19], calcium [20], ATP [21] have been reported to enhance serine racemase activity, whereas NADH, NO [22] and membrane lipids like phosphatidylinositol 4,5-bisphosphate (PIP2) [2] inhibit the activity [23]. Furthermore, serine racemase activity was proposed to be regulated by physical interactions with other proteins, such as the glutamate-receptor-interacting protein (GRIP)[24], the protein interacting with C kinase (PICK1) and Disrupted in Schizophrenia 1 (DISC1)[25].

2.1 ATP binding

In 2002, Wolosker et al. described the allosteric activation of murine serine racemase by ATP, which is not hydrolyzed during the catalytic cycle. The binding site for ATP is located in a pocked at the interdimeric interface (Figure 1.5) and was identified by co-crystallizing serine racemase with the ATP stable analog adenylyl-imidodiphosphate (AMP-PCP).

The ATP site is surrounded by Ala115 and Tyr119 of the small domain, Asn25, Lys52, Met53 and Asn311 of the large domain (Figure 1.6) Recently, the mechanism of regulation has been thoroughly characterized [26] [21]. ATP binds serine racemase with strong cooperativity and increases the affinity of the active site ligand glycine. Conversely, glycine stabilizes a protein conformation that binds ATP non-cooperatively and with high affinity, indicating a cross-talk between allosteric and active sites. Marchetti at al. measured the β-elimination and racemization activity of serine racemase using L-serine and D-serine as substrates, with and without ATP. The binding curve of ATP showed a sigmoidal shape, indicating positive cooperativity. In addition, the effect of ATP binding on the PLP fluorescence spectrum indicates that ATP induces a conformational change in the active site [21].

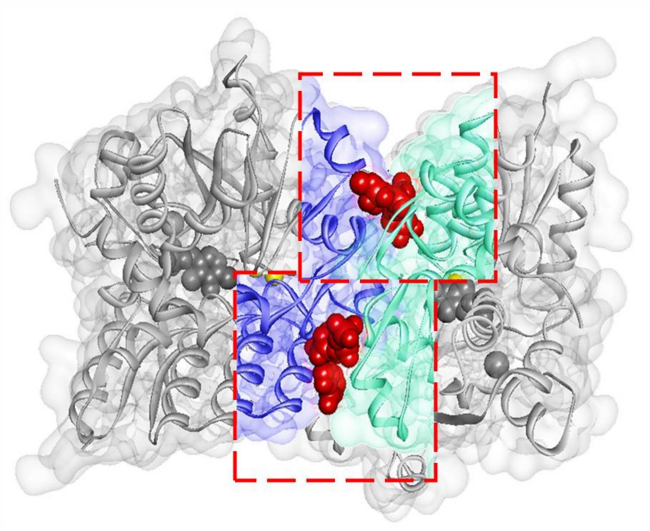

***Figure 1.5**. The model is based on PDB entry 3L6B, reported as a homodimer, which binds Mg2+ at the metal binding site but not ATP. The ATP binding site was approximately defined by overlapping the structure of hSR with that from Schizosaccharomyces pombe (PDB 1WTC, reported as a dimer), in complex with the ATP analog AMP-PCP. In red the two ATP molecules at the dimer interface.*

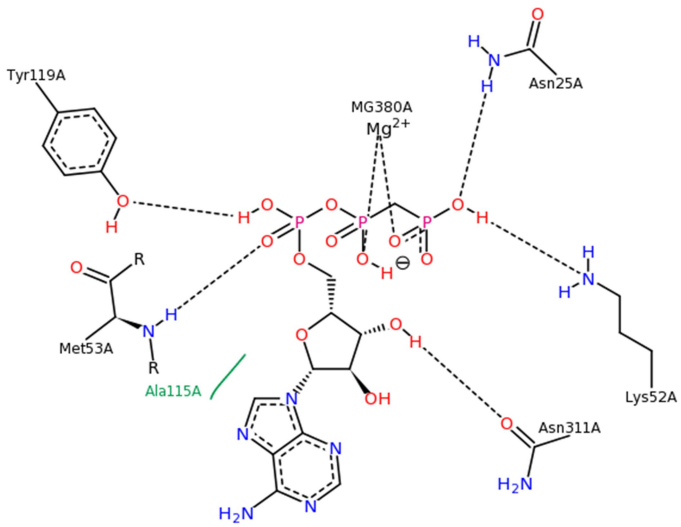

***Figure 1.6.** Interaction of the ATP-Mg^{2+} complex with hSR at the dimer interface, obtained by homology modeling of the homologous Schizosaccharomyces pombe protein (PDB 1WTC).*

2.2 Metal ions

Other positive allosteric effectors are the divalent cations Ca^{2+} and Mg^{2+}. Mg^{2+} is considered the physiological ligand because of its intracellular concentration, higher than that of Ca^{2+}. As a matter of fact, Ca^{2+} is normally in the nanomolar range in neuronal cytosol [19]. However, Ca^{2+} intracellular concentrations fluctuate significantly as a result of the activation of calcium-dependent signal pathways. The binding site of divalent cations involves residues Glu210, Ala214, Asp216. [27,28]. Their symmetry-related binding sites were recognized crystallographically and involve residues Glu210, Asp216 and Ala214 (human SR numbering, about 10 Å apart from the active site and 25 Å from the ATP-binding site (Figure 1.8). The site is largely conserved in mammalian, plant and yeast homologs (Figure 1.7) [29]. However, it is not conserved in SR from the hyperthermophilic archaeon *Pyrobaculum islandicum*, which, as expected, is not affected by ATP or by divalent cations [30].

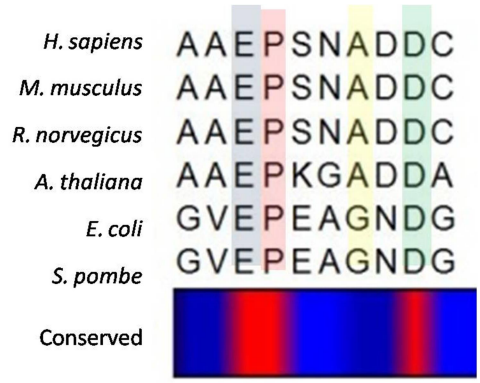

Figure 1.8. *Conserved residues in the binding site of metal ions in serine racemase homologous proteins*

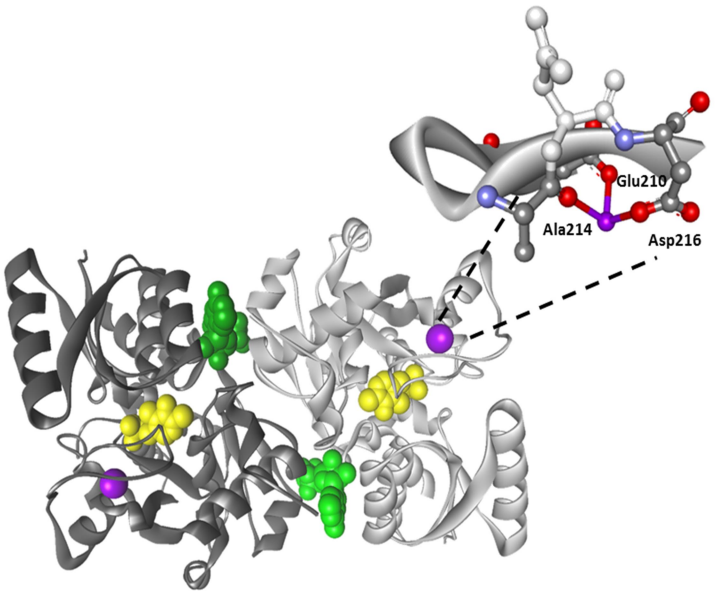

***Figure 1.7**. Metal binding sites of hSR. Model of human SR indicating the positions of Mg2+, ATP, and pyridoxal 5'-phosphate, represented in purple, green and yellow, respectively. The model is based on PDB entry 3L6B, reported as a homodimer, which binds Mg2+ at the metal binding site but not ATP. The ATP binding site was approximately defined by overlapping the structure of hSR with that from Schizosaccharomyces pombe (PDB 1WTC, reported as a dimer), in complex with the ATP analog AMP-PCP. Zoom: detail of the metal-binding site.*

2.3 Inhibitory effect of NADH

More recently, a role of the glycolytic flux in serine racemase regulation was observed, as suggested by the inhibition of serine racemase by NADH [2]. The nicotinamide mononucleotide, the NADH precursor, was recently showed to determine an inhibition comparable with that of 2,2-dichloromalonate, the best serine racemase inhibitor identified so far [31]. The inhibition is determined by the N-substituted 1,4-dihydronicotinic ring, which binds at the dimer interface close to the allosteric binding site for ATP [32]

3. Interactors of serine racemase

In addition to small molecule effectors and post-translational modifications, SR function is regulated by the interactions with specific proteins. Particularly, the C-terminal end, located near the ATP binding site, is important in terms of serine racemase regulation because it mediates the interaction with protein partners such as DISC1 (Disrupted in Schizophrenia 1). Moreover, it was shown that serine racemase interacts directly with glyceraldehyde-3-phosphate dehydrogenase (GAPDH) and the activation of glycolysis increases this interaction. Suzuki at al. revealed that GAPDH suppresses serine racemase activity by direct binding to GAPDH and through NADH, the product of GAPDH reaction. NADH promotes the dissociation of ATP from serine racemase [2].

3.1. DISC1 and serine racemase

St Clair and collaborators began to investigate cytogenetic databases for cases of psychiatric illness and discovered DISC1 [33]. From cytogenetic studies conducted in 1970 on boys of a large Scottish family [34], a regular Mendelian autosomal dominant anomaly was found and shown to be linked to major psychiatric disorders, including schizophrenia, major depression and bipolar disorder. The gene associated to these psychiatric illnesses was found to be carried by the (1;11) (q42.1;q14.3) translocation. The mechanism by which this translocation could have caused the observed phenotypes was not clear at the time. However, the most likely explanation was that the translocation disrupted a gene at one of the breakpoints. St Clair and collaborators did not follow up this idea until ten years after the description of the apparent inheritance pattern.

The study of the translocation by Millar and collaborators found that, while the region surrounding the breakpoint on chromosome 11 did not contain genes, the area on chromosome 1 adjacent to the breakpoint was gene-rich [35]. Particularly, there were two genes that were directly disrupted by the translocation and these

became known as Disrupted in Schizophrenia 1 and 2 (DISC1 and DISC2, OMIM accession numbers 605210 and 606271 respectively). It was later discovered that DISC2 was antiparallel and antisense to DISC1 [36], leaving DISC1 as the only protein-coding gene. Although this pattern of inheritance is unusual in complex psychiatric diseases, the analysis of the translocation has shown that, when inherited, there is about a fifth-fold increase in the risk of developing schizophrenia, bipolar disorder or recurrent major depression [37].

Previous studies performed with a mouse model have shown that the C-terminus truncated form of DISC1 is unable to bind serine racemase and induce serine racemase degradation and D-serine depletion [38], suggesting a role of DISC1 to prevent the ubiquitination of serine racemase (Fig. 1.9). As a consequence, the diminished production of D-serine reflects on the decrease of NMDA neurotransmission.

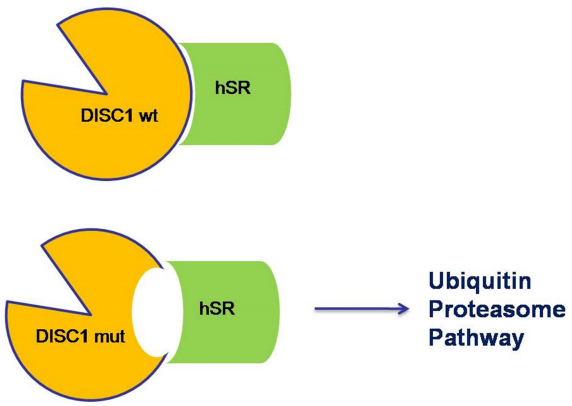

Figure 1.9. *DISC1 protect serine racemase from ubiquitination*

3.1.1 Biology of DISC1

The DISC1 gene has a sequence length of 415 kb [35], which encodes a protein of 854 residues with an N-terminal head domain and a long helical C-terminal tail domain [39]. The gene has a large number of isoforms, which range greatly in size

and composition due to alternate splicing. There are currently a total of twenty-three isoforms of DISC1 reported on the NCBI Gene database, but a further twenty-four have been identified [40] giving a total of forty-seven. The most commonly expressed transcript in the DISC1 gene is known as the long (L) isoform and consists of thirteen exons [35]. This isoform has been the subject of the majority of the investigations on DISC1 function.

3.1.2 Expression patterns of DISC1

Although DISC1 is expressed in a number of tissues, particularly the heart, the placenta, the kidneys and the pancreas, research has mostly focused on its expression in the brain, particularly during development, both during embryogenesis and in the post-natal period. The areas of expression within the adult brain are broad and include the hippocampus, the cortex, the hypothalamus, the brain stem and the cerebellum [41]. In the past, DISC1 was thought to be primarily localized to neurons. Recent studies have revealed that DISC1 is also expressed in glial cells, including astrocytes [38]. Additionally, through studies in mice, they concluded that the expression within the brain changes over time. [42]. From this, they concluded that DISC1 dysfunctions may have effects on the development and function of the hippocampus [43]. The fact that DISC1 expression takes place in the brain, and specifically during the development of the brain of both rats and humans, provides some basis for the hypothesis that DISC1 could be involved in psychiatric illness in humans.

3.2. GAPDH and serine racemase

Serine racemase activity was reported to be affected by glycolytic metabolism, which is strongly regulated in neurons, since they require enormous amount of energy to maintain continuous neurotransmission. Astrocytes support neurons for energy production and previous studies have revealed that activation of

NMDA receptors requiring binding of glutamate co-agonist, stimulate glycolysis in astrocytes. Moreover, glycolysis inhibition affects the glutamate transport. These results suggest that the glycolytic metabolism is involved in regulating synaptic glutamate levels and, in general, is involved in excitatory neurotransmission. Moreover, in the central nervous system, the L-serine biosynthesis pathway starts from the intermediate of glycolysis, 3-phosphoglycerate (Fig. 1.10). Finally, glycolysis regulates intracellular ATP level and drives indirectly the availability of ATP for serine racemase. It was recently discovered that GAPDH and NADPH can inhibit serine racemase activity by direct binding.

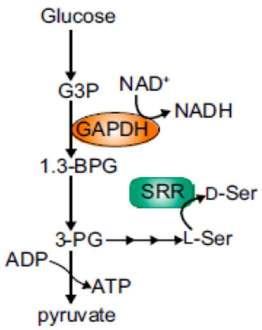

Figure 1.10. *Hypothetical regulation of serine racemase by glycolysis biosynthesis. [2]*

3.2.1. Glyceraldehyde-3-phosphate dehydrogenase

Glyceraldehyde-3-phosphate dehydrogenase is an important enzyme of glycolysis and is itself a potential drug target because cancer cells and several pathogens rely on glycolysis for energy production. It is a homotetrameric enzyme (Fig. 1.12 [44]) that catalyzes the conversion of glyceraldehyde-3-phosphate (G3P) into 1,3-biphosphoglycerate (1,3-BPG), with the concomitant reduction of nicotinamide adenine dinucleotide (NAD+) to NADH (Fig. 1.11). The active site has a catalytic cysteine.

The mechanism of reaction consists of several steps: the cysteine of the active site attacks the aldehydic group of glyceralhyde-3-phospate with nucleophilic bond, forming a thiohemiacetal intermediate. NAD^+ oxidizes the thiohemiacetal intermediate via direct hydride (H:-) transfer, resulting in the formation of a thioester intermediate and NADH product. Upon NADH displacement by NAD^+ Pi binds to the GAPDH-thioester-NADH ternary complex and nucleophilically attacks the thioester intermediate to form 1,3-BPG product. The structure of the enzyme has been determined and consists of four subunits of 37 KDa each (Figure 1.12).

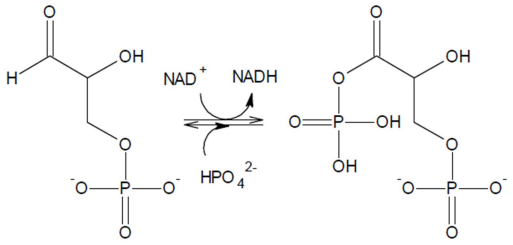

Figure 1.11. *Reaction catalysed by GAPDH*

***Figure 1.12**. Structure of human GAPDH (PDB entry5C7O)*

3.2.2. GAPDH as anti-protozoan drug target

Inhibitors of the GAPDH from *Trypanozoma cruzi*, and *Trypanozoma brucei* have been already identified, with potential selectivity toward the parasitic enzyme with respect to the human homologue. These parasites are responsible for the trypanosomiasis in humans, Chagas disease in South America and sleeping sickness in Africa. Another pathogen is *Plasmodium falciparum,* which causes the most dangerous form of malaria in humans. 250 million cases of malaria worldwide have been reported. The GAPDH homologue of *Plasmodium falciparum* presents a 50% similarity with the human homologue, according to their alignment (Fig.1.13), giving the possibility to design selective inhibitors.

Derivatives of acivicin with a nucleus of 3-bromo-isoxazoline have been designed and tested on *Plasmodium falciparum* homologue [45]. These potential inhibitors are designed to allow the access to the active site where they cause the inactivation of GAPDH with an irreversible mechanism. Bruno at al. showed that these compounds selectively bind Cys153 of the active site, without involvement of

the other residues. In the following chapter, the selectivity of some of these compounds is reported, demonstrating that these molecules are potential inhibitors of pathogenic GAPDHs with low inhibitory effects on human homologue. Also 2-phenoxy-1,4-naphthoquinone has been identified as covalent inhibitor of the *Trypanosoma brucei* homologue, and herein we will investigate its binding to several homologs.

```
H.sapiens       MGKVKVGVNGFGRIGRLVTRAAFNSGKVDIVAINDPFIDLNYMVYMFQYDSTHGKFHGTV   60
P.falcparum     MAVTKLGINGFGRIGRLVFRAAFGRKDIEVVAINDPFMDLNHLCYLLKYDSVHGQFPCEV   60
                *. .*:*:********** ****.  .:::*******:***:: *:::***.**:*   *

H.sapiens       KAENGKLVINGNPITIFQERDPSKIKWGDAGAEYVVESTGVFTTMEKAGAHLQGGAKRVI   120
P.falcparum     THADGFLLIGEKKVSVFAEKDPSQIPWGKCQVDVVCESTGVFLTKELASSHLKGGAKKVI   120
                .  :* *:*. : :::* *:***:* **.. .: * ****** * * *.:**:****:**

H.sapiens       ISAPS-ADAPMFVMGVNHEKYDNSLKIISNASCTTNCLAPLAKVIHDNFGIVEGLMTTVH   179
P.falcparum     MSAPPKDDTPIYVMGINHHQYDTKQLIVSNASCTTNCLAPLAKVINDRFGIVEGLMTTVH   180
                :***   *:*::***:**.:**..  *:******************:*.************

H.sapiens       AITATQKTVDGPS--GKLWRDGRGALQNIIPASTGAAKAVGKVIPELNGKLTGMAFRVPT   237
P.falcparum     ASTANQLVVDGPSKGGKDWRAGRCALSNIIPASTGAAKAVGKVLPELNGKLTGVAFRVPI   240
                * **.* .*****  ** ** ** **.****************:*********:*****

H.sapiens       ANVSVVDLTCRLEKPAKYDDIKKVVKQASEGPLKGILGYTEHQVVSSDFNSDTHSSTFDA   297
P.falcparum     GTVSVVDLVCRLQKPAKYEEVALEIKKAAEGLLKGVLGYTEDEVVSQDFVHDNRSSIFDM   300
                ..******.***:*****:::   :*:*:** ***:*****.:***.**  *.:** **

H.sapiens       GAGIALNDHFVKLISWYDNEFGYSNRVVDLMAHMASKE 335
P.falcparum     KAGLALNDNFFKLVSWYDNEWGYSNRVLDLAVHITNN- 337
                 **:****:*.**:******:******:** .*::.:
```

Figure 1.13. *Sequence alignment of GAPDH Homo sapiens and Plasmodium falciparum homologs.*

3.3. Other protein interactors of serine racemase

In addition to GAPDH and DISC1, serine racemase was suggested to be regulated by the AMPA receptor-binding protein o 'glutamate receptor interacting protein' (GRIP), which enhances serine racemase activity and D-serine release from glia. GRIP contains a PDZ domain interacting protein, which is recognized by three

carboxyl-terminal amino acids of murine serine racemase with a well characterized consensus sequence (-V-S-V-)[24]. In 2006, Snyder et al. also reported the interaction of hSR with PICK1 (protein interacting with C-kinase). PICK1 contains a PDZ domain, as well, responsible for protein-protein interaction which bind to the C-terminus of hSR. How PICK1 and GRIP interact to regulate serine racemase is still unclear, but they are both dependent on the phosphorylation status of AMPA receptors [15, 25]. The phosphorylation at Ser-880 causes dissociation of GRIP, which can bind serine racemase, and, on the other hand, keeps PICK1 linked. AMPA receptor in astrocytic glia uses these proteins as mediators to regulate serine racemase activity [46]. Another interactor of SR is Golga-3, a protein that binds to the cytosolic face of the Golgi apparatus and stabilizes mouse serine racemase levels through inhibition of its ubiquitination [47].

ABBREVATIONS:

PLP, 5-pyridoxal phosphate; NMDA, N-methyl D-aspartate receptors; Asc-1 alanine-serine-cysteine transporter; DAO, D-amino acid oxidase; ASCT1, alanine/serine/cysteine/threonine transporter; NAD^+, nicotinamide adenine dinucleotide (oxidized form); NADH, nicotinamide adenine dinucleotide (reduced form); ATP, adenosine triphosphate; DISC1, Disrupted in Schizophrenia 1, hSR human serine racemase.

REFERENCES

1. Foltyn, V.N., et al., *Serine racemase modulates intracellular D-serine levels through an alpha,beta-elimination activity.* J Biol Chem, 2005. **280**(3): p. 1754-63.
2. Suzuki, M., et al., *Glycolytic flux controls D-serine synthesis through glyceraldehyde-3-phosphate dehydrogenase in astrocytes.* Proc Natl Acad Sci U S A, 2015. **112**(17): p. 13.
3. Wolosker, H., *Serine racemase and the serine shuttle between neurons and astrocytes.* Biochim Biophys Acta, 2011. **11**(66): p. 9.
4. Goto, M., et al., *Crystal structure of a homolog of mammalian serine racemase from Schizosaccharomyces pombe.* J Biol Chem, 2009. **284**(38): p. 25944-52.
5. Wolosker, H., D.T. Balu, and J.T. Coyle, *The Rise and Fall of the D-Serine-Mediated Gliotransmission Hypothesis.* Trends in Neurosciences. **39**(11): p. 712-721.
6. Smith, M.A., et al., *The structure of mammalian serine racemase: evidence for conformational changes upon inhibitor binding.* J Biol Chem, 2010. **285**(17): p. 12873-81.
7. Goto, M., et al., *Crystal structure of a homolog of mammalian serine racemase from Schizosaccharomyces pombe.* J Biol Chem, 2009. **284**(38): p. 25944-52.
8. Zou, L., et al., *Crystal structure of maize serine racemase with pyridoxal 5'-phosphate.* Acta Crystallogr F Struct Biol Commun, 2016. **72**(Pt 3): p. 165-71.
9. Simanshu, D.K., H.S. Savithri, and M.R. Murthy, *Crystal structures of Salmonella typhimurium propionate kinase and its complex with Ap4A: evidence for a novel Ap4A synthetic activity.* Proteins, 2008. **70**(4): p. 1379-88.
10. Gallagher, D.T., et al., *Structure and control of pyridoxal phosphate dependent allosteric threonine deaminase.* Structure. **6**(4): p. 465-475.
11. Yamada, T., et al., *Crystal structure of serine dehydratase from rat liver.* Biochemistry, 2003. **42**(44): p. 12854-65.

12. Omi, R., et al., *Crystal structures of threonine synthase from Thermus thermophilus HB8: conformational change, substrate recognition, and mechanism.* J Biol Chem, 2003. **278**(46): p. 46035-45.
13. Yoshimura, T. and M. Goto, *d-Amino acids in the brain: structure and function of pyridoxal phosphate-dependent amino acid racemases.* FEBS Journal, 2008. **275**(14): p. 3527-3537.
14. Wolosker, H., et al., *Purification of serine racemase: Biosynthesis of the neuromodulator d-serine.* Proc Natl Acad Sci U.S.A., 1999. **96**(2): p. 721-725.
15. Wolosker, H., et al., *Purification of serine racemase: biosynthesis of the neuromodulator D-serine.* Proc Natl Acad Sci U.S.A., 1999. **96**(2): p. 721-5.
16. Balu, D.T., et al., *d-Serine and Serine Racemase are Localized to Neurons in the Adult Mouse and Human Forebrain.* Cel MolNeurobiol, 2014. **34**(3): p. 419-435.
17. Ehmsen, J.T., et al., *D-serine in glia and neurons derives from 3-phosphoglycerate dehydrogenase.* J Neurosci, 2013. **33**(30): p. 12464-9.
18. Ehmsen, J.T., et al., *Serine in Glia and Neurons Derives from 3-Phosphoglycerate Dehydrogenase .* J Neurosci, 2013. **33**(30): p. 12464-12469.
19. de Miranda, J., et al., *Cofactors of serine racemase that physiologically stimulate the synthesis of the N-methyl-d-aspartate (NMDA) receptor coagonist d-serine.* Proc Natl Acad Sci U.S.A., 2002. **99**(22): p. 14542-14547.
20. Cook, S.P., et al., *Direct calcium binding results in activation of brain serine racemase.* J Biol Chem, 2002. **277**(31): p. 27782-92.
21. Marchetti, M., et al., *ATP binding to human serine racemase is cooperative and modulated by glycine.* FEBS Journal, 2013. **280**(22): p. 5853-5863.
22. Mustafa, A.K., et al., *Nitric oxide S-nitrosylates serine racemase, mediating feedback inhibition of d-serine formation.* Proc Natl Acad Sci U.S.A., 2007. **104**(8): p. 2950-2955.
23. Mustafa, A.K., et al., *Glutamatergic regulation of serine racemase via reversal of PIP2 inhibition.* Proc Natl Acad Sci U.S.A., 2009. **106**(8): p. 2921-2926.

24. Kim, P.M., et al., *Serine racemase: activation by glutamate neurotransmission via glutamate receptor interacting protein and mediation of neuronal migration.* Proc Natl Acad Sci U S A, 2005. **102**(6): p. 2105-10.
25. Fujii, K., et al., *Serine racemase binds to PICK1: potential relevance to schizophrenia.* Mol Psychiatry, 2006. **11**(2): p. 150-7.
26. Neidle, A. and D.S. Dunlop, *Allosteric Regulation of Mouse Brain Serine Racemase.* Neurochem Res, 2002. **27**(12): p. 1719-1724.
27. De Miranda, J., et al., *Cofactors of serine racemase that physiologically stimulate the synthesis of the N-methyl-D-aspartate (NMDA) receptor coagonist D-serine.* Proc Natl Acad Sci U S A, 2002. **99**(22): p. 14542-7.
28. Strisovsky, K., et al., *Mouse brain serine racemase catalyzes specific elimination of L-serine to pyruvate.* FEBS Lett, 2003. **535**(1-3): p. 44-8.
29. Baumgart, F. and I. Rodriguez-Crespo, *D-amino acids in the brain: the biochemistry of brain serine racemase.* FEBS J, 2008. **275**(14): p. 3538-45.
30. Ohnishi, M., et al., *Purification and characterization of serine racemase from a hyperthermophilic archaeon, Pyrobaculum islandicum.* J Bacteriol, 2008. **190**(4): p. 1359-65.
31. Vorlova, B., et al., *Malonate-based inhibitors of mammalian serine racemase: kinetic characterization and structure-based computational study.* Eur J Med Chem, 2015. **89**: p. 189-97.
32. Bruno, S., et al., *Human serine racemase is allosterically modulated by NADH and reduced nicotinamide derivatives.* Biochem J, 2016. **473**(20): p. 3505-3516.
33. St Clair, D., et al., *Association within a family of a balanced autosomal translocation with major mental illness.* The Lancet, 1990. **336**(8706): p. 13-16.
34. Jacobs, P.A., et al., *Studies on a family with three cytogenetic markers.* Annals of Human Genetics, 1970. **33**(4): p. 325-336.
35. Millar, J.K., et al., *Disruption of two novel genes by a translocation co-segregating with schizophrenia.* Hum Mol Gen, 2000. **9**(9): p. 1415-1423.

36. Taylor, M.S., et al., *Evolutionary constraints on the Disrupted in Schizophrenia locus.* Genomics, 2003. **81**(1): p. 67-77.

37. Blackwood, D.H.R., et al., *Schizophrenia and Affective Disorders—Cosegregation with a Translocation at Chromosome 1q42 That Directly Disrupts Brain-Expressed Genes: Clinical and P300 Findings in a Family.* Am J Hum Gen, 2001. **69**(2): p. 428-433.

38. Ma, T.M., et al., *Pathogenic disruption of DISC1-serine racemase binding elicits schizophrenia-like behavior via D-serine depletion.* Mol Psychiatry, 2013. **18**(5): p. 557-67.

39. Surpili, M.J., T.M. Delben, and J. Kobarg, *Identification of Proteins That Interact with the Central Coiled-Coil Region of the Human Protein Kinase NEK1.* Biochemistry, 2003. **42**(51): p. 15369-15376.

40. Nakata, K., et al., *DISC1 splice variants are upregulated in schizophrenia and associated with risk polymorphisms.* Proc Natl Acad Sci U.S.A., 2009. **106**(37): p. 15873-15878.

41. Schurov, I.L., et al., *Expression of disrupted in schizophrenia 1 (DISC1) protein in the adult and developing mouse brain indicates its role in neurodevelopment.* Mol Psychiatry, 2004. **9**(12): p. 1100-10.

42. Ma, L., et al., *Cloning and characterization of Disc1, the mouse ortholog of DISC1 (Disrupted-in-Schizophrenia 1).* Genomics, 2002. **80**(6): p. 662-72.

43. Miyoshi, K., et al., *Disrupted-In-Schizophrenia 1, a candidate gene for schizophrenia, participates in neurite outgrowth.* Mol Psychiatry, 2003. **8**(7): p. 685-94.

44. Danshina, P.V., et al., *Structural analyses to identify selective inhibitors of glyceraldehyde 3-phosphate dehydrogenase-S, a sperm-specific glycolytic enzyme.* Mol Hum Reprod, 2016. **26**.

45. Bruno, S., et al., *Discovery of covalent inhibitors of glyceraldehyde-3-phosphate dehydrogenase, a target for the treatment of malaria.* J Med Chem, 2014. **57**(17): p. 7465-71.

46. Hanley, J.G., *PICK1: A multi-talented modulator of AMPA receptor trafficking.* Pharmacol Ther, 2008. **118**(1): p. 152-160.

47. Dumin, E., et al., *Modulation of D-serine levels via ubiquitin-dependent proteasomal degradation of serine racemase.* J Biol Chem, 2006. **281**(29): p. 20291-302.

Chapter 2

Divalent cations as effectors of serine racemase

Abstract

Mg^{2+} and Ca^{2+} bind both at a specific site of hSR and, as ATP-metal complexes, at the ATP-binding site. We cloned, expressed and purified hSR from *E. coli* and we evaluated the binding of Mg^{2+} and Ca^{2+} in the absence and presence of ATP. Mg^{2+} shows an EC_{50} of 28±3 μM, whereas Ca^{2+} has an EC_{50} 4.5-fold higher. In the presence of ATP, Mg^{2+} binding leads to 10-fold enzyme activation, whereas Ca^{2+} binding leads to a 5-fold activation. This finding suggests that an increase in Ca^{2+} concentration can cause enzyme inhibition, although the physiological significance is not established. Both metals produce a similar thermal stabilization of hSR and a stabilization of a tetramer in comparison to the metal-stripped protein. The additional binding of the ATP-Mg^{2+}complex further activates the enzyme and further shifts the quaternary state toward the tetramer.

This work has been accepted for publication in BBA - Proteins and Proteomics (2017).

Authors' contributions: Marilena Margiotta carried out the cloning and the purification of a serine racemase construct with a cleavable His-tag, specifically designed for the experiments on metals. She carried out part of the enzymatic characterization and all the experiments on thermal stability at the Structural Biology and Genomics Platform at the CBI-IGBMC, Illkirch, France. Valentina Orlandi carried out part of the enzyme assays. Francesco Marchesani and Gianluca Paredi carried out the gel filtration experiments.

1. Introduction

The divalent cations Ca^{2+} and Mg^{2+} have long been identified as positive allosteric effectors of hSR [1, 2]. Their symmetry-related binding sites (Fig. 2.1) were recognised crystallographically and involve residues Glu210, Asp216 and Ala214 (hSR numbering), 10 Å apart from the active site and 25 Å from the ATP-binding site (Fig. 2.1). This site is conserved in plant and yeast homologs [3] but not in SR from the hyperthermophilic archaeon *Pyrobaculum islandicum,* which, as expected, was not affected by ATP or by divalent cations [4]. On the other hand, SR from the soil-living mycetozoa *Dictyostelium discoideum* is also modulated by Na^{+}, which binds at the same site as Mg^{2+} [5]. Functionally, the activation by divalent cations was first proposed as a Ca^{2+} sensing system, although it was objected that the alternative ligand Mg^{2+} has a much higher intracellular concentration [6] and would be, therefore, a more likely physiological ligand. However, considering the excitability of neurons and the highly variable Ca^{2+} concentration within the excitation cycle, the activation by Ca^{2+} was not ruled out in specific cellular compartments or under specific cellular conditions [3].

In addition to the specific metal binding sites, the ATP-Mg^{2+}\Ca^{2+} complexes bind cooperatively [7] at two symmetry-related sites [1] at the dimer interface [5] resulting in a strong activation, especially of the β-elimination reaction [1, 8, 9]. Crystallographic data on *Schizosaccharomyces pombe* SR, murine SR and human SR have provided structural details on the binding of ATP-metal complexes and on the allosteric conformational changes it produces [5, 10].

Experimentally, the investigation of SR activation by Ca^{2+} is complicated by its effect on D-serine release *in vivo* [11] and by the requirement of divalent cations for ATP binding, with different affinities depending on the protein conformation [7]. Moreover, the investigation of the modulation of hSR activity by either Mg^{2+} or Ca^{2+} in the presence of ATP is tangled by the multiple equilibria involved and requires the precise determination of free ions concentration in solution.

In this study, the calculation of free ion concentrations through dedicated software [12] allowed us to show that Ca^{2+} and Mg^{2+} activate hSR to a different extent. Moreover, we show that the binding of ATP and Mg^{2+} is associated with a change in the quaternary state of hSR and thermal stabilization, suggesting a molecular basis for the enzyme allosteric properties.

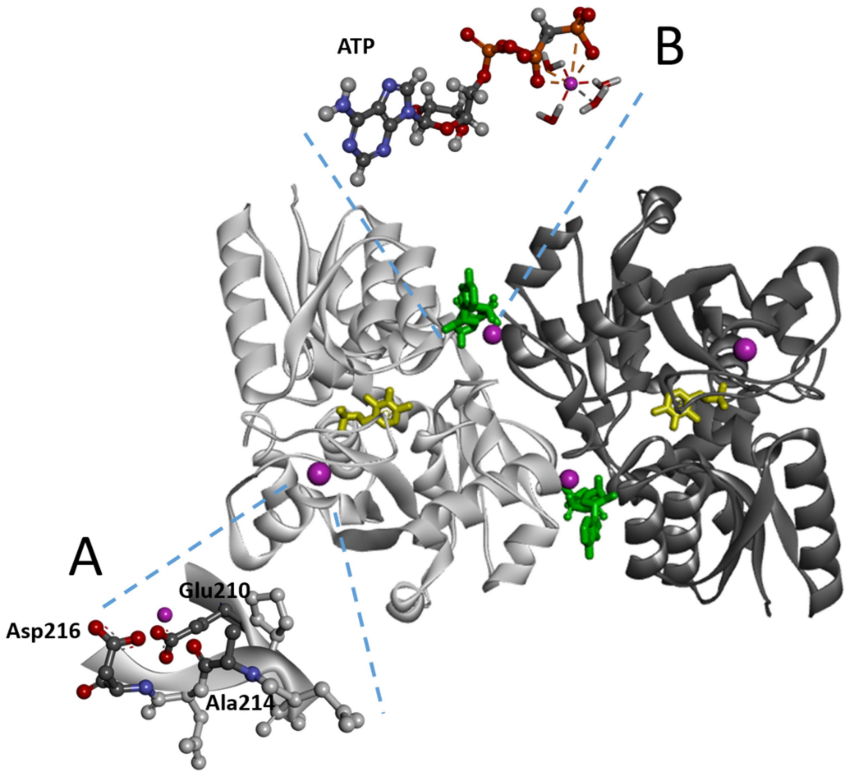

***Figure 2.1**. Model of human SR indicating the positions of Mg^{2+}, ATP-Mg^{2+} and pyridoxal 5'-phosphate, represented in purple, green and yellow, respectively. The model is based on PDB entry 3L6B, reported as a homodimer, which binds Mg^{2+} at the metal binding site but not ATP. The ATP binding site was approximately defined by overlapping the structure of hSR with that from Schizosaccharomyces pombe (PDB 1WTC, also reported as a dimer), in complex with the ATP analog AMP-PCP. Insets: **A)** detail of the metal- binding site **B)** Details of the ATP-Mg2+ (Ca2+) binding sites. Whereas the molecular model of inset A is derived from a crystallographic structure, the model of inset B is only inferred from the superimposition of hSR and SpSR.*

2. Material and Methods

2.1. Chemicals and Materials

Chemicals were of the best commercial quality available and were purchased from Sigma-Aldrich (St. Louis, MO, USA), with the exception of tris (2-carboxyethyl) phosphine (TCEP), from Apollo Scientific. Recombinant D-amino acid oxidase (DAAO) of *Rhodotorula gracilis* was a generous gift from Professor Loredano Pollegioni, University of Insubria, Varese, Italy. The plasmid for His-tagged TEV protease expression and the plasmid containing His-tagged thioredoxin were both generously provided by Professor Christopher S. Hayes, UC Santa Barbara, Santa Barbara, CA, USA [13, 14].

2.2. Enzyme preparation

To remove the polyhistidine tag, a potential metal chelator, the gene encoding for hSR in a pET-28-derived plasmid [7] has been amplified by PCR using the primers 5'-TTTGGATCCGAGAATCTATATTTTCAATCTGGTACTTGTGCTCAGTACTGCATCTC-3' and 5'-CCCCTCGAGCTAAACAGAAACAGACTGATAGGAAGCTGGCC-3'. The construct was subcloned into a pET21b-derived expression vector (pSH21 trx) in frame with the gene encoding for His-tagged thioredoxin (Fig. 2.2). The expression vector contains a site for the TEV protease at the N-terminus for trx-tag removal (Fig. 2.3). The fusion protein was expressed in BL21 (DE3)-RIL cells, which were lysed by lysozyme incubation (45 minutes at 4°C), followed by sonication in a buffer containing 50 mM Na2HPO4, 150 mM NaCl, 4 mM TCEP, 50 µM PLP, 0.2 mM PMSF, 0.2 mM benzamidine, 1.5 µM pepstatine, pH 8.0. The fusion protein was purified using a TALON® Resin (Clontech, CA, USA) and incubated with His-tagged-TEV protease (60 µg per mg of protein) for 3 hours at 4°C to remove the His-tagged thioredoxin fragment. After dialysis to remove imidazole, the uncleaved protein and the His-tagged TEV protease were removed by further incubation with the TALON® matrix. The cleaved protein was supplemented of 400 µM EDTA to remove all residual

metal ions from the Co2+resin that could promote protein precipitation [15] and then extensively dialyzed into a buffer containing 50 mM TEA, 150 mM NaCl, at pH 8.0. Finally, hSR was concentrated to 33.6 µM and flash-frozen in 20 µl aliquots. The pSH21P:trx-TEV expression vector was provided by Professor Christopher S. Hayes, MCDB, University of California, Santa Barbara. The protein sequence of the construct is reported in Figure 2.3.

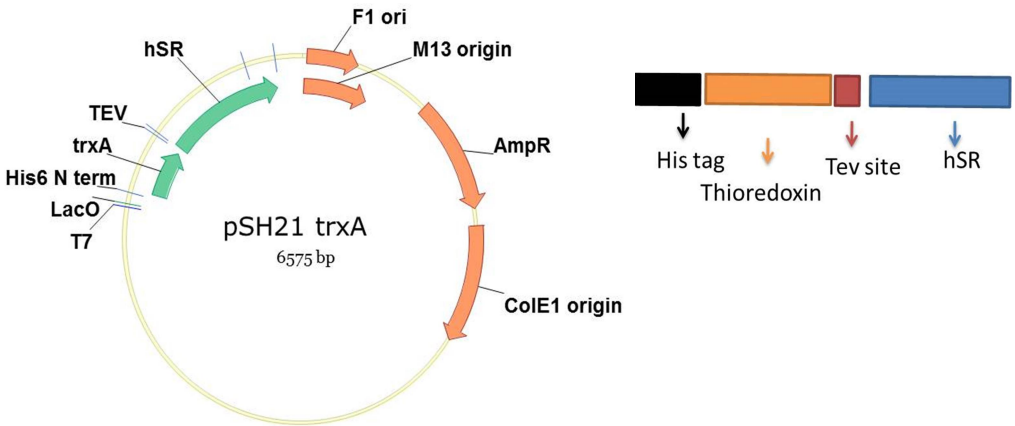

Figure 2.2. A) *derived pET21b-expression vector after the cloning of serine racemase gene located downstream the His-tag, thioredoxin and TEV protease site.* ***B)*** *schematic representation of the recombinant serine racemase gene.*

ATGGCTCATCATCACCACCATCACAGCGATAAAATTATTCACCTGACTGACGACAGTT
TTGACACGGATGTACTCAAAGCGGACGGGGCGATCCTCGTCGATTTCTGGGCAGAG
TGGTGCGGTCCGTGCAAAATGATCGCCCCGATTCTGGATGAAATCGCTGACGAATAT
CAGGGCAAACTGACCGTTGCAAAACTGAACATCGATCAAAACCCTGGCACTGCGCC
GAAATATGGCATCCGTGGTATCCCGACTCTGCTGCTGTTCAAAAACGGTGAAGTGGC
GGCAACCAAAGTGGGTGCACTGTCTAAAGGTCAGTTGAAAGAGTTCCTCGACGCTA
ACCTGGCGGGATCCGAGAACCTGTATTTTCAGTCTGGTACTTGTGCTCAGTATTGCA
TCTCCTTTGCTGATGTTGAAAAAGCTCATATCAACATTCGAGATTCTATCCACCTCACA
CCAGTGCTAACAAGCTCCATTTTGAATCAACTAACAGGGCGCAATCTTTTCTTCAAAT
GTGAACTCTTCCAGAAAACAGGATCTTTTAAGATTCGTGGTGCTCTCAATGCCGTCA
GAAGCTTGGTTCCTGATGCTTTAGAAAGGAAGCCGAAAGCTGTTGTTACTCACAGCA
GTGGAAACCATGGCCAGGCTCTCACCTATGCTGCCAAATTGGAAGGAATTCCTGCTT
ATATTGTGGTGCCCCAGACAGCTCCAGACTGTAAAAAACTTGCAATACAAGCCTACG
GAGCGTCAATTGTATACTGTGAACCTAGTGATGAGTCCAGAGAAAATGTTGCAAAAAG
AGTTACAGAAGAAACAGAAGGCATCATGGTACATCCCAACCAGGAGCCTGCAGTGAT
AGCTGGACAAGGGACAATTGCCCTGGAAGTGCTGAACCAGGTTCCTTTGGTGGATG
CACTGGTGGTACCTGTAGGTGGAGGAGGAATGCTTGCTGGAATAGCAATTACAGTTA
AGGCTCTGAAACCTAGTGTGAAGGTATATGCTGCTGAACCCTCAAATGCAGATGACT
GCTACCAGTCCAAGCTGAAGGGGAAACTGATGCCCAATCTTTATCCTCCAGAAACCA
TAGCAGATGGTGTCAAATCCAGCATTGGCTTGAACACCTGGCCTATTATCAGGGACC
TTGTGGATGATATCTTCACTGTCACAGAGGATGAAATTAAGTGTGCAACCCAGCTGGT
GTGGGAGAGGATGAAACTACTCATTGAACCTACAGCTGGTGTTGGAGTGGCTGCTG
TGCTGTCTCAACATTTTCAAACTGTTTCCCCAGAAGTAAAGAACATTTGTATTGTGCTC
AGTGGTGGAAATGTAGACTTAACCTCCTCCATAACTTGGGTGAAGCAGGCTGAAAGG
CCAGCTTCTTATCAGTCTGTTTCTGTTTAA

***Figure 2.3**. Serine racemase sequence. Histidine Tag is in green, the Tev protease site is in red, the thioredoxin coding sequence is in black and the serine racemase coding sequence is in blue.*

2.3. β-elimination activity assay

Activity assays for L-serine β-elimination [8, 15] were carried out in a solution containing 50 mM TEA, 2 mM ATP, 50 µM PLP, 5 mM dithiothreitol (DTT), 1 mM $MgCl_2$, 150 mM NaCl, 60 U/ml LDH (Sigma L2625) and 300 µM NADH, pH 8.0, at 37°C. The concentration of either EDTA, $CaCl_2$, $MgCl_2$ or ATP was modified in some experiments, as specified. The reaction was started by adding hSR at a concentration of 0.3-0.5 µM, unless otherwise stated. All reactions were carried out at 37°C. For the evaluation of the dependence of the activity on the concentration of divalent cations, either in the absence or presence of ATP, EDTA at concentrations ranging from 0 to 2.5 mM was added to enzyme solutions containing either 500 µM $MgCl_2$ (10-fold the EC_{50}, see below) or 833 µM

$CaCl_2$ (10-fold the EC_{50}, see below). In the presence of ATP, $MgCl_2$ and$CaCl_2$, exhibiting a higher EC_{50} (see below), were used at 2 mM concentration. The concentration of free Mg^{2+} or Ca^{2+} was calculated using the software Max chelator [12], which takes into account the simultaneous binding equilibria of divalent cations with EDTA and ATP, at a given pH, temperature and ionic strength.

2.4. Racemization assay.

The initial rate of D-serine formation by hSR under different conditions was determined through a discontinuous assay based on the oxidation of D-serine by D-amino acid oxidase (DAAO), with production of hydrogen peroxide [7, 16]. The assay solution contained 50 mM TEA, 150 mM NaCl, 50 µM PLP and 47 mM L-serine, which was preliminarily purified by incubation with DAAO to eliminate traces of D-serine in the commercial product [7]. Additionally, either ATP, $CaCl_2$, $MgCl_2$ or EDTA, were added at different concentrations as specified for each experiment. The reaction was triggered by addition of 1.5 µM hSR. Hydrogen peroxide was reacted with *o*-dianisidine in the presence of horseradish peroxidase to form a chromophoric species, which was treated with sulphuric acid to increase its solubility. The absorbance of the chromophoric product was measured using a HALO LED 96 microled reader (Dynamica) set at 550nm. The corresponding D-serine concentration was calculated based on a calibration curve obstained by directly reacting D-serine solutions with DAAO.

2.5. Evaluation of thermal stability

The thermal stability of hSR under different conditions was evaluated using a a Prometheus NT.48 instrument (NanoTemper Technologies GmbH), which detects intrinsic protein fluorescence changes upon thermal unfolding by monitoring tryptophan emission at 330 nm and 350 nm.Thermal unfolding experiments were performed in a temperature range from 20°C to 90°C at a rate of 1°C /minute, resulting in a data point density of 10 points/°C. For each condition, 12 µl of samples per capillary were prepared

with 0.4 µg of hSR. Stability for hSR has been estimated in: i) 50 mM TEA, 150 mM NaCl, 5 mM EDTA ii) 50 mM TEA, 150 mM NaCl, 2 mM $MgCl_2$ iii) 50 mM TEA, 150 mM NaCl, 2 mM $CaCl_2$ iv) 50 mM TEA, 150 mM NaCl, 2 mM $CaCl_2$, 2 mM ATP,v) 50 mM TEA, 150 mM NaCl, 2 mM $MgCl_2$, 2 mM ATP, at both pH 7.0 and pH 8.0. Moreover the condition v) 50 mM TEA, 150 mM NaCl, 2 mM $MgCl_2$, 2 mM ATP was tested with 20 mM of glycine and 2 mM of malonate (Table 2.1). The melting temperatures were determined by detecting the maximum of the first derivative of the fluorescence ratio (F330/F350).

Condition	***TEA***	***NaCl***	***EDTA***	***$MgCl_2$***	***$CaCl_2$***	***ATP***	***Glycine***	***Malonate***
I	*50mM*	*150mM*	*2mM*					
II	*50mM*	*150mM*		*2mM*				
III	*50mM*	*150mM*			*2mM*			
IV	*50mM*	*150mM*			*2mM*	*2mM*		
V	*50mM*	*150mM*		*2mM*		*2mM*		
VI	*50mM*	*150mM*		*2mM*		*2mM*	*20mM*	
VII	*50mM*	*150mM*		*2mM*		*2mM*		*2mM*

Table 2.1. *Conditions tested to investigate the thermal stability of serine racemase.*

3. Result and discussion

3.1. Protein purification and metal stripping

The presence of a His-tag, a potential metal chelator, did not allow for the use of the hSR construct previously designed [7, 15], as its removal using the thrombin cleavage site was hindered by the relative instability of hSR in the conditions required for proteolysis [15]. For this reason, a new His-tag-thioredoxin-SR fusion protein has been designed and digested with His-tagged TEV protease in only 3 hours at 4°C, directly in the imidazole-containing IMAC elution buffer. This procedure led to a >95% cleavage yield in a short period of time. The uncleaved fusion protein and the His-tagged TEV protease were efficiently removed with a TALON resin (Clontech, CA, USA). Overall, the final purity was >98% (Fig. 2.4).

We previously observed that incubation of hSR with EDTA prevented protein precipitation and reduced enzyme activity [15]. In order to obtain metal-free hSR for the evaluation of Ca^{2+} and Mg^{2+} effect on protein activity, EDTA had to be added and consequently considered in the equilibria. The dependence of enzyme activity on EDTA concentration was preliminary measured (Fig. 2.5). The minimal EDTA concentration needed to completely strip hSR of metals was found to be dependent on the concentration of L-serine in the enzyme assay suggesting the presence of divalent cations as contaminants. For L-serine concentration of 21.7 mM (around the K_M), 50 μM EDTA was required to reach basal activity (Fig. 2.5). Enzyme assays were designed accordingly, by adding both EDTA and divalent cations at various concentrations and by calculating the concentration of the free ions using Maxchelator software [12].

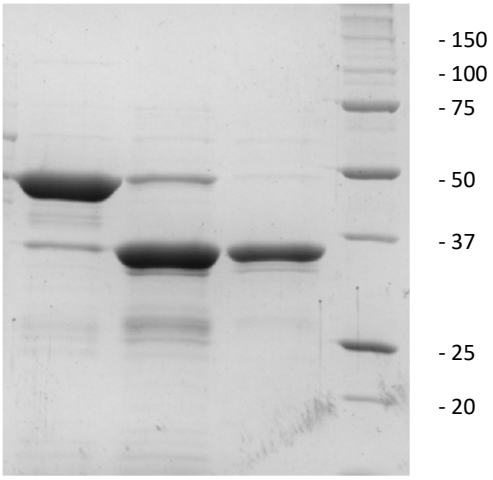

Figure 2.4. *SDS-PAGE of HisTag-TRX-hSR purification. Lane 1: full length HisTag-TRX-hSR after purification on a TALON resin. Lane 2: hSR after cleavage of the HisTag-TRX portion by incubation with TEV protease for 3 hours at 4°C. Lane 3: hSR after elimination of HisTag-TRX and unreacted HisTag-TRX-hSR using a TALON resin. Lane 4: BioRad Precision Plus Protein™ Marker.*

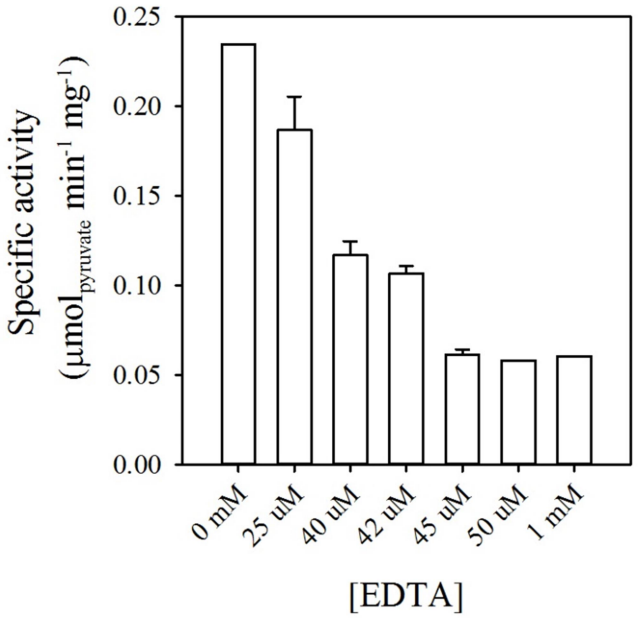

Figure 2.5. *β-elimination activity of purified hSR as a function of EDTA concentration with 21.7 mM L-serine*

3.2. Effect of cations on hSR activity in the absence of ATP

The dependence of hSR activity on either Ca^{2+} or Mg^{2+} concentration in the absence of ATP was reported in Fig. 2.6A. The binding curves were hyperbolic in both cases, indicating absence of cooperativity. The $EC_{50}$was 28 ± 3 μM for Mg^{2+} and 126 ± 7 μM for Ca^{2+}, a 4.5-fold difference in affinity. At saturation, Mg^{2+} produced a 10-fold enzyme activation in comparison to the stripped enzyme, 20% higher than the activation brought about by Ca^{2+}.

To investigate whether this difference was associated to an effect on the V_{max} or the K_M, the dependence of activity on L-serine concentration was determined at saturating concentrations of the two ions (Fig. 2.6B, Table 2.2).

	1 mM EDTA	**+ 1 mM $MgCl_2$**		**+ 2 mM $CaCl_2$**	
	No ATP	**No ATP**	**+ 2 mM ATP**	**No ATP**	**+2 mM ATP**
K_M (mM)	895±245	158±16	22.5 ± 1.5	179±22	32±3
k_{cat} (min^{-1})	13 ± 1	45 ± 1	201 ± 1	39 ± 1	114 ± 1
k_{cat}/K_M (min^{-1} mM^{-1})	0.013	0.28	9.13	0.22	3.56

Table 2.2. *Steady state parameters of hSR in the absence and presence of magnesium and calcium ions, and in the absence and presence of ATP.*

The K_M for L-serine was found to be almost identical in the presence of Ca^{2+} or Mg^{2+} (179 ± 22 mM and 158 ± 16 mM, respectively), and much lower than that in their absence (895 ± 245 mM) (Fig. 2.6B). The k_{cat} was 45 ± 1 min^{-1} in the presence of Mg^{2+} and 39 ± 1 min^{-1} in the presence of Ca^{2+}, a 15% difference. In comparison, the k_{cat} of metal-stripped hSR was 13 ± 1 min^{-1}. Therefore, the catalytic parameters in the absence of ATP

were very similar in the presence of either ions, with an effect on both the K_M and the k_{cat} in comparison to the stripped enzyme. The effect on K_M indicates that Ca^{2+} and Mg^{2+} in the absence of ATP behave as non-essential binding activators [17], with different affinity but with a similar capability to bring about the conformational modifications responsible for hSR activation.

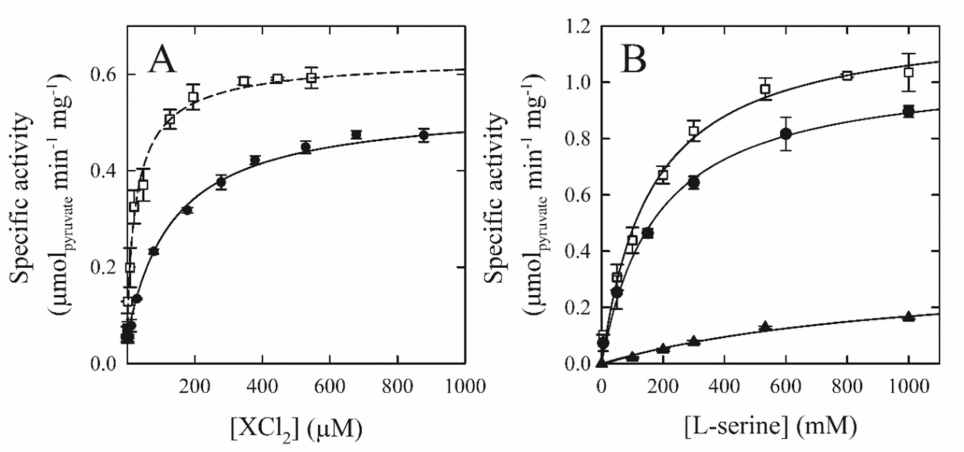

Figure 2.6. A) *Titrations of hSR with $MgCl_2$ (open squares) or $CaCl_2$ (closed circles) in the absence of ATP. The β-elimination reactivity was measured at L-serine concentration of 167 mM, a value close to the K_M in the absence of ATP. The bars were the standard errors of two replicates.* ***B)*** *Dependence of the L-serine β-elimination activity of hSR in the absence of ATP and presence of either 1 mM $CaCl_2$ (closed circles), 1 mM $MgCl_2$ (open squares), or 1 mM EDTA (closed triangles). The solid curves were the fitting to the Michaelis-Menten equation.*

3.3. Binding of ATP to hSR in the absence and presence of divalent cations

The binding of ATP in the presence of either Ca^{2+} or Mg^{2+} at 2 mM concentration was characterized to elucidate the ATP binding properties of the metal-bound forms of hSR. The evaluation of protein-metal binding equilibria required a precise evaluation of the concentration of metals in solution, considering that ATP chelates both ions. To overcome this possible limit, all binding equilibria with ATP and EDTA were taken into account [12]. In the presence of Mg^{2+}, ATP binds with a EC_{50} of 206 ± 15 µM and a Hill coefficient of 1.7 ± 0.1 (Fig. 2.7). In the presence of Ca^{2+}, ATP exhibited a EC_{50} of 595 ± 34 µM and a Hill coefficient of 1.8 ± 0.2 (Fig. 2.7). Interestingly, the activation by ATP in the presence of Ca^{2+} was only half that of Mg^{2+} (Fig. 2.7). The difference in maximal activation possibly reflects the reduced capability of the ATP-Ca^{2+} complex to shift the conformational equilibrium towards the fully activated enzyme form. Metal-stripped hSR bound ATP with a EC_{50} of 16 ± 1 mM (Fig. 2.7, inset), 80-fold higher than that in the presence of saturating concentrations of Mg^{2+} and much higher than intracellular ATP concentrations, confirming the essential role of divalent cations for ATP-mediated activation. Even in the absence of divalent cations, ATP binding was cooperative, with a Hill coefficient of 2.1 ± 0.2 [7]. The recently described aspartate racemase activity of hSR was modulated by the ATP-Mg^{2+} and ATP-Ca^{2+}complexes to the same extent as the hSR activity, with the former producing double the activation [18].

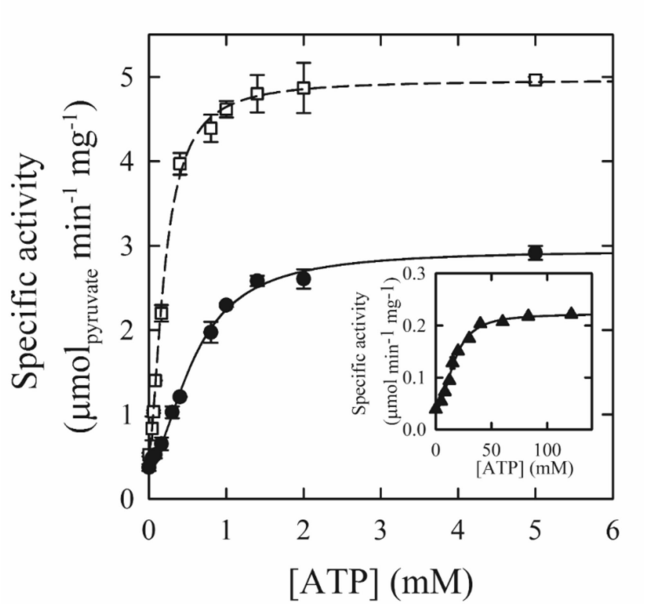

Figure 2.7. *Dependence of the β-elimination activity of hSR on ATP concentration in the presence of 2 mM $CaCl_2$ (closed circles) and 2 mM $MgCl_2$ (open squares), at 167 mM L-serine (the K_M in the absence of ATP. The bars were the standard errors of two replicates.* ***Inset:*** *Dependence of the β-elimination activity of hSR on ATP in the presence of 1 mM EDTA, at 167 mM L-serine (the K_M in the absence of ATP). The solid line was the fitting to a sigmoidal isotherm with an EC_{50} of 16±1 mM and a Hill coefficient of 2.1±0.2. The bars were the standard errors of two replicates.*

3.4. Binding of metals to hSR in the presence of ATP

Under most physiological conditions hSR is likely to operate under saturating ATP concentrations [19, 20] (Table 2.3). Therefore, the binding of Ca^{2+} and Mg^{2+} in the presence of ATP is investigated to characterize their binding equilibria both for the metal binding site and for the ATP binding site (as ATP-metal complexes). Considering the high EC_{50} of hSR for uncomplexed ATP, its contribution to hSR activation at 2 mM concentration could be neglected in the analysis.

In the presence of 2 mM ATP, both Ca^{2+} and Mg^{2+} produced hSR activation, with EC_{50} of 194 ± 6 μM and 17.3 ± 0.5 μM, respectively (Fig. 2.8A). These values were

consistent with those measured in the absence of ATP, 126 ± 7 μM for Ca^{2+} and 28 ± 3 μM for Mg^{2+}, respectively. Considering that the intracellular concentration of free Mg^{2+} in neurons was estimated in the range 400-600 μM [6] (Table 2.3), it appears that Mg^{2+} is the likely physiological ligand of hSR at this site, achieving near saturation at typical intracellular concentrations, as already suggested [1]. Ca^{2+} average concentration is estimated to be in the nanomolar range in the neuronal cytosol [21] (Table 2.3), where hSR has been consistently detected. However, the cytosolic Ca^{2+} concentrations in neurons can locally reach up to 100 μM in micro domains below the plasma membrane, within the nucleus or in proximity of mitochondria or the endoplasmic reticulum [22, 23], within the range of the observed EC_{50} for hSR. Therefore, it cannot be excluded that local fluctuations in Ca^{2+} concentration can result in the local inhibition of SR. Moreover, it is now clear that hSR is widely distributed in cells other than neurons, including uroepithelial cells, renal tubular cells, Schwann cells, chondrocytes, osteoblasts and keratinocytes [24]. The Ca^{2+}-mediated regulation of hSR might therefore involve cells other than neurons, where Ca^{2+} concentration can undergo larger fluctuations and where the subcellular localization of hSR has not be fully established.

The sigmoidal binding curves indicated cooperativity for metal binding and a fitting to sigmoidal equation yielded a Hill coefficient close to 2. This showed that, once the enzyme binds the divalent cation at its binding site, it concomitantly also binds the ATP-metal complex at the ATP binding site, resulting in a full activation. The activation at saturation is 50% higher for Mg^{2+}, confirming that the Ca^{2+}-ATP complex was less efficient than the Mg^{2+}-ATP complex at activating the enzyme. This effect is due both to a larger K_M for L-serine and a lower k_{cat}, as determined by measuring the dependence of the β-elimination activity on L-serine concentration at saturating concentrations of both metals and ATP (Fig. 2.8B). Interestingly, under physiological L-Ser concentrations, estimated to be around 1mM in neuronal cells[8], the enzyme was under-saturated and it operates under k_{cat}/K_M conditions, at which the Mg^{2+} effect on activity was 2.5-fold larger than that of Ca^{2+}.

Compartment	**Condition**	**$[Ca^{2+}]_{free}$**	**$[Mg^{2+}]_{free}$**	**[ATP]**
Cytosol	At rest	~100 nM [21]	400-600 μM [6]	~1-5 mM [19, 20]
	Activated	500-1000 nM [21]		
	Microdomains	~100 μM [22, 23]		

Table 2.3. *Concentration of ATP, Ca^{2+} and Mg^{2+} in the cytosol of neurons*

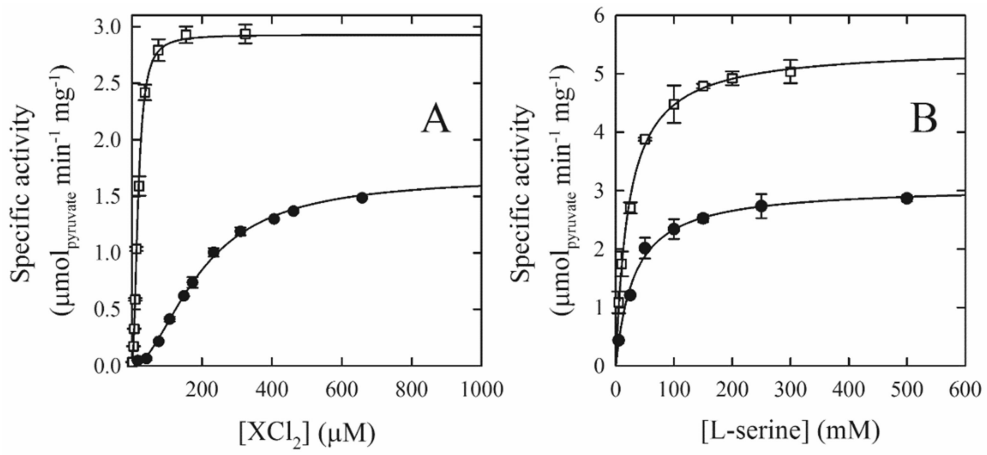

Figure 2.8. A) *Dependence of the β-elimination reactivity of hSR on $MgCl_2$ concentration (open squares) or $CaCl_2$ concentration (closed circles), at 2 mM ATP, 21.7 mM L–serine (the K_M in the presence of ATP). All assays were carried out at 37°C. The bars were the standard errors for duplicates.* ***B)*** *Dependence of the L-serine β-elimination activity of hSR in the presence of 2 mM ATP and in the presence of 2 mM $MgCl_2$ (open squares) or 2 mM $CaCl_2$ (closed circles). The K_M was 24 ± 4 mM in the presence of Mg^{2+} and 31 ± 6 mM in the presence of Ca^{2+}. The kinetic parameter resulting from the analysis of the curves with the Michaelis-Menten model were reported in Table 2.2.*

The racemization activity under the same conditions confirmed a partial activation by Ca^{2+} (Fig. 2.9A). The different ATP-mediated effects in the presence of Mg^{2+} or Ca^{2+} suggested that an intracellular increase in Ca^{2+} concentration could reduce hSR

activity, both because it would promote ATP dissociation (considering the higher EC_{50}) and produce a decrease in the Mg^{2+}-associated activation. As expected, β-elimination assays carried out in the presence of 1 mM Mg^{2+} and 2 mM ATP show that high concentrations of Ca^{2+} reduce hSR activity (Fig. 2.9B).

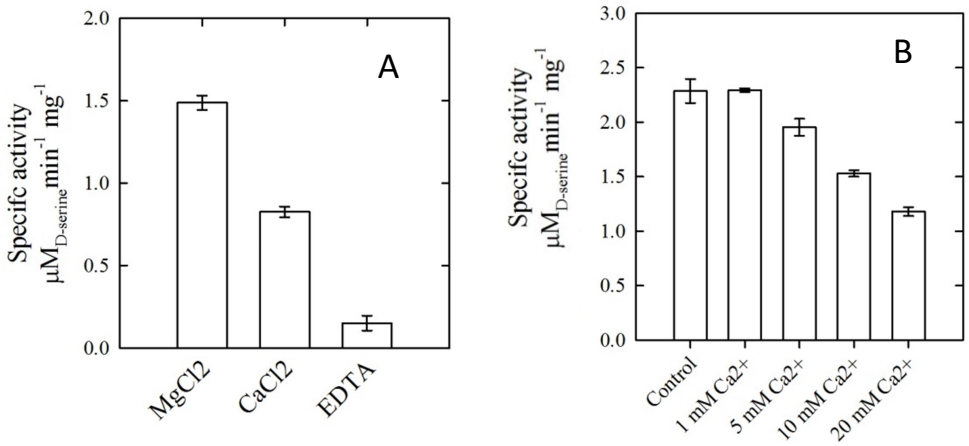

Figure 2.9. *. **A)** Effect of either 2 mM $MgCl_2$ or 2 mM $CaCl_2$ on L-serine racemization activity of hSR in comparison with the reactivity in the presence of 1 mM EDTA (absence of divalent cations), at 46.7 mM L-serine (two-fold the K_M) and 2 mM ATP. hSR was added at 1.5 μM concentration. **B)** Effect of Ca^{2+} on hSR β-elimination activity in the presence of 1 mM Mg^{2+}.*

3.5. Effect of cations on hSR thermal stability

The thermal stability of hSR under different conditions differed significantly depending on the presence of allosteric effectors (Fig. 2.10).

The melting temperature (T_m) of hSR in the absence of bound metals at pH 8 was 54 ± 1 °C and increased to 60 ± 2 °C upon addition of saturating concentrations of either Ca^{2+} or Mg^{2+} (Fig. 2.11). Further addition of ATP resulted in a slight decrease in T_m (57.6 ± 0.7 °C) that could reflect an increase in protein flexibility associated with the fully catalytically

active enzyme conformation. From a structural point of view, the decreased thermal stability could reflect the enlargement of the groove between monomers observed upon binding of ATP [25]. The ATP-Ca^{2+} complex brought about a further decrease in T_m, at 55.3 °C, in comparison to the ATP-Mg^{2+} complex, mirroring the lower catalytic activity under these conditions. The same trend was measured at pH 7.0, with an even larger stabilization by metals, with a T_m increasing from 48 ± 3 to 60 ± 2 °C in their presence. As at pH 8.0, addition of ATP in the presence of Mg^{2+} resulted in a destabilization, with a T_m of 56 ± 2 °C (Fig. 2.11). Moreover, both at pH 7 and at pH 8, the addition of glycine and malonate led to a conformation with highest melting temperature compare to the all tested conditions (Fig. 2.12). Glycine increases viscosity of the medium and was associated to a higher activity of hSR. Malonate is a competitive inhibitor of the enzyme, binding at a subside of the active site [26].

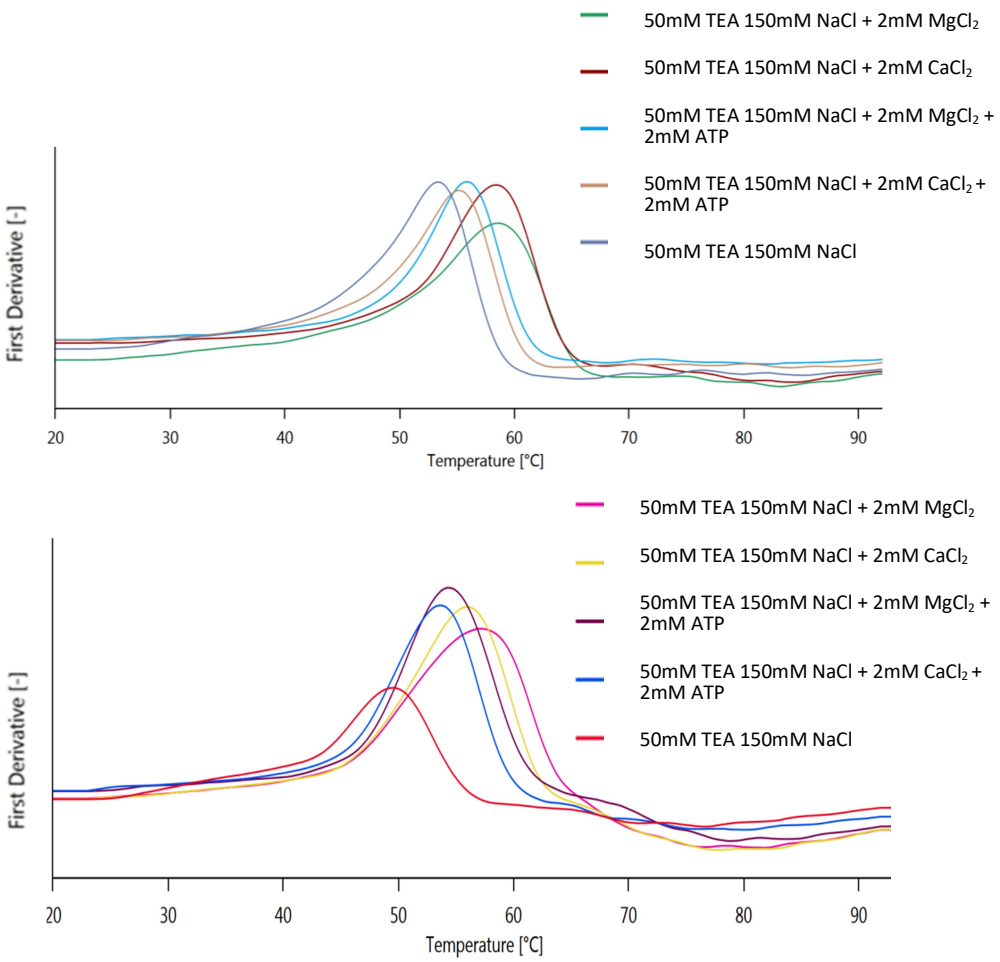

Figure 2.10. *Data from Prometheus NT.48 show changes in fluorescence emission at 330 nm in the presence of metal ions and/or ATP and corresponding first derivatives of the F330/F350 ratio. The same conditions were investigated at pH 8 (top panel) and pH 7 (bottom panel).*

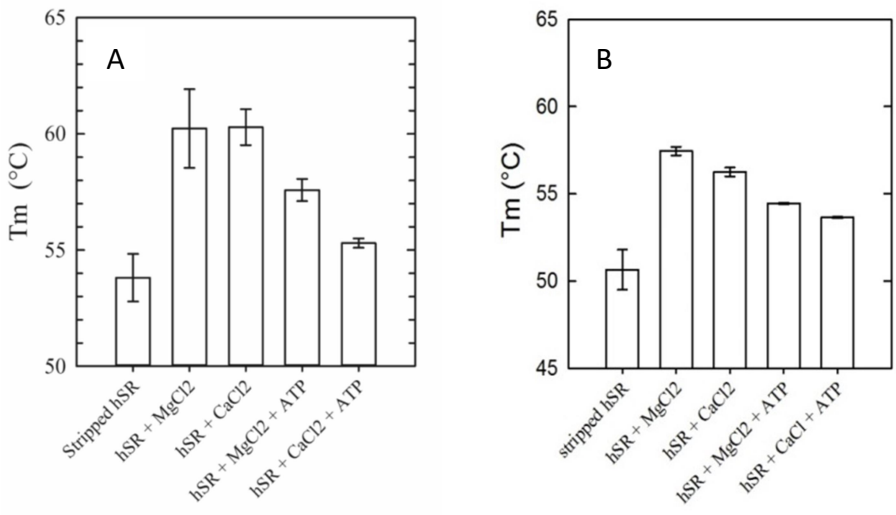

Figure 2.11. *Melting temperature of hSR under different conditions: i) 50 mM TEA, 150 mM NaCl, 5 mM EDTA (stripped hSR) ii) 50 mM TEA, 150 mM NaCl, 2 mM $MgCl_2$ iii) 50 mM TEA, 150 mM NaCl, 2 mM $CaCl_2$ iv) 50 mM TEA, 150 mM NaCl, 2 mM $MgCl_2$, 2 mM ATP, v) 50 mM TEA, 150 mM NaCl, 2 mM $CaCl_2$, 2 mM ATP,* ***A)*** *at pH 8.0* ***B)*** *at pH 7.*

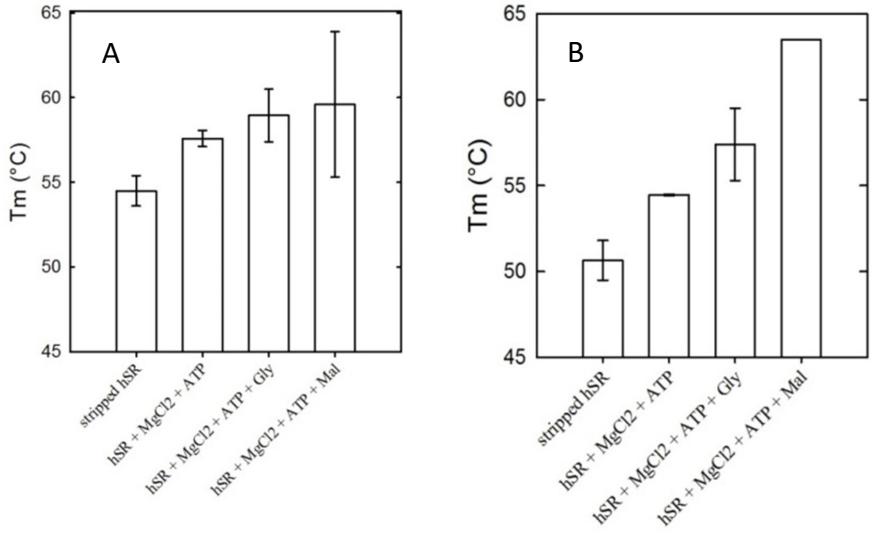

Figure 2.12. *Melting temperature of serine racemase under different condition: i) 50 mM TEA, 150 mM NaCl, 5 mM EDTA (stripped hSR) ii)50 mM TEA, 150 mM NaCl, 2 mM $MgCl_2$, 2mM ATP iii) 50 mM TEA, 150 mM NaCl, 2 mM $MgCl_2$, 2mM ATP 20mM glycine iii) 50 mM TEA, 150 mM NaCl, 2 mM $MgCl_2$, 2mM ATP, 1mM malonate.* ***A)*** *at pH 8* ***B)*** *at pH 7.*

4. Conclusions

The regulation of hSR activity and dynamics by metal ions, although established since the identification of the enzyme, has never been fully characterized. Here, we show that Ca^{2+} and Mg^{2+} bind with different affinity to the metal-binding site and stabilize the enzyme. In the presence of ATP, they mediate a different maximal activation, suggesting a possible Ca^{2+}-induced decrease in hSR activity at transiently high concentrations. Moreover, the quaternary equilibrium of hSR depends on both cations and ATP. The observation that hSR exists as an equilibrium between a poorly active dimer and an active ATP-bound tetramer opens the possibility of drug-targeting the interdimeric interface in the attempt to modulate hSR activity, a much sought after goal [27] [28] which has so far delivered only discouraging results [29, 30] [31] [32].

ABBREVATIONS:

PLP, 5'-pyridoxal phosphate; ATP, adenosine triphosphate; ADP, adenosine diphosphate; AMP, adenosine monophosphate; AMW, apparent molecular weight; hSR, human serine racemase; TEA, triethanolamine; NADH, nicotinamide adenine dinucleotide (reduced form); SpSR, *Schizosaccharomyces pombe* serine racemase.

REFERENCES

1. De Miranda, J., et al., *Cofactors of serine racemase that physiologically stimulate the synthesis of the N-methyl-D-aspartate (NMDA) receptor coagonist D-serine.* Proc Natl Acad Sci U S A, 2002. **99**(22): p. 14542-7.
2. Strisovsky, K., et al., *Mouse brain serine racemase catalyzes specific elimination of L-serine to pyruvate.* FEBS Lett, 2003. **535**(1-3): p. 44-8.
3. Baumgart, F. and I. Rodriguez-Crespo, *D-amino acids in the brain: the biochemistry of brain serine racemase.* FEBS J, 2008. **275**(14): p. 3538-45.
4. Ohnishi, M., et al., *Purification and characterization of serine racemase from a hyperthermophilic archaeon, Pyrobaculum islandicum.* Journal of Bacteriology, 2008. **190**(4): p. 1359-65.
5. Goto, M., et al., *Crystal structure of a homolog of mammalian serine racemase from Schizosaccharomyces pombe.* J. Biol. Chem., 2009. **284**(38): p. 25944-52.
6. Jahnen-Dechent, W. and M. Ketteler, *Magnesium basics.* Clin Kidney J, 2012. **5**(Suppl 1): p. i3-i14.
7. Marchetti, M., et al., *ATP binding to human serine racemase is cooperative and modulated by glycine.* FEBS Journal, 2013. **280**(22): p. 5853-63.
8. Foltyn, V.N., et al., *Serine racemase modulates intracellular D-serine levels through an alpha,beta-elimination activity.* Journal of Biological Chemistry, 2005. **280**(3): p. 1754-63.
9. Neidle, A. and D.S. Dunlop, *Allosteric regulation of mouse brain serine racemase.* Neurochem Res, 2002. **27**(12): p. 1719-24.
10. Smith, M.A., et al., *The structure of mammalian serine racemase: evidence for conformational changes upon inhibitor binding.* J. Biol. Chem., 2010. **285**(17): p. 12873-81.
11. Marchetti, M., et al., *ATP binding to human serine racemase is cooperative and modulated by glycine.* FEBS J., 2013. **280**(22): p. 5853-63.

12. Bers, D.M., C.W. Patton, and R. Nuccitelli, *A practical guide to the preparation of Ca(2+) buffers.* Methods in Cell Biology, 2010. **99**: p. 1-26.
13. Koskiniemi, S., et al., *Selection of orphan Rhs toxin expression in evolved Salmonella enterica serovar Typhimurium.* PLoS Genet, 2014. **10**(3): p. e1004255.
14. Ruhe, Z.C. and C.S. Hayes, *The N-terminus of GalE induces tmRNA activity in Escherichia coli.* PLoS One, 2010. **5**(12): p. e15207.
15. Marchetti, M., et al., *Regulation of human serine racemase activity and dynamics by halides, ATP and malonate.* Amino Acids, 2015. **47**(1): p. 163-73.
16. Molla, G., et al., *Enzymatic detection of D-amino acids.* Methods in Molecular Biology, 2012. **794**: p. 273-89.
17. Purich, D.L. and R.D. Allison, *The Enzyme Reference: A Comprehensive Guidebook to Enzyme Nomenclature, Reactions, and Methods* 2002: Academic Press.
18. Ito, T., et al., *Serine racemase is involved in d-aspartate biosynthesis.* J Biochem, 2016.
19. Genc, S., I.A. Kurnaz, and M. Ozilgen, *Astrocyte-neuron lactate shuttle may boost more ATP supply to the neuron under hypoxic conditions--in silico study supported by in vitro expression data.* BMC Syst Biol, 2011. **5**: p. 162.
20. Gribble, F.M., et al., *A novel method for measurement of submembrane ATP concentration.* J Biol Chem, 2000. **275**(39): p. 30046-9.
21. Berridge, M.J., P. Lipp, and M.D. Bootman, *The versatility and universality of calcium signalling.* Nat Rev Mol Cell Biol, 2000. **1**(1): p. 11-21.
22. Berridge, M.J., *Calcium microdomains: organization and function.* Cell Calcium, 2006. **40**(5-6): p. 405-12.
23. Rizzuto, R. and T. Pozzan, *Microdomains of intracellular Ca2+: molecular determinants and functional consequences.* Physiol Rev, 2006. **86**(1): p. 369-408.
24. Montesinos Guevara, C. and A.R. Mani, *The role of D-serine in peripheral tissues.* Eur J Pharmacol, 2016. **780**: p. 216-23.

25. Goto, M., et al., *Crystal structure of a homolog of mammalian serine racemase from Schizosaccharomyces pombe.* J Biol Chem, 2009. **284**(38): p. 25944-52.
26. Vorlová, B., et al., *Malonate-based inhibitors of mammalian serine racemase: Kinetic characterization and structure-based computational study.* European Journal of Medicinal Chemistry, 2015. **89**: p. 189-197.
27. Campanini, B., et al., *Serine racemase: a key player in neuron activity and in neuropathologies.* Front Biosci, 2013. **18**: p. 1112-28.
28. Conti, P., et al., *Synthesis and in vitro/in vivo evaluation of the antitrypanosomal activity of 3-bromoacivicin, a potent CTP synthetase inhibitor.* ChemMedChem, 2011. **6**(2): p. 329-33.
29. Dellafiora, L., et al., *Expanding the chemical space of human serine racemase inhibitors.* Bioorg Med Chem Lett, 2015. **25**(19): p. 4297-303.
30. Vorlova, B., et al., *Malonate-based inhibitors of mammalian serine racemase: kinetic characterization and structure-based computational study.* Eur J Med Chem, 2015. **89**: p. 189-97.
31. Smith, A.C., et al., *High-throughput cell transplantation establishes that tumor-initiating cells are abundant in zebrafish T-cell acute lymphoblastic leukemia.* Blood, 2010. **115**.
32. Toney, M.D., *Controlling reaction specificity in pyridoxal phosphate enzymes.* Biochim Biophys Acta, 2011. **1814**(11): p. 1407-18.

Chapter 3

Disrupted in Schizophrenia-1 as interactor of serine racemase

Abstract

A chromosomal translocation of the DISC1 (Disrupted in Schizophrenia 1) gene has been associated to behavioral abnormalities associated to schizophrenia and other neurodegenerative disorders. Recently, it was shown that DISC1 binds hSR in cells and that a pathogenic truncation of DISC1 prevents the two proteins from interacting. We expressed DISC1 in insect cells with a baculovirus expression system, alone and in co-expression with hSR. We confirmed that DISC1 and hSR interact when they are co-expressed. We showed that DISC1 partially inhibits hSR activity at equimolar concentrations.

Authors' contribution: Marilena Margiotta performed the expression and purification of DISC1 at the Institute of genetic, molecular and cellular biology (IGBMC) of Strasbourg. In collaboration with Francesco Marchesani, she carried out the enzyme assays.

1. Introduction

Escherichia coli is a robust and inexpensive expression organism for the production of recombinant proteins, but there are few limitations for the production of eukaryotic proteins. In particular, bacteria are unable to accomplish the posttranslational modifications and folding events required for the generation of fully functional eukaryotic proteins. Many eukaryotic proteins expressed in bacteria are often produced as truncated polypeptides or become insoluble as inclusion bodies, which might be very difficult to recover.

DISC1 is a large protein (854 amino acid), partially unstructured. It undergoes SUMOylation at one specific lysine residue and phosphorylation at one specific serine residue [14] [15]. Because of the predicted instability, it was decided to carry out its expression in eukaryotic cells, either alone or in co-expression with hSR. Insect cell lines are generally considered easy to cultivate compared to mammalian cell lines and can be maintained either in suspension or in monolayers. Most insect cell culture media utilize a phosphate buffering system and do not require CO_2 incubators. Insect cells promote good protein folding and many posttranslational modifications.

Baculoviruses have been exploited as expression vectors for insect cells since 1983 [2]. They are rod-shaped, double stranded DNA viruses which infect and kill the cells of a large number of invertebrate species, especially insects. The most common baculovirus used for expression studies is the *Autographa californica* multiple nuclear polyhedrosis virus (AcMNPV), which infects the lepidopteran species *Spodoptera frugiperda*. AcMNPV particles are surrounded by a protective matrix consisting of the protein polyhedrin [3], which permits survival in the environment and efficient dissemination to the hosts. Polyhedrin, which makes up most of the polyhedron, is expressed under the control of the extremely strong viral promoter *pPolh, i*n the late phase of the infection*,* and can represent up to 50% of the total cellular proteins of an infected cell. In cell cultures, the polyhedrin coat is not essential for virus propagation.

Therefore, the gene encoding for polyhedrin can be removed and substituted with that encoding for the desired heterologous proteins under the control of the *pPolh* promoter. Insect cells infected by recombinant baculoviruses can overexpress target proteins with yields that can reach several hundreds of milligrams per liter of culture. More importantly, the cytoplasmic environment of the insect cells allows for proper protein folding and for most post-translational modifications found in vertebrates, which are very often crucial for the folding/function of the target protein [4] [6].

As the baculovirus genome is generally considered too large for direct insertion of foreign gene in vitro, the gene of interest is first cloned into a transfer vector containing sequences that flank the polh gene in the viral genome. Virus DNA and transfer vector are then co-transfected into the host cell and homologous recombination between the flanking sequences common to both DNA molecules occurs. This causes the insertion of the gene of interest into the viral genome at the polh locus, resulting in the production of a recombinant virus genome. The genome then undergoes replication within the host nucleus, generating recombinant viruses.

The formation of the recombinant virus is a significant bottleneck in the process. In principle, there are three methods for the insertion of foreign genes into baculoviruses: recombination within insect cells, recombination in *E. coli* (or yeast) cells and ligation in vitro [7]. For this project, the recombination in insect cells was used.

1.1 Recombination in *E. coli*

The recombination in *E. coli* is based on Tn7-mediated transposition. The bacmids include a bacterial replicon, a kanamycin resistance marker, and attTn7, the target site for the bacterial transposon Tn7. For recombination to occur, the *E. coli* cells must contain the baculovirus shuttle vector, which can replicate in *E. coli* as a plasmid, and a helper plasmid encoding for the Tn7 transposition proteins. The expression cassette, containing the target gene and the gene for antibiotic resistance (gentamycin), flanked by the left and right ends of Tn7 (attL and attR), is carried through a donor plasmid or transfer

vector. The cassette transposes from the donor plasmid to the target bacmid, affording the recombinant bacmid [8] (Fig 3.1).

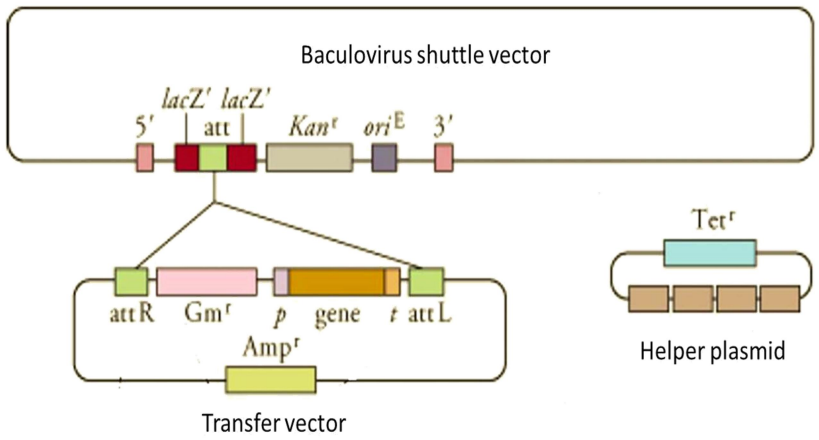

Figure 3.1. *Schematic transposition of target gene (in orange) from the transfer vector to the recombinant shuttle bacmid in a bacterial cell. In this example, the transposition interrupts the gene coding for β-galatosidase (lacZ) that hydrolyze X-gal to produce a blue product. This approach simplifies the selection of recombinant bacmids in a white/blue screening.*

1.2 Recombination in insect cells

Site-specific recombination in *E. coli* may require multiple cloning steps, whereas the latest recombination process in insect cells can reduce the time, increase efficiency and facilitate the screening. Moreover, insect cells constitutively express the recombination machinery that eukaryotic cells use for the recombination of homologous chromosomes.

Historically, recombinant baculovirus expression vectors within insect cells were produced using the highly ineffective homologous recombination process between a transfer vector containing the gene of interest and the parental virus DNA. Insect cells co-transfected with the two circular DNAs produced a mixture of both recombinant and parental viruses, with a recombination yield of around 0.1% of total virus produced. This

limitation was circumvented by the use of linearized viral DNA which cannot initiate a viral infection unless recombination with the transfer vector occurs. However, even with the use of linear DNA, the recombinant yield was around 30%. [9].

To improve the efficacy of recombination, two Bsu36I restriction sites were engineered into the polyhedrin locus of baculovirus DNA to permit linearization of the viral genome prior to co-transfection. Plus, the cleavage with Bsu36I truncates both ORF1629 and ORF603, which encode for essential genes for virus replication. This product gave rise to a higher frequency of recombinant virus production, but s background wild type may still result either from incomplete digestion or by re-ligation *in vivo* of the two Bsu36I fragments.

Further improvements employed gene knockout of ORF1629, part of which was replaced by a low copy bacterial replicon and a resistance marker (Chloramphenicol) to provide a marker for the gene knockout, surrounded by two Bsu36I sites (Fig. 3.2) [10]. The linearization of the viral DNA results in a partial deletion of the essential gene ORF1629 [9]. These bacmid DNAs, which can be amplified in *E. coli*, do not replicate in insect cells, because the essential gene ORF1629 is interrupted. The homologous recombination that occurs between the viral DNA and an appropriate transfer plasmid will re-circularizes the bacmid, restore replication, eliminate the bacterial replicon in the polyhedrin locus, and knock-in the gene of interest [11]. As it is not possible for non-recombinant viruses to replicate, there is no need for any selection system, so this engineered bacmid considerably simplifies and reduces the production of recombinant viruses to a one-step procedure in insect cells. Overall, the deletion of ORF1629 in the parental virus increased the yield of recombinant virus to more than 90%.

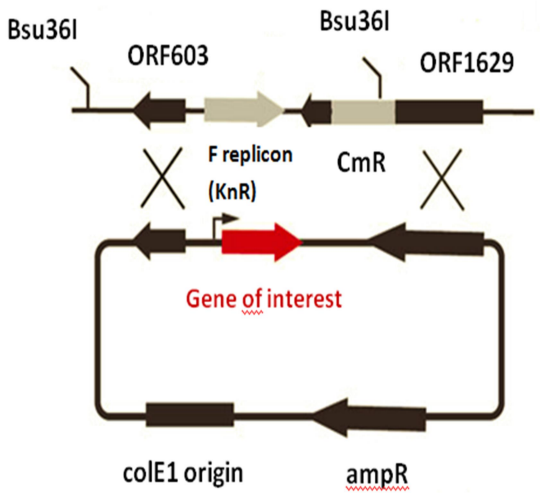

Figure 3.2. *Construction of the recombinant baculovirus by homologous recombination. Linearized viral DNA (BAC10:KO1629) is co-transfected in Sf9 insect cells with a transfer vector containing the gene of interest. Homologous recombination restores the essential ORF1629, allowing viral replication and expression of the desired protein [1].*

Today, ready-to-use and genetically optimized linearized baculovirus DNA can be purchased from a number of sources. For standard applications and/or initial construct evaluation, the BAC10:KO1629 bacmid [9] is a reference source of viral DNA. It consists of the wild type AcMNPV genome with two Bsu36I restriction sites, kanamycin or chloramphenicol resistance markers inserted at the polyhedron locus (Fig. 3.2).

2. Materials and methods

2.1. Preparation of the transfer vector

2.1.1. Restriction/ligation based cloning

The pMF dual transfer vector (Fig. 3.3) used in this study belongs to a set of vectors based on PAC8 vector Backbone designed to facilitate expression screening and enable consistent comparisons of the impact of partners on expression, solubility and purification. These vectors contain two expression cassettes driven by two late viral promoters: the polyhedrin promoter (*pPolh*) and the p10 promoter.

The gene for hSR (1083 bp) with an N-terminal histidine affinity tag, available in a pET28 bacterial expression vector, was inserted in pMF transfer vector with restriction/ligation-based cloning techniques using the NheI and XhoI restriction sites (Figure 3.2). The synthetic full-length gene encoding for DISC1 (2679 bp) (GeneArt), was cloned in a pMF transfer vector, individually and with hSR for co-expression, using the BamHI and XbaI restriction sites. hSR was positioned under the control of the p10 promoter and DISC1 under that of the *pPolh* promoter.

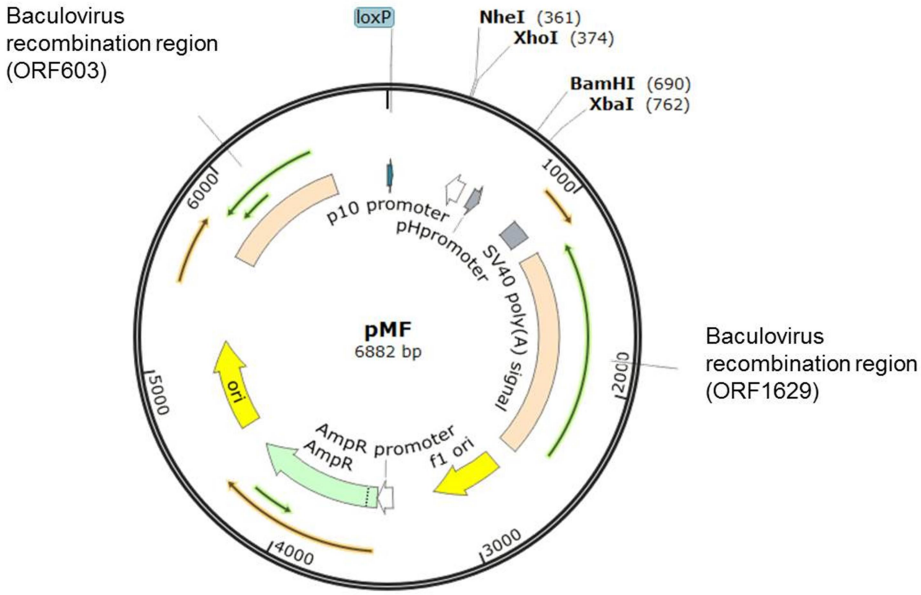

Figure 3.3. *Graphic map of pMF transfer vector. It contains the site-specific recombination site (LoxP) for Cre-LoxP, a resistance marker for ampicillin (AmpR), the expression cassettes comprising promoters (pPolh, p10), multiple cloning sites, terminators (SV40, HSVtk) and the colE1 origin of replication for a high copy number replication in E. coli.*

Two different constructs of DISC1 were tested for purification purposes:

1) DISC1 in frame with a Twin-Strap-tag at the N-terminus

2) DSIC1 in frame with both a Flag Tag at C-terminal end and a Twin-Strep-tag at the N-terminus.

The resulting final sequence for DISC1 containing both affinity tags is reported in Figure 3.4 and the amino acid sequences of the affinity tags are reported in Table 3.1.

The FlagTag sequence was added to DISC1 sequence through PCR using the pair of primers (Table 3.2) DISC1_PmlI F and FlagTag R. The PCR product of 1287 bp was

digested with PmlI and XbaI and inserted in the pMF vector already containing the N-terminal part of DISC1.

MASAWSHPQFEKGGGSGGGSGGSAWSHPQFEKENLYFQGPGGGPQGAPAAAGGGGVSHR
AGSRDCLPPAACFRRRRLARRPGYMRSSTGPGIGFLSPAVGTLFRFPGGVSGEESHHSESRAR
QCGLDSRGLLVRSPVPKSAAAPTVTSVRGTSAHFGIQLRGGTRLPDRLSWPCGPGSAGWQQE
FAAMDSSETLDASWEAACSDGARRVRAAGSLPSAELSSNSCSPGCGPEVPPTPPGSHSAFTS
SFSFIRLSLGSAGERGEAEGCPPSREAESHCQSPQEMGAKAASLDGPHEDPRCLSRPFSLLAT
RVSADLAQAARNSSRPERDMHSLPDMDPGSSSSLDPSLAGCGGDGSSGSGDAHSWDTLLRK
WEPVLRDCLLRNRRQMEVISLRLKLQKLQEDAVENDDYDKAETLQQRLEDLEQEKISLHFQLPS
RQPALSSFLGHLAAQVQAALRRGATQQASGDDTHTPLRMEPRLLEPTAQDSLHVSITRRDWLL
QEKQQLQKEIEALQARMFVLEAKDQQLRREIEEQEQQLQWQGCDLTPLVGQLSLGQLQEVSKA
LQDTLASAGQIPFHAEPPETIRSLQERIKSLNLSLKEITTKVCMSEKFCSTLRKKVNDIETQLPALL
EAKMHAISGNHFWTAKDLTEEIRSLTSEREGLEGLLSKLLVLSSRNVKKLGSVKEDYNRLRREVE
HQETAYETSVKENTMKYMETLKNKLCSCKCPLLGKVWEADLEACRLLIQSLQLQEARGSLSVED
ERQMDDLEGAAPPIPPRLHSEDKRKTPLKVLEEWKTHLIPSLHCAGGEQKEESYILSAELGEKC
EDIGKKLLYLEDQLHTAIHSHDEDLIQSLRRELQMVKETLQAMILQLQPAKEAGEREAAASCMTA
GVHEAQAGAPDYKDDDDK

Figure 3.4. *DISC1 amino acid sequence (final construct). In red, is the Twin-Strep tag; in green is the linker, in blue is the Tev protease site, and in violet the Flag tag*

Name	**Sequence**
His Tag	5’-GTGATGATGATGATGATG-3’
Strep Tag	5’- TGGAGCCACCCGCAGTTCGAGAAA-3’
Flag Tag	5’- GACTACAAGGACGACGATGACAAG-3’

Table 3.1. *Tag sequences added to terminal ends of DISC1 and serine racemase*

Name	Sequence
DISC1_BamHI F	5'- CCGTCCCACCATCGGGCGCGGATCC ATGGCTAGCGCATGGAGCCACCCGCAGTTCG -3'
DISC1_XbaI R	5'- CTCGACAAGCTTGTCGAGACTGCAGGCTCTAGATCAGGCTTGTGCTTCGTGGACACCA GCTGTC -3'
DISC1_PmlI F	5'- GAACCCACTGCTCAGGACAGCTTGCACGTGTCC -3'
DISC1_PmlI R	5'- GAAGCCAGTCTCGTCTCGTGATGGACACGTGCAA -3'
Universal F	5'-CTATAAATATTCCGGATTATTCATACCGTCCCACCATCGGGCGCGGATCC-3'
Universal R	5'- ATTATGATCCTCTAGTACTTCTCGACAAGCTTGTCGAGACTGCAGGCTCTAGA -3'
hSR F	5'- TGCATCAGCTGCTAGCTTAAACAGAAACAGACTGATAAGAAGCTGG-3'
hSR R	5'- CACCCGGGATCTCGAGCCATGGGCAGCAGCCATC-3'
FlagTag R	5'-GGCTCTAGATCACTTGTCATCGTCGTCCTTGTAGTCTGGCGCGCCGGCTTGTGCTTCGTG GACACCAGCTGTCATG-3'

Table 3.2. *Primer sequences used for PCR reactions*.

2.1.2. Alternative cloning: SLIC

In parallel with the traditional techniques using restriction enzymes, a novel cloning method, the sequence and ligation-independent cloning (SLIC) (Fig. 3.5) [12] was used to clone the gene encoding for full-length DISC1 in the pMF transfer vector. SLIC allows the assembly of multiple DNA fragments in a single reaction using in vitro homologous recombination and single-strand annealing. SLIC mimics in vivo homologous recombination by relying on exonuclease-generated ssDNA overhangs in insert and vector fragments, and the assembly of these fragments by recombination in vitro.

The procedure for SLIC cloning was as follows:

- Digest the pMF vector with the restriction enzymes BamHI and XhoI
- Purify of the resulting fragment from an agarose gel using the QIAquick Gel Extraction Kit (Qiagen).

- Perform PCR amplification of the insert using Phusion DNA polymerase to generate separately two PCR products using four primer pairs (Table 3.2, Figure 3.5). *DISC1_PmlI R* and *DISC1_BamHI F* were used to amplify the N-terminal end of the gene. *DISC1_PmlI F* and *DISC1_XbaI R* were designed to amplify the C-terminal end. Then each fragment was used as template for the second PCR with, respectively, DISC1_PmlI R and *Universal F* primers for N-terminal end; DISC1_PmlI F with *Universal R* for C-terminal end. The second round of PCRs added the 30bp homologous region to the vector at both 5' ends of the fragments. The primers pair *DISC1_PmlI F* and *DISC1_PmlI R,* which overlaps on the 3' end, created an overlapping homology of 55 bp between the two PCR products (Fig.3.4).
- Digest the template with 20 U of *DpnI* and incubate at 37°C for 1 h
- Purify the PCR products using a QIAquick PCR purification column (Qiagen).
- Treat 1 µg of vector and 1 µg of each insert separately, in 50 µl reaction at 22 °C per 15 min (time depending on the length of the homologous region) with 0.5 U of T4 DNA polymerase and 5 µl Buffer 1X (New England Biolabs, NE Buffer 2.1) containing 50 mM NaCl, 10 mM Tris-HCl, 10 mM $MgCl_2$, 100 µg/ml BSA.
- Stop the reaction with 1/10 volume of 10 mM dCTP (Deoxycytidine triphosphate).
- Mix 200 ng of vector (6810 bp) and 200 ng per each fragments (~1300 bp) with a 1:5 insert-to-vector molar ratio in 10 µl annealing reaction with 1X ligation Buffer (50 mM Tris-HCl, 10 mM $MgCl_2$, 1 mM ATP, 10 mM DTT pH 7.5) and incubate at 37°C for 30 min.
- Use 5 µl of annealing reaction to transform 50 µl of chemical competent cells (*E. coli* DH5α) and plate them on the LB agar plate containing 100 µg/mL ampicillin.
- Confirm the insertion through colony PCR
- Extract and purify the plasmid DNA from the positive colonies
- Perform the restriction analysis with PmeI/AvrII (located outside the expression cassette), and with *PmlI* (unique site of DISC1 sequence). Sequencing using the

corresponding gene specific primers: *Universal F, Universal R* and *DISC1_PmlI F* and *DISC1_PmlI R* in case of DISC1 and with *hSR F* and *hSR R* for hSR.

- Prepare the Midi-prep of the sequence-validated plasmid, precipitate and dry the plasmid DNA under the sterile hood and resuspend it in sterile ultrapure water.

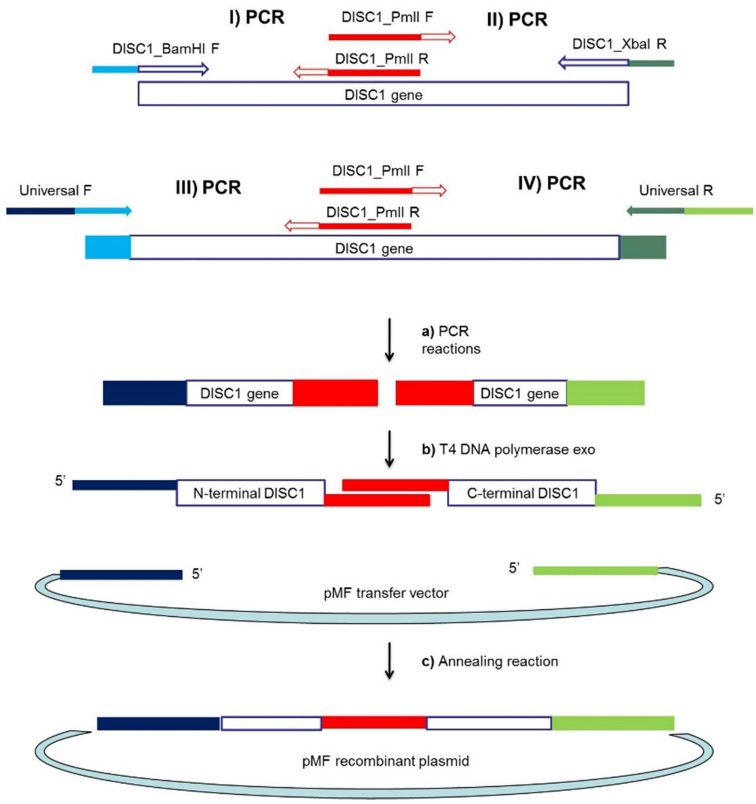

Figure 3.5. *SLIC cloning strategy.* ***a)*** *Amplification of DISC1 gene using four PCR reactions: I) DISC1_PmlI R and DISC1_BamHI F primers amplify N-terminal region, II) DISC1_PmlI F and DISC1_XbaI R primers amplify C-terminal region, III and IV) Universal F and Universal R primers add at 5' ends 30 bp homology region to the vector.* ***b)*** *Incubation of PCR products and vector with T4 DNA polymerase with exonuclease activity to generate 5' overhangs.* ***c)*** *The ssDNA assembly by homologous recombination.*

2.2. Linearized Viral DNA for co-transfection

The bacmid BAC10:KO1629 was amplified in *E. coli*, purified using a plasmid/bacmid isolation kit, and linearized to enhance recombination efficiency, following the following protocol.

- Pre-culture: inoculate 3 mL of LB medium containing 50 µg/mL kanamycin and 34 µg/mL chloramphenicol with a single colony of DH10B BAC10:KO1629 from a freshly prepared plate and incubate at 37 °C for 8 h
- Culture: Add 200 µL of the pre-culture into a 1 L Erlenmeyer containing 200 mL of LB with the appropriate combination of antibiotics and incubate at 37 °C for 12–16 h. The culture should be grown to an OD of 2.0–3.0 at 600 nm, which corresponds to 1.2–1.8 g of wet cells and is enough for 20 µg bacmid purification.
- Bacmid extraction purification using a commercially available purification kit: The procedures include an isopropanol precipitation to concentrate DNA, followed by a washing step with 70 % ethanol to remove traces of salts. After centrifugation, the ethanol is removed and the DNA pellet air-dried at room temperature.
- Resuspend the dried bacmid pellet with 200 µL of sterile ultrapure H_2O. Quantify and store the sample at 4 °C.
- As homologous recombination is more efficient with linear DNA than with the circular DNA, the purified bacmid is finally linearized using the restriction enzyme Bsu36I. To digest 1 µg of bacmid, prepare 25 µl of the solution with 2.5 µL 10× NEB3 buffer, and 1 µL Bsu36I (NEB) (10 U/µL). Then incubate for 2 h at 37 °C.
- Analyze the digestion by gel electrophoresis.
- Precipitate again the linearized bacmid with isopropanol and ethanol, aliquot in 20 µL (1 µg/µL) and store at 4 °C for 1–2 month or at -20 °C for long-term storage.

2.3. Generation and amplification of recombinant Baculovirus

The most common cellular lines suitable for the expression of recombinant proteins is the Sf9 insect cell line, a clonal isolate derived from the parental *Spodoptera frugiperda* cell line IPLB-Sf-21-AE developed form ovaries, best known as Sf21. For efficient transfection, virus amplification, and protein production, healthy cells are absolutely required. Cells should be maintained in exponential growth phase, should not be overgrown, and passages should be limited. A doubling time of 18–24 h and a continuous viability >95 % are prerequisites for successful work.

To generate recombinant baculoviruses, the transfer vector (Fig. 3.3) suitable for homologous recombination is co-transfected with linearized viral DNA (Fig. 3.6) in insect cells. This allows integration of the expression cassette into the viral genome which will be replicated and leads to virus production. The co-transfection supernatant represents the first virus stock (V0), which can be used for small-scale expression test. The subsequent amplification will be suitable for large-scale expression [1].

2.3.1. Co-transfection of Transfer Plasmid and Viral DNA

To perform the co-transfection, two methods have been already optimized: The Lipofectamine method and the calcium phosphate method. Both procedures were carried out to obtain the insertion of the genes of interest and to get more possibilities of success.

I) Lipofectamine method.

- Seed 1 ×106 Sf9 cells with 1.6 mL insect cell culture medium (Grace's Insect Medium, L-glutamine and NHCO3, G8142-SIGMA) in a 6-well plate and let the cells adhere for 20 min at 27 °C.
- Under the sterile hood, mix 2.5 µg of DNA transfer vector with 1 µg of linearized bacmid in 150 µL of insect cell culture medium in tube A. Separately dilute 15 µL of Lipofectamine transfection reagent (LIPOFECTAMINE*2000 Invitrogen Reagent

1mg/ml) into 135 µL of insect cell culture medium. Include negative control without the transfer plasmid and positive control with transfer vector expressing the DsRed protein.

- Add the DNA solution (from tube A) to the Lipofectamine solution (to tube B, respect the addition order) gently, drop-wise and incubated at room temperature (RT) for 5 min. Extended incubation may lead to formation of large and difficult to transfect DNA/transfection agent complexes.
- Mix 300 µL of DNA/Lipofectamine solution drop wise with the cells, homogenize by dropping surface and incubate at 27 °C. The day after add 1.5 mL of medium containing serum (10% FBS) to the cell and return to the incubator for at least 5 days.
-

II) Calcium phosphate method

- Add 2 ×106 Sf9 cells in 5 ml insect cell culture medium (Grace's Insect Medium, L-glutamine and NHCO3, G8142-SIGMA) in 25 cm2 flasks (Fig. 3.7) and incubate at 27°C per 30 min.
- Mix 2.5 µg of transfer vector, 1 µg of linearized Bacmid and add 750 µl of Hepes Buffer in tube A. Optionally, prepare a negative control with Bacmid and just Hepes buffer. Separately prepare a mixture with 680 µl of Grace's Insect Medium with 75 µl of Fetal Cow Serum (FCS) in tube B. Respecting the order, add the solution from tube A to tube B gently and drop wise, and incubate the mixture at room temperature (RT) for 15 min.
- Remove the media from the 25 cm2 flask and add the DNA mixture to insect cells (1.5 ml per each flask), and incubate them for 4h at 27 °C;
- 4 hours later add 5 ml of fresh Grace's Insect Medium with 10 % FCS and return to the incubator for at least 5-7 days.

- From the second day, the cells are observed daily under an inverted microscope in search for infected cells. These cells should swell, stop dividing, and appear uniformly rounded with enlarged nuclei while confluent cell grow should be seen in non-transfected cell control (without DNA mixture). Cells expressing the DsRed fluorescent protein should be present in the positive control (with bacmid and transfer plasmid) and should not be in negative control.
- After 5-7 days, when more than 50 % of cells in the positive control express the DsRed fluorescent protein, carefully, collect the cell culture and centrifuge at 1200 rpm for 7 min. The supernatant is the first generation of virus is called V0. V0 can be stored at 4 °C for at least 3–6 months, protected from light.

Figure 3.7. *Cell culture Flasks*

2.3.2. Protein expression test

V0 was used for an initial screening to determine if the protein(s) of interest were expressed. For the screening, the following procedure was carried out:

- Prepare 25 ml of Sf21 insect cells culture in suspension at the concentration of 0.6 × 106 Sf21 and add 1 ml of V0 (just collected from co-transfection)

- The first, the second and the third day after infection, take an aliquot of culture (1 ml), count the cells and prepare the samples for Western Blot analysis. Centrifuge at 12000 rpm for 5 min at 4 °C remove the media, resuspend the cells in PBS solution (106 cells in 100 µl) or lysis buffer supplemented with EDTA-free protease inhibitor cocktail (if the protein showed to be insoluble and degraded) and sonicate them for 30 seconds (0.5 sec ON-0.5 sec OFF) using 3 mm probe with an amplitude of 60 %.
- Centrifuge the lysate at 12000 rpm for 5 min at 4 °C, transfer the supernatants in fresh tubes, add the loading buffer and analyze the soluble and insoluble extracts by SDS-PAGE and Western Blot analysis.

2.3.3. Virus amplification from adherent cultures

Recombinant V0 virus stock can be amplified before large-scale recombinant production. Healthy and in exponential growth phase insect cells are infected with a small quantity of virus, at a very low multiplicity of infection (MOI) (less than one virus per cell). In these conditions, few cells were infected initially and multiple rounds of replication occurred to obtain high virus titers. When cells are infected at high MOI, all the cells are initially infected and only a single round of replication will occur, giving poor virus amplification. After the first round of amplification, a high-titer viral stock, called V1, is obtained. The second and the third round of amplification afford the V2 and V3 virus stocks, respectively.

Procedure for amplification from adherent cultures:

- Add 2.0 x 10^6 Sf9 cells in 25 cm^2 flask in 5 ml of Grace's Insect Medium and incubate the flask for 30 min at 27 °C until the cells adhere to the surface. Then discard the medium and add 1 ml of V0 (low potency).

- After 1 h incubation at 27 °C, add 5 mL of Grace's Insect Medium with 10 % FCS to the same 25 cm^2 flask and then incubate again per 5-7 days. We left the incubation until cytopathic effect occurred, i.e. when 50% of cells or more collapse.
- Harvest the virus with centrifuge at 25000 rpm per 10 min to remove cells debris. The supernatant containing the virus is stored at 4 °C and protect it from the light. This is the V1 virus stock.

V1 is sufficient for initial protein expression studies. If large volumes of virus are required second step of amplification is repeated to obtain V2 or V3.

2.4. Optimization and Small-Scale Expression of Proteins

The yield of the recombinant protein, as well as its quality, is affected by a myriad of factors. Thus, once a concentrated baculovirus stock has been amplified, optimization experiments are required before large-scale expression and purification can take place. Experiments started from small-scale purification to get preliminary information on protein solubility and expression yield. For the infection, we used Sf21 cells grown in suspension and we infected them with a high MOI (about 5 viral particles per cell), one viral particle per cell, to get all cells infected synchronously. The cultures were harvested three days after infection.

2.4.1. Small scale purification of hSR

- Infect 50 ml of Sf21 insect cell culture at the concentration of 0.7-1 x 10^6 cells/ml growing in Rich medium (Grace's insect Medium Supplemented with L-glutamine 30 g/l Lactalbumine Hydrolysate 3 g/l yeastolate) with 0.5 ml of V1 (recombinant virus with hSR gene).

- Three days after infection centrifuge the cells at 4000 rpm for 15 min at 4 °C and discarded the supernatant. Then wash the cell pellet with 50 mL of PBS supplemented with 10 % glycerol followed by centrifugation at 4000 rpm for 10 min.
- Resuspended the cells in 5 ml of lysis buffer (50 mM Na2HPO4; 150 ml NaCl, pH 8.0 at 4°C; TCEP 5 mM, stock at pH7.0; PLP 50 µM) supplemented with EDTA-free protease inhibitor cocktail at recommended concentration and sonicate for 30 s (0.5 sec ON-0.5 sec OFF) using 3 mm probe with an amplitude of 60%.
- Centrifuge the lysate at 20000 rpm for 30 min at 4 °C T and incubate the soluble extract with equilibrated Ni-NTA resin at 4 °C per 60 min, using 100 µL of resin for batch purification.
- Use 500 µL spin-column to wash the resin three times with 800 µL of washing buffer (50 mM Na2HPO4, 300 mM NaCl, 5 mM Imidazole, pH 8.0 a 4 °C), supplemented with Imidazole to limit a-specific binding to Ni-NTA resin. Then elute two times with 800 µL of elution buffer (50 mM Na2HPO4, NaCl 150mM, 250 mM Imidazole, pH 8.0 a 4 °C). Add 1 mM EDTA to the purified eluted protein.
- The imidazole was removed using desalting column, prior to equilibration with 15 ml of Storage Buffer (50 mM TEA pH 8.0). All steps were monitored using SDS-PAGE with Coomassie staining and/or with Western blot in case of low expression levels.

2.4.2. Small scale purification of DISC1

- Infect 200 ml of Sf21 insect cell culture (0.7-1 x10^6 cells/ml) with recombinant virus for the expression of DISC1.
- Three days after infection the cells are centrifuged at 4000 rpm for 15 min at 4 °C and wash the cell pellet with 50 mL of PBS supplemented with 10 % glycerol followed by centrifugation at 4000 rpm for 10 min.

- Resuspend the cells in 30 mL of lysis buffer (50 mM Tris-HCl, 400 mM NaCl, 10 mM MgCl2at pH 8, 10% glycerol) supplemented with EDTA-free protease inhibitor cocktail.
- Sonicate the cells for 30 s (0.5 sec ON-0.5 sec OFF) with amplitude of 60 %, and centrifuge the lysate at 20000 rpm for 30 min at 4 °C.
- Incubate the soluble extract with 200 µL of equilibrated Strep-Tactin Super flow High Capacity (IBA) resin for 60 min at 4 °C with gently mixing on a slow end-over-end rotator.
- Wash the resin with 500 µl spin-columns three times with lysis buffer and elute two times with 200 µL of elution buffer, supplemented with 10 mM desthiobiotin.
- After the first incubation with Strep-Tactin resin, the flow through is incubated with ANTI-FLAG M2 Affinity Gel (Sigma A2220) for 3 h at 4 °C. Proceed with nine washing steps with 1 ml lysis buffer, and perform elution overnight with 100 µL of lysis buffer supplemented with 1mg/ml of specific competitor Peptide (PD157).
- Analyze the samples with SDS-PAGE and Western blot to verify the molecular weight and expression level of DISC1 in these conditions.

2.5. β-elimination activity of hSR in the presence of DISC1

L-Serine β-elimination activity assays, already described in chapter 2, were performed in the presence of DISC1 to evaluate its effects on hSR activity. Due to the instability of DISC1, the assay was performed with the storage Buffer of DISC1, and the kinetics control was carried out with same Buffer stripped of DISC1, at pH8 37°C. The Buffer contains 50 mM Tri-HCl, 400 mM NaCl, 10 mM $MgCl_2$, 10 % glycerol, supplemented with 2mM ATP, 133 µM L-serine, 30 U/LDH for the reaction. hSR was added at a concentration of 88 nM, in order to have 1.45-fold molar excess of DISC1 with a concentration of 128 nM.

3. Results and Discussion

3.1. Gene cloning in pMF

The DISC1 gene (2679 bp) was inserted in pMF transfer vector using sequence-ligation independent cloning (SLIC), and the insert size was verified by restriction analysis (Fig. 3.8).

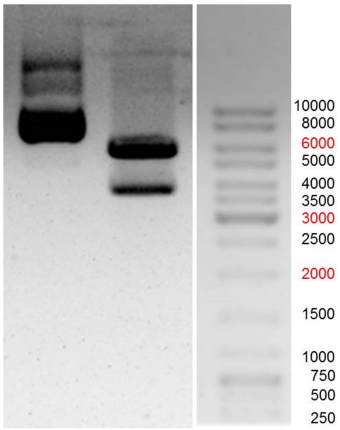

Figure 3.8. *Restriction analysis to verify the right size of the insert DISC1. Line 1. Plasmid not digested, line 2. Digestion with PmeI and AvrII (fragments length expected: 3715 bp for the insert and 5780 bp for the backbone).*

As described in Materials and Methods, we amplified the gene as two fragments in order to increase the efficiency of SLIC cloning. hSR was also inserted in pMF vector using restriction-ligation dependent cloning. Then, the two genes were subcloned together in pMF with restriction-ligation dependent cloning. Also in this case DISC1 gene was inserted as two fragments, and at C-terminal end a Flag-tag was added. The recombinant plasmid was verified with restriction analysis using BamHI (located at N-terminal end of the insert) and AscI (located between the insert and the Flag-tag) (Fig. 3.9)

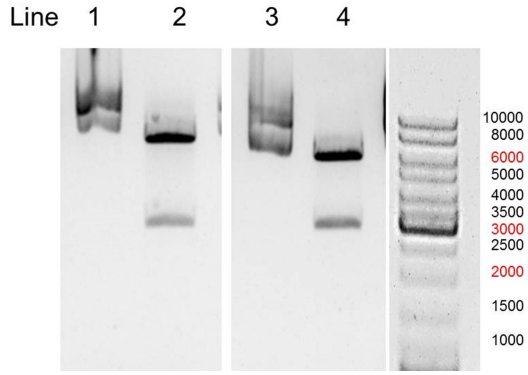

***Figure 3.9**. Restriction analysis of plasmid DNA to verify the cloning of serine racemase and DISC1 in pMF and the cloning of DISC1 after addition of Flag-tag. Line1. pMF_serine racemase_DISC1 plasmid not digested, line 2. pMF_serine racemase_DISC1 digested with BamHI and AscI (expected fragments size 2683 bp and 7923 bp) line 3. pMF_DISC1 not digested, line 4. pMF_DISC1 digested with BamHI and AscI (expected fragments size 2683 bp and 6845 bp).*

3.2. Expression

Various cell lines, ratios of Bacmid-to-plasmid DNA, incubation times and cell densities were tested to find the optimum conditions for both hSR and DISC1 expression. The optimized protocol described in subsequent experiments is outlined in Material and Methods.

The Western Blot analysis with anti-His antibody showed the high expression level and the integrity of hSR at different MOI (multiplicity of infection) (Fig. 3.10), whereas DISC1 was largely insoluble and it was observed in the cellular debris pellet after centrifugation (Fig. 3.11). The Western blot analysis with anti-Strep antibody for DISC1 showed a degradation of the protein at the C-terminal end, and denoted the necessity to optimize the conditions of purification (Fig. 3.11). Four main bands were detected, corresponding to 100 KDa, which matches exactly with the molecular weight of DISC1, 36 kDa, 28 kDa, and 17 KDa. In the following western blot analysis, the same bands were detected, indicating a partial degradation.

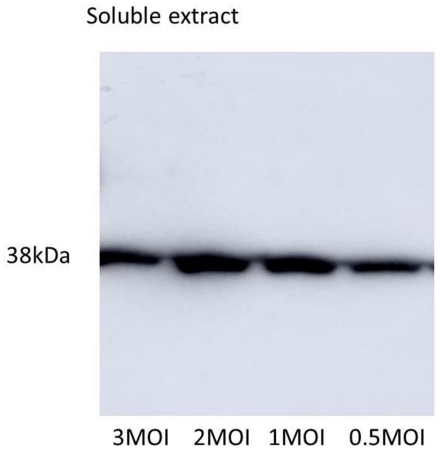

Figure 3.10. *Western blot analysis of cleared lysate from Sf21 insect cell with expressed hSR; the cells were infected with different MOI (number of viral particles/number of cells).*

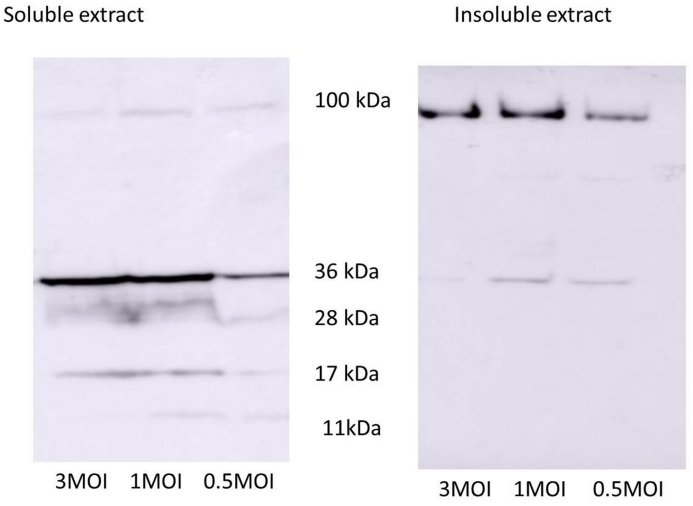

Figure 3.11. left*) Western blot analysis of cleared lysate from Sf21 insect cell with expressed DISC1, the cells were infected with different MOI (number of viral particles/number of cells).* ***right****) Insoluble extract derived from centrifugation of the same lysates.*

3.3. Purification of DISC1

The purification of DISC1 proved to be difficult. Different issues were identified, mostly associated to the degradation of the full-length protein and its precipitation in inclusion body. Several steps were taken in the attempt to optimize the purification protocol, including use of different lysis buffers, homogenization, and the use of inhibitors of proteases. At last, a Flag Affinity Tag was added to C-terminal end of DISC1.

As we already detailed, we performed DISC1 purification using both a *Strep-Tactin* resin and an *ANTI-FLAG Affinity Gel* resin. However, we noticed, since the first purification, that DISC1 does not bind to the Strep resin efficiently, possibly because of steric effect or improper folding (Fig. 3.12). By using the Flag Tag at the C-terminal, we purified a small quantity of full-length soluble DISC1. The protocol was repeated with 1 liter of Sf21 insect culture, but the yield was barely 0.2 mg in total of full-length DISC1 and a new band of 55kDa corresponding degradation of DISC1 was detected. The expression conditions are yet not optimal, and future experiments will aim at purifying under denaturing conditions to recover the insoluble protein.

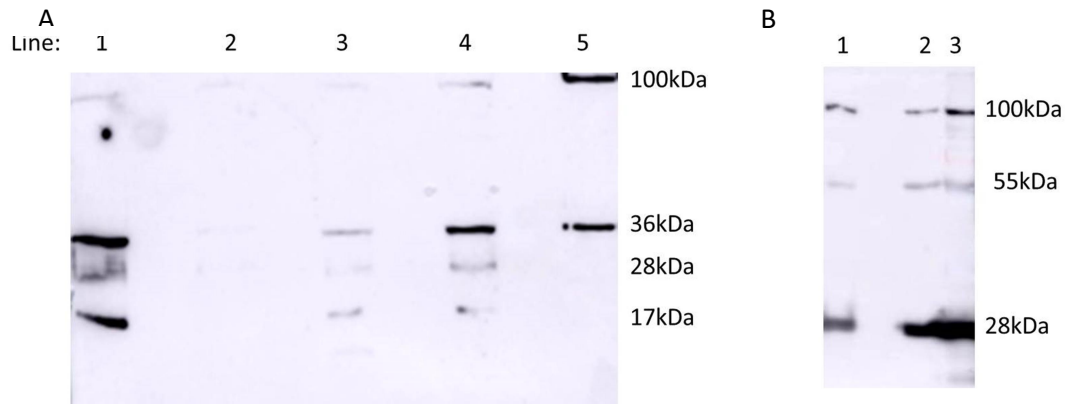

Figure 3.12. A) *Western blot analysis showing DISC1 bands detected with antibody anti-Strep after purification with Strep-Tactin resin. The bands detected from DISC1 elution are not intense because of low expression level and not optimized condition of purification. line1: positive control, line 2: DISC1 elution, line 3: flow through, line 4: soluble fraction, line 5: insoluble fraction.* ***B)*** *western blot analysis with antibody anti-Flag after purification with ANTI-FLAG Affinity resin Line 1: DISC1 elution, line 2: flow through, line 3: soluble fraction.*

3.4. Co-expression and co-purification

Working with recombinant baculoviruses containing both the hSR and the DISC1 gene, we performed purification test to determine full-length DISC1-hSR complex. To this end, we aim to purify DISC1 with *Strep-Tactin* resin to pull down DISC1 using C-terminal tag and then we re-loaded the flow through with Ni-NTA resin to bind hSR co-expressed with DISC1 in the same lysate. To demonstrate the direct interaction, we performed two Western Blot analyses with anti-His antibody to detect the presence of hSR in DISC1 elution (Fig. 3.13A) and with anti-Strep antibody to identify DISC1 in elution from Ni-NTA resin (Fig. 3.13B). The interpretation of the results is ambiguous since we did not succeed in the purification of full-length DISC1. Fig. 8 shows a clear band of 38 kDa correspond to hSR in DISC1 elution after incubation with Strep-Tactin resin, but absence of DISC1 when hSR is pulled down with Ni-NTA resin. This likely indicates weak interactions between the two proteins or a low expression of DISC1 compared to hSR.

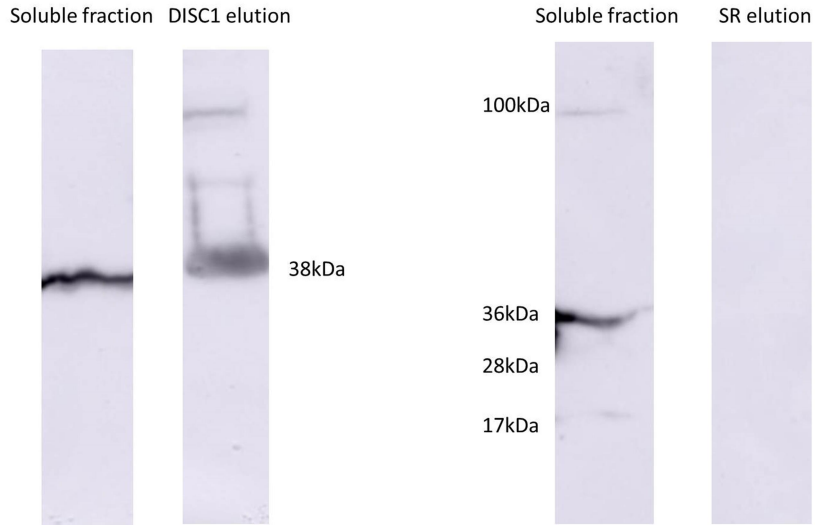

***Figure 3.13**. **A)** Western blot showing hSR band detected with anti-His antibody after elution from Strep-Tactin resin. **B)** Western blot showing DISC1 bands detected with anti-Strep antibody after incubation of the same lysate with Ni-NTA.*

Moreover, we performed a pull down assay (Fig. 3.15) with *ANTI-FLAG Affinity Gel* resin followed by western blot with antibody anti-His for three different constructs (hSR and DISC1 individually and two proteins together). For each construct, we loaded 20 µl of cleared lysate prepared with sonication and centrifugation of three different cell pellets. Removing all the background coming from the Flag resin, the lysate with co-expressed SR and DISC1 has a band corresponding to 38 KDa (molecular weight of hSR more intense compare to the other samples, and in the lysate containing just DISC1 was not even detect any band of that size. These results suggested a direct interaction between DISC1 and hSR (Fig. 3.14).

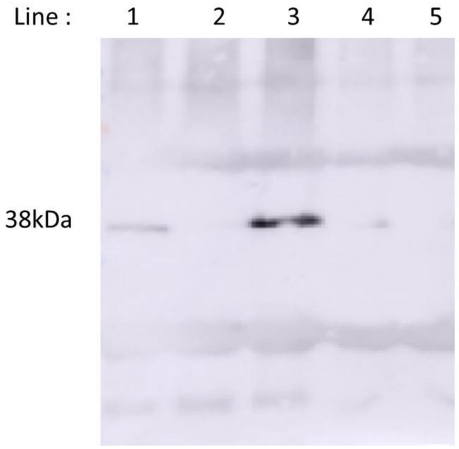

***Figure 3.14**. Pulldown assay with ANTI-FLAG Affinity Gel and following detection of His Tag at the N-terminal of serine racemase. Line 1: serine racemase expressed individually, line 2: DISC1 expressed individually, line 3: co-expression, line 4: crude extract of Sf21 insect cells, line 5: ANTI-FLAG Affinity Gel.*

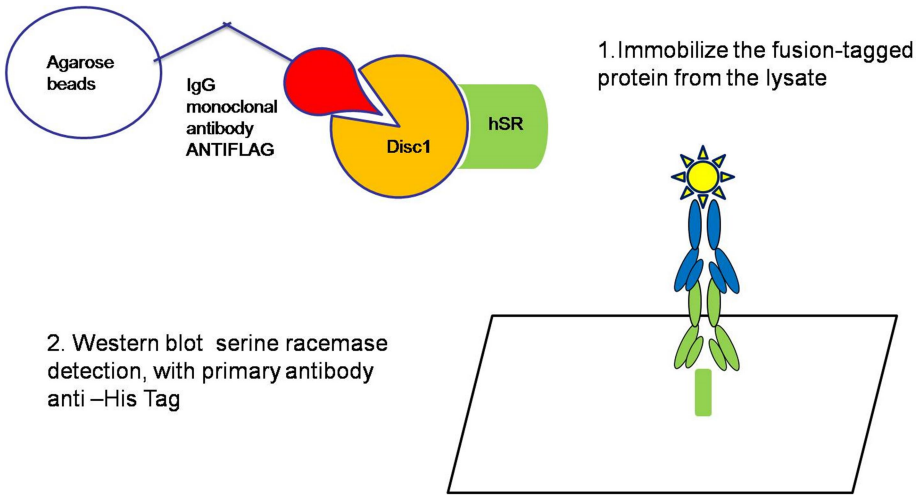

Figure 3.15. *Pull down assay of Flag fusion-tagged proteins.*

3.5. Interaction of DISC1 with hSR

DISC1 showed to be very insoluble and unstable, limiting the range of protein concentrations for enzymatic assays. For this reason, to evaluate the interaction of full-length DISC1 with hSR we adapted the hSR β-elimination assay, reported in [13], working with a 5-fold lower concentration of hSR. Equimolar concentrations of full-length DISC1 produced a 20% decrease of hSR activity (Figure 3.16). The reference activity was measured using the storage Buffer of DISC1 stripped of DISC1 itself, proving that DISC1 was the only responsible of the effect. These preliminary results are promising and require further investigations and larger amounts of DISC1.

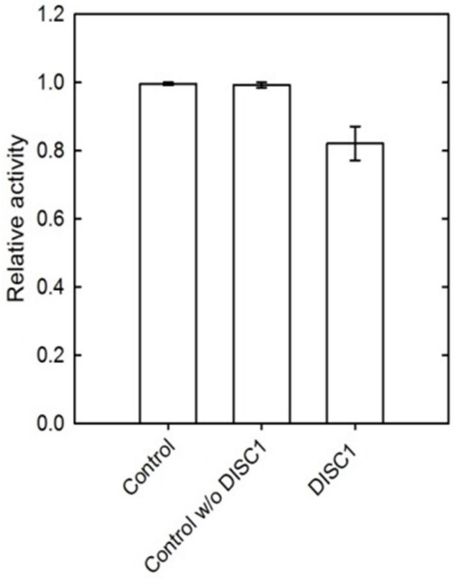

***Figure 3.16**. β-elimination activity of serine racemase measured in the presence of 128 nM DISC1. Two references, one was carried out with the solution 50 mM TEA, 2 mM ATP, 50 µM PLP, 5 mM DTT, 2 mM MgCl2, 150 mM NaCl, 30 U/ml LDH, 300 µM NADH, and 88nM hSR. The other was carried out in absence of DISC1, in the solution containing 50 mM Tri-HCl, 400 mM NaCl, 10 mM MgCl2, 10 % glycerol, which is the storage Buffer of DISC1 supplemented of 2 mM ATP, 133 µM L-serine, 30 U/LDH and 88 nM of hSR. The error bars are the standard error of two replicates.*

4. Conclusion

The genes of DISC1 and hSR were correctly inserted in different bacmids for the expression and the co-expression in insect cells. The early evaluation for DISC1 expression revealed the difficulty to obtain the pure and full-length protein, which limited our investigation and further characterization. However, around 0.2 mg of protein per 1 liter of culture at 30 % purity was finally obtained, using the Flag affinity tags. hSR was obtained at much higher yields (2 mg per 1 liter of culture) at 80 % purity. The preliminary inhibition studies of the β-elimination activity of hSR and pull down assays demonstrated the interaction between the two proteins, which will be further characterized.

ABBREVATIONS:

ATP, adenosine triphosphate; pPolh, polyhedrin promoter; hSR serine racemase; NAD+, nicotinamide adenine dinucleotide (oxidized form); NADH, nicotinamide adenine dinucleotide (reduced form);

REFERENCES

1. Osz-Papai, J., et al., *Insect Cells–Baculovirus System for the Production of Difficult to Express Proteins*, in *Insoluble Proteins: Methods and Protocols*, E. García-Fruitós, Editor. 2015, Springer New York: New York, NY. p. 181-205.
2. Smith, G.E., M.D. Summers, and M.J. Fraser, *Production of human beta interferon in insect cells infected with a baculovirus expression vector.* Mol Cell Biol, 1983. **3**(12): p. 2156-65.
3. Smith, G.E., M.J. Fraser, and M.D. Summers, *Molecular Engineering of the Autographa californica Nuclear Polyhedrosis Virus Genome: Deletion Mutations Within the Polyhedrin Gene.* J Virol, 1983. **46**(2): p. 584-93.
4. Emery, V.C., *Baculovirus expression vectors : choice of expression vector.* Methods Mol Biol, 1992. **8**: p. 287-307.
5. Kost, T.A. and C.W. Kemp, *Fundamentals of Baculovirus Expression and Applications.* Adv Exp Med Biol, 2016. **896**: p. 187-97.
6. Albala, J.S., et al., *From genes to proteins: high-throughput expression and purification of the human proteome.* J Cell Biochem, 2000. **80**(2): p. 187-91.
7. Wang, Y., N. Stojiljković, and J.A. Jehle, *Cloning of complete genomes of large dsDNA viruses by in vitro transposition of an F factor containing transposon.* Journal of Virological Methods, 2010. **167**(1): p. 95-99.
8. Luckow, V.A., et al., *Efficient generation of infectious recombinant baculoviruses by site-specific transposon-mediated insertion of foreign genes into a baculovirus genome propagated in Escherichia coli.* Journal of Virology, 1993. **67**(8): p. 4566-4579.
9. Zhao, Y., D.A.G. Chapman, and I.M. Jones, *Improving baculovirus recombination.* Nucleic Acids Research, 2003. **31**(2): p. e6.
10. Abdulrahman, W., et al., *The Production of Multiprotein Complexes in Insect Cells Using the Baculovirus Expression System*, in *Structural Proteomics: High-*

Throughput Methods, R.J. Owens, Editor. 2015, Springer New York: New York, NY. p. 91-114.

11. Kitts, P.A. and R.D. Possee, *A method for producing recombinant baculovirus expression vectors at high frequency.* Biotechniques, 1993. **14**(5): p. 810-7.
12. Li, M.Z. and S.J. Elledge, *Harnessing homologous recombination in vitro to generate recombinant DNA via SLIC.* Nat Meth, 2007. **4**(3): p. 251-256.
13. Marchetti, M., et al., *ATP binding to human serine racemase is cooperative and modulated by glycine.* FEBS Journal, 2013. **280**(22): p. 5853-5863.

14 Tankou, S., et al., *SUMOylation of DISC1: a potential role in neural progenitor proliferation in the developing cortex*. Mol Neuropsychiatry, 2016. **2**(1): p. 20-27.

15 Ishizuka, K., et al., *DISC1-dependent switch from progenitor proliferation to migration in the developing cortex*. Nature, 2011. **473**(7345): p. 92-6.

Chapter 4

Glyceraldehyde 3-phosphate dehydrogenase and NADH as effectors of human serine racemase

Abstract

It was recently suggested that the binding of GAPDH and/or NADH suppresses hSR activity, in a supposed regulation of D-serine synthesis through the glycolytic flux. In this work, we cloned, expressed and purified human GAPDH and we partially characterized its interaction with hSR. We show that the reported effect on the murine serine racemase-GAPDH interaction is not seen for the human homologs and we suggest that it is rather associated to a bias of the experiment. Indeed, the substrate of GAPDH, glyceraldehyde 3-phosphate, which was added to the mixture, is a week inhibitor of hSR, explaining the reported results. Moreover, we investigated in depth the inhibition of the GAPDH product NADH, showing that it produces a partial inhibition, albeit with an IC_{50} several fold higher than physiological intracellular concentrations. By dissecting the NADH molecule, we discovered that the inhibitory determinant is the N-substituted 1,4-dihydronicotinamide ring. Particularly, the NADH precursor 1,4-dihydronicotinamide mononucleotide exhibited a partial mixed-type inhibition, with a K_I of 18 ± 7 μM. Docking simulations suggested that all 1,4-dihydronicotinamide derivatives bind at the interdimeric interface, with the ring positioned in an unoccupied site next to the ATP binding site. This newly recognized allosteric site could be exploited for the design of high affinity hSR effectors to finely modulate D-serine homeostasis.

Part of this work was published in the Biochemical Journal (2016) [1].

Candidate's contribution: Marilena Margiotta carried out the cloning, expression and purification of the human GAPDH and part of the enzyme assays. Francesco Marchesani performed most of the human serine racemase activity assays and Luca Dellafiora performed the computational analysis.

1. Introduction

Recently, it was reported that glycolytic enzyme, GAPDH and its product, NADH, inhibit hSR, suggesting a physiological regulation of hSR activity by the glycolytic flux in neurons [2]. Here, we thoroughly investigated the inhibition of hSR by NADH and by some of its analogues, derivatives and metabolic precursors. Indeed, some of the NADH precursors formed in the kynurenine pathway are involved in the glutamatergic neurotransmission, including kynurenic acid (KYNA) [3], quinolinic acid (QUIN) [4], 3-hydroxykynurenine (3-HK) [5] and xanthurenic acid (XA) [6]. More recently, the NADH metabolic precursor nicotinamide mononucleotide (NMN) was shown to accumulate after nerve injury - reaching intracellular concentrations in the micromolar range - and to promote axon degeneration [7].

Neurons need energy to maintain a continuous neurotransmission and the astrocytes represent the key to support neurons. Specifically, astrocytes balance the glycolytic flux by glutamate synaptic level. The glutamate is linked to molecular signal that switches on glucose utilization pathways to accomplish the energy requirement. On the other hand, inhibition of glutamate uptake prevents the stimulation of the glycolytic pathway. At the glutamatergic synapsis NMDA receptors are activated by glutamate and by a second co-agonist, D-serine. D-serine production is as well regulated in astrocytes and neurons through specific mechanism still not well defined.

Pull-down assay of mouse brain lysate using recombinant hSR with GST and co-immunoprecipitation identified endogenous interaction of hSR with GAPDH. GAPDH

inhibits D-serine production through direct binding as shown that Lys84 mutant GAPDH, with reduced interaction, restores partly hSR activity. Moreover, mutants of GAPDH with decreased activity still interact with hSR but lead to a lower rate of inhibition, suggesting that the metabolites of GAPDH enzymatic reaction. NADH also contributes to the inhibition of hSR activity.

GAPDH needs G3P substrate to stabilize the interaction suggesting the need of a conformational change to bind hSR. hSR, as well, require Mg^{2+} -ATP complex to stabilize the protein folding and to increase the interaction in a dose-dependent manner.

2. Materials and Methods

2.1. Materials

Chemicals were of the best commercial quality available and were purchased from Sigma-Aldrich (St. Louis, MO, USA), with the exception of tris (2-carboxyethyl) phosphine (TCEP), from Apollo Scientific (Bredbury, UK), $NADP^+$ and NADPH, from Boehringer Ingelheim and 1-methyl-1,4-dihydronicotinamide (MNA-red) from Toronto Research Chemicals (Toronto, Canada). Recombinant D-amino acid oxidase (DAAO) from *Rhodotorula gracilis* was a generous gift from Professor L. Pollegioni, University of Insubria, Varese, Italy. Porcine DAAO was acquired from Sigma Aldrich.

2.2. Enzyme preparation

Recombinant hSR was expressed as a His-tagged fusion protein encoded in a pET28a-derived plasmid [8] transformed into *E. coli* BL21 CodonPlus (DE3)-RIL cells (Merck-Millipore, Darmstadt, Germany). Purification was carried out using a TALON® His-Tag Purification Resin (Clontech, CA, USA), as previously described [9].

The synthetic human GAPDH gene (NCBI protein accession NP_001276675.1) (Fig. 4.1) was codon optimized for the expression in E.coli (GeneArt Life Technology) and cloned in pET28b(+) expression vector with Histidine Tag at N-terminus followed by a thrombin cleavage site. The recombinant pET28b(+)-derived plasmid was transformed into E.coli BL21 CodonPlus (DE3)-RIL cells (Merck-Millipore, Darmstadt, Germany). Cells were grown in Luria-Bertani (LB) medium at 37°C and protein expression was induced 1 mM isopropyl β-D-1-thiogalactopyranoside (IPTG). After 4 hours from induction, the cells were harvested and washed through centrifugation and resuspension cycles. The paste was finally resuspended in a lysis buffer containing 20 mM tris (hydroxymethyl) aminomethane (TRIS), 0.5 M NaCl, 20 mM imidazole at pH 8.0 and cells were disrupted by sonication. The soluble fraction was recovered by ultracentrifugation (Sorvall OTD-65B)

and loaded onto a Ni Sepharose Fast Flow column (Amersham). The protein was eluted with a linear gradient using a solution containing 20 mM TRIS, 0.5 M NaCl, 0.5 M imidazole at pH 7.4. The recovered protein was dialyzed against a solution containing 10 mM triethylamine (TEA), 1 mM EDTA, 10 mM potassium phosphate, at pH 7.6, concentrated to a final concentration of 200 µM as assessed by the Bradford method and incubated with thrombin (2 Units/ml) for 24 hours at 37°C, followed by gel filtration. The hGAPDH solution was flash-frozen in small aliquots and stored at -80°C. Protein purity was assessed by densitometry of Coomassie-blue-stained bands of an SDS-PAGE gel using a Chemidoc gel imaging system (Biorad, CA, USA).

2.3. Preparation of 1-methyl-1,4-dihydronicotinamide and 1,4-dihydronicotinamide mononucleotide

1,4-dihydronicotinamide mononucleotide (NMN-red) was prepared from β-nicotinamide mononucleotide (NMN-ox, Sigma-Aldrich) by stoichiometric reduction with sodium dithionite under anaerobic conditions [10], followed by desalting in an acetone\water mixture, drying in SpeedVac™ (Thermo Scientific™) and resuspension in a 50% DMSO\water solution. Reduction was confirmed by ^{1}H NMR spectra recorded on a Bruker 400 MHz spectrometer in 20 mM Na_2HPO_4 buffer, pH 8.0 (10% D_2O), by the presence of a peak at 7.07 ppm, typical of the reduced NADH nicotinamide ring. The concentration of the reduced species was determined spectrophotometrically based on the reported extinction coefficients [10].

2.4. Racemization activity assay

The initial rate of conversion of L-serine into D-serine by hSR was determined via a discontinuous assay based on the oxidation of D-serine by DAAO, as already described. [9, 11, 12]. The assay mixture contained 50 mM TEA, 150 mM NaCl, 50 µM PLP, 50 mM L-serine and 1.5 µM hSR, unless otherwise stated. L-serine was preliminarily purified by incubation with DAAO for several hours to eliminate contaminant traces of D-serine [9].

The reaction was triggered by the addition of hSR and the mixture was periodically sampled to estimate the concentration of D-serine, as previously described [9]. Briefly, D-serine reacts with DAAO to give hydrogen peroxide, which then reacts with *o*-dianisidine in the presence of horseradish peroxidase (HRP), the chromophoric product was treated then with sulfuric acid to increase solubility. The absorbance of the chromophoric product was measured using a HALO LED 96 microplate reader (Dynamica) set at 550 nm.

2.5. β-elimination activity assay

As already described the velocity of L-serine β-elimination by hSR was monitored through a coupled assay with LDH [9, 13]. The LDH-coupled assay was carried out in the same solution of previous experiments, containing 50 mM TEA, 2 mM ATP, 50 µM PLP, 5 mM DTT, 2 mM $MgCl_2$, 150 mM NaCl, 30 U/ml LDH, 300 µM NADH, pH 8.0, at 37°C. L-serine was added at different concentrations depending on the experiment. The reaction was triggered by addition of 0.45 µM hSR and NADH consumption was followed at 340 nm using a Varian 4000 spectrophotometer. In some experiments, the concentrations of either NADH or ATP were modified, as specified. As NADH affects hSR activity, its concentration was assessed spectrophotometrically at the exact time when the velocity was measured. It was therefore possible to assess reaction rates at NADH concentrations lower than those initially added for the assay.

The same kinetic experiments were also performed in the presence of a 10-fold excess (4 µM) of recombinant human GAPDH and in the presence of G3P at 1 mM, 2 mM, 4 mM, 10 mM concentration. The β-elimination assay was performed as described before, with a fixed concentration of 50 mM L-serine, pH 8, at 37 °C.

2.6. β-elimination activity in presence and absence of GAPDH and G3P

β-elimination activity was measured with a discontinuous assay based on the conversion of pyruvate to lactate by LDH, in the presence and absence of GAPDH and

G3P. The discontinuous assay was necessary to dissect the effect of GAPDH, NADH and G3P on hSR and GAPDH.

The reactions were carried out in a solution with 2 mM ATP, 5 mM $MgCl_2$, and 0.148 µM hSR. 1.5 µM GAPDH and 10 mM G3P were added either individually or together. The reaction was triggered by the addition of 50 mM L-serine at 37 °C. Aliquots were taken at different time (0 min, 3 min, 5 min and 10 min) and incubated at 100 °C to stop the reaction by enzyme denaturation. To calculate the concentration of pyruvate produced by hSR, 4 U of LDH and 1 mM NADH in each aliquot were added to trigger the conversion of pyruvate to lactate and the oxidation of NADH to NAD^+. After 1 hour of incubation at 37 °C, the concentration of NADH was measured at 340 nm using a microplate reader (HALO LED 96). The values were expressed in relative activity of hSR.

2.7. Inhibition assays

The inhibition of either the hSR β-elimination or racemization activities by different compounds was initially evaluated at 2 mM concentration. For the active compounds, the IC_{50} was determined through β-elimination assays at several inhibitor concentrations. The potential effect of each compound on the activity of the coupled enzymes LDH, DAAO and HPR was preliminary evaluated in the presence of their substrates, i.e. pyruvate, D-serine and hydrogen peroxide, respectively.

The dependence of the initial rate on inhibitor concentration at different L-Ser concentrations was fitted to the equation describing a hyperbolic mixed-type inhibition (Equation 1) [14].

$$v = \frac{V_{max}\frac{[S]}{K_M} + \beta V_{max}\frac{[S][I]}{\alpha K_M K_I}}{1 + \frac{[S]}{K_M} + \frac{[I]}{K_I} + \frac{[S][I]}{\alpha K_M K_I}} \qquad \text{Equation 1}$$

where [*S*] and [*I*] are the concentrations of L-Ser and inhibitor in the assay, respectively, K_M is the Michaelis-Menten constant, α is a coefficient that indicates the difference in affinity of the inhibitor for the free enzyme and the ES complex, K_I is the inhibition constant and β is a coefficient that describes the degree of inhibition (also called efficacy).

3. Results and discussion

3.1. Protein expression and purification

A typical preparation of hGAPDH yielded 8 mg of protein per liter of culture at >99% purity, as assessed by SDS-PAGE and densitometric analysis. Incubation with thrombin resulted in the complete removal of the His-tag, with minimal loss of soluble protein (Fig. 4.2).

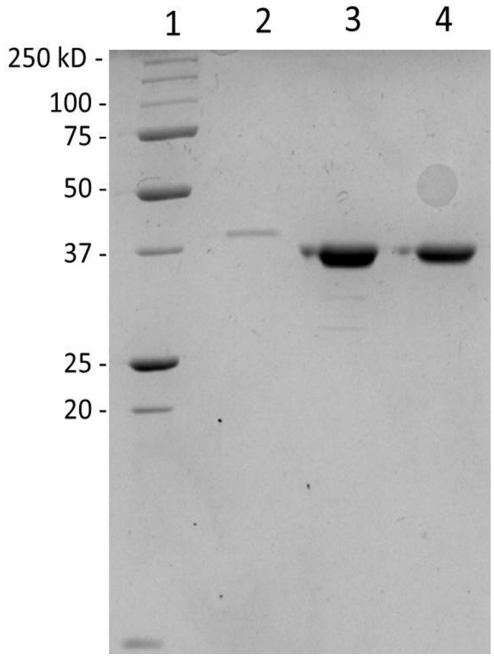

Figure 4.2. *SDS gel of hGAPDH purification. Lane 1: Biorad Precision Plus Protein Standards 2. Purified hGAPDH prior to thrombin cleavage 3. Purified and concentrated GAPDH after thrombin digestion 4. Purified hGAPDH after purification with G100 gel filtration chromatography.*

3.2. Inhibition of hSR by reduced NADH and NADPH

The effect of NADH, NAD^+, NADPH and $NADP^+$ was tested on the racemization and β-elimination activities of hSR in the presence of 50 mM L-serine, 2 mM ATP, 2 mM $MgCl_2$ and 2 mM of each dinucleotide (Fig. 4.5).

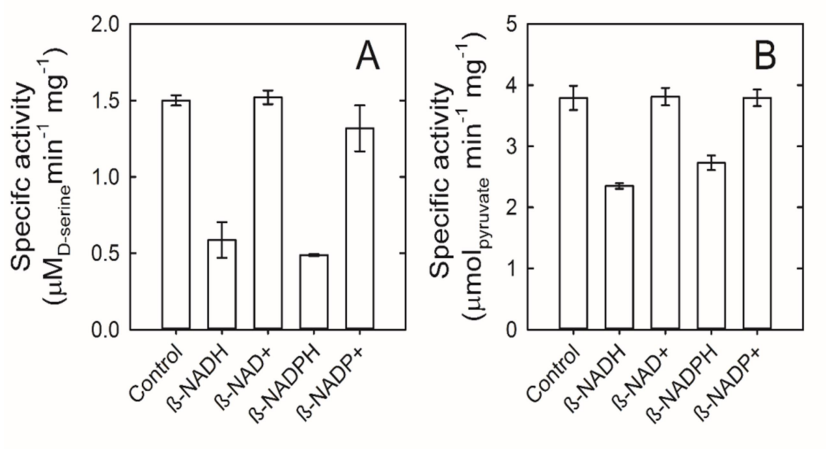

Figure 4.5. *A, Effect of NADH, NAD^+, NADPH and $NADP^+$ on L-serine racemization. The control experiment was carried out by incubating 1.5 μM hSR in a 50 mM TEA-buffered solution containing 50 mM L-serine, 2 mM ATP-Mg at pH 8.0. NAD^+, NADH, $NADP^+$ and NADPH were added at 2 mM concentration. The error bars are the standard error of two replicates. B, Effect of NADH, NAD^+, NADPH and $NADP^+$ on the L-serine β-elimination reaction. The reference experiment was carried out by incubating 0.45 μM hSR in a TEA-buffered solution containing 50 mM L-serine, 2 mM ATP, 2 mM $MgCl_2$. NAD^+, NADH, $NADP^+$ and NADPH were added at 2 mM concentration. The error bars are the standard error of two replicates.*

NADH and NADPH reduce the racemization activity by about 50% and the β-elimination activity by about 36%. The difference is ascribed to the difficulty to extrapolate the maximum velocity from the β-elimination assays, where NADH is present (vide infra). The inhibition did not depend on the incubation time of hSR with NADH, nor by the presence of reducing agents, such as TCEP or dithiothreitol (data not shown).

Interestingly, the oxidized forms NAD^+ and $NADP^+$ did not lead to any significant changes in hSR activity. All compounds produced partial inhibition, with different residual activities at saturating concentrations. The resulting IC_{50}s were 246±63 μM for NADH, 177±63 μM for MNA-red and 51±15 for NMN-red. The maximum inhibition was 36% for NADH, 25% for MNA-red and 47% for NMN-red.

3.3. ATP competition for the same site

The partial structural similarity of NADH and ATP suggest a competition for the same site, although the opposite effect [15]. However, a 10-fold excess of ATP did not remove NADH inhibition in the β-elimination assays to any extent (Fig. 4.6). NAD+ not only did not produce any inhibition (Fig. 4.5), but it also did not compete with NADH, as a 5-fold excess did not restore the original activity. Overall, these results suggest that NADH binds to an allosteric site at least partially distinct from the ATP binding site**.**

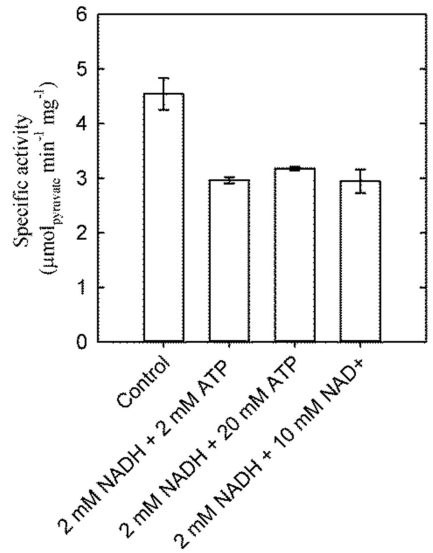

Figure 4.6. *Effect of ATP and NAD+ on NADH inhibition. In the presence of 2 mM NADH, a 30% decrease in activity is observed in comparison with the control (0.3 mM NADH, 2 mM ATP, 2 mM MgCl2). Addition of 20 mM ATP did not restore full activity, ruling out competition for the same site. Addition of NAD+ in a 5-fold excess with respect to NADH did not affect the inhibition. All assays were carried out in the presence of 50 mM L-serine, 2 mM MgCl2, at 37°C. Each error bar is the s.e.m. of two replicates.*

3.4. Identification of the inhibitory determinant of NADH

The NADH\NAD$^+$ fragments 1-methyl-1,4-dihydronicotinamide (MNA-red), 1,4-dihydronicotinamide mononucleotide (NMN-red), their oxidized forms 1-methylnicotinamide (MNA-ox) and β-nicotinamide monucleotide (NMN-ox), the fully reduced form of MNA-ox - 1-methyl 3-piperidinecarboxamide (MPCA) (Fig. 4.7), ADP and sodium pyrophosphate were screened at 2 mM concentration using the β-elimination assay to identify the inhibitory determinant of NADH. ADP did not bring about any inhibition, as it had emerged already by investigating its possible binding to the ATP binding site [16]. Pyrophosphate ions at 2 mM concentration produced an inhibition of around 60%, which has been already associated to Mg^{2+} chelation [17]. NMN-red and MNA-red inhibited hSR by 46% and 25%, respectively (Fig. 4.8).

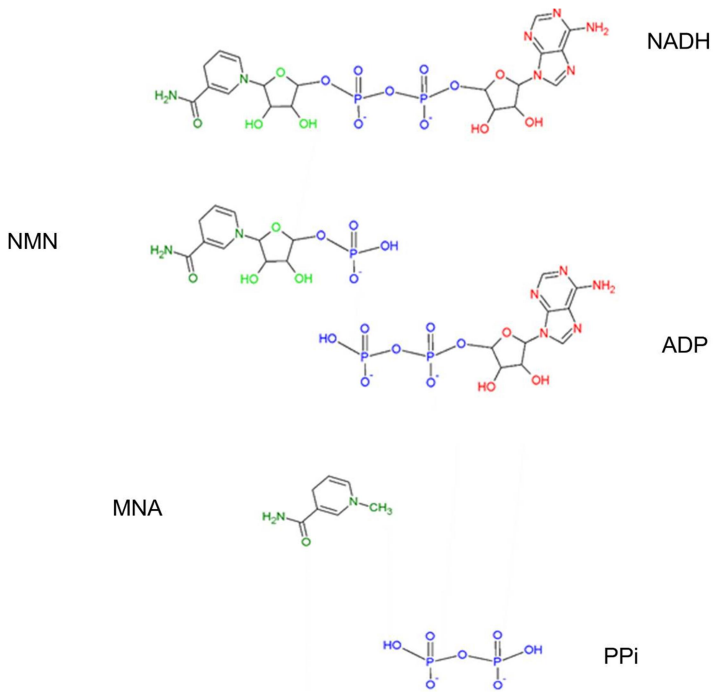

Figure 4.7*. NADH analogues and precursors tested as inhibitors of serine racemase in this study.*

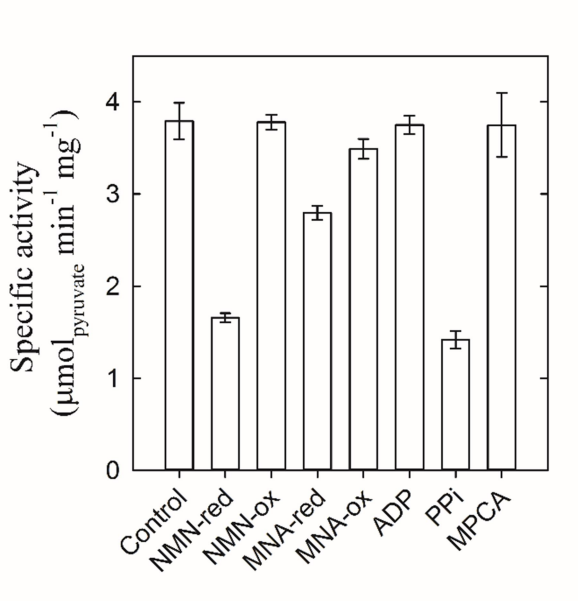

Figure 4.8. *Effect of MNA-red, MNA-ox, NMNred, NMN-ox, ADP, pyrophosphate and MPCA at 2 mM concentration on the β-elimination reaction of hSR in the presence 2 mM ATP and 50 mM L-serine. Each error bar is the s.e.m. of two replicates.*

Overall, it can be concluded that the inhibition determinant of NADH is the N-substituted 1,4-dihydronicotinic ring. The redox state of the 1,4-dihydronicotinic ring is crucial, as neither the oxidized forms (NAD^+, $NADP^+$, NMN-ox, MNA-ox) nor the fully reduced piperidinic form (MPCA) showed any inhibitory activity. The redox forms of the nicotinamidic ring differ both in net charge at neutral pH and conformation, offering indications on the binding properties of the pocket.

3.5. Dependence of β-elimination activity on GAPDH and G3P

The β-elimination activity coupled with LDH reactions in discontinuous assay showed the effect of GAPDH and G3P on hSR activity. The glycolytic enzyme did not

influence serine racemase, indicating limited possibility of their interactions. Instead, in the presence of 2 mM G3P hSR reduced its activity of about 10% (fig. 4.9A). The increase in the concentration of G3P up to 10 mM caused a lowering of 80 % of relative activity (Fig. 4.9B). The inhibitory effect was related to the presence of G3P not to GAPDH, as was previously thought, since in the absence of the glycolytic enzyme it was still possible to detect the inhibition. The dependence of β-elimination activity on G3P is reported in Figure 4.10.

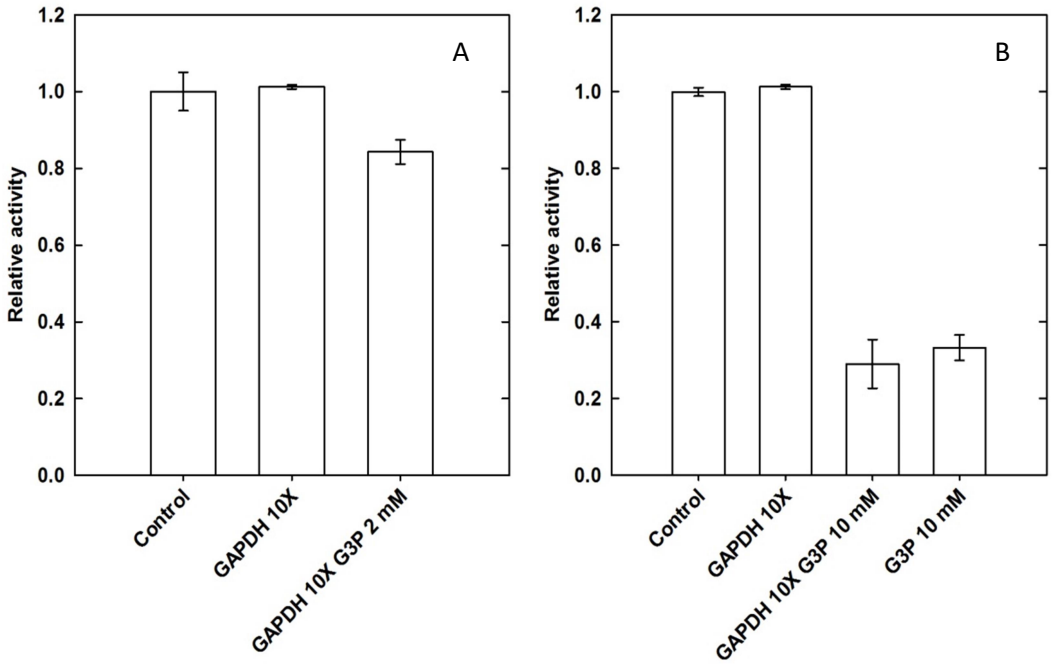

Figure 4.9. *Effect of GAPDH and G3P on β-elimination activity. The control was carried out in a solution containing 2 mM ATP, 5 mM $MgCl_2$, 0.148 µM of hSR, and 10 µl of storage buffer of GAPDH. GAPDH was added in a concentration 10-fold in excess compared to hSR (1.5 µM)* ***A)*** *G3P was added at 2 mM concentration with GAPDH.* ***B)*** *10 mM G3P was tested with and without GAPDH. The error bars are the standard error of two replicates.*

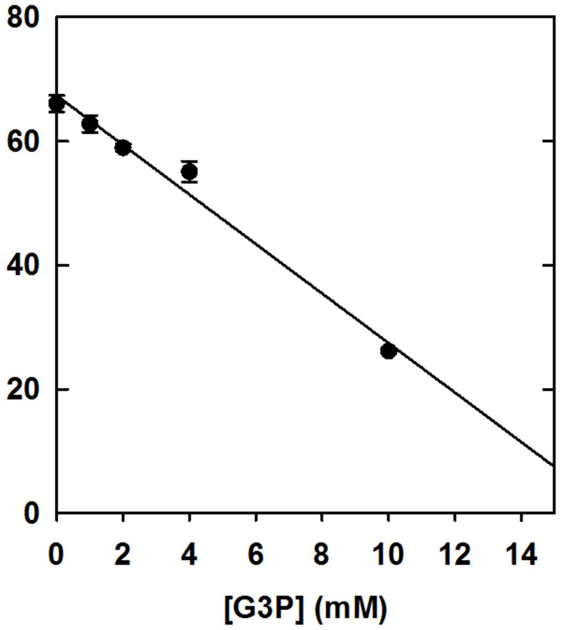

***Figure 4.4**. Dependence of β-elimination activity on the concentration of G3P. The reference experiment was carried out in the absence of G3P.*

4. Conclusion

The intracellular concentration of free NAD species in the cytosol of mammalian cells is estimated to be around 300 μM. The NAD^+/NADH ratio heavily favours the oxidized form, that is 700 fold more concentrated than the reduced form [18]. Considering the partial inhibition and the relatively high IC_{50}, it appears unlikely that NADH could have a role in hSR modulation under physiological conditions. However, it cannot be ruled out that an altered redox state of the cell might increase the concentration of NADH to a value sufficient to exert some degree of hSR inhibition. NADPH is the prevailing form in the redox equilibrium with $NADP^+$, but its cytosolic concentrations are much lower than those of NADH.

The site for the 1,4-nicotinamidic ring is a novel allosteric site that might be exploited for the fine tuning of hSR activity. Up to now, only weak inhibitors directed to the active site have been identified, particularly malonate and its derivatives. A key limitation of these inhibitors is that they are not particularly suitable for modifications, as the hSR active site is very small. The binding pocket for the 1,4-nicotinamidic ring might offer a better option for the development of higher affinity, more specific inhibitors.

The direct interaction of hSR with GAPDH and the relation between glycolytic activity and production of D-serine, previously showed by Suzuki et al. [19] was not confirmed by the β-elimination assays for hSR. Indeed, we suggest that their experiment was biased by the presence of G3P, which showed to be a week inhibitor of hSR at millimolar concentration.

ABBREVATIONS:

ADP, adenosine diphosphate; ATP, adenosine triphosphate; DAAO, D-amino acid oxidase; G3P, glyceraldehyde 3-phosphate; GAPDH, Glyceraldehyde 3-phosphate dehydrogenase; hSR, human serine racemase; KYNA, kynurenic acid; MNA-ox, 1-methylnicotinamide; MNA-red, 1-methyl-1,4-dihydronicotinamide; MPCA, 1-methyl 3-piperidinecarboxamide;

NA, nicotinic acid; NAD+, nicotinamide adenine dinucleotide (oxidized form); NADH, nicotinamide adenine dinucleotide (reduced form); Nam, nicotinamide; NMDARs, N-methyl D-aspartate receptors; NMN-ox, β-nicotinamide monucleotide; NMN-red, 1,4-dihydronicotinamide mononucleotide; (2,3-pyridinedicarboxylic acid); QUIN, quinolinic acid; TCEP, tris(2-carboxyethyl)phosphine; TRP, tryptophan; XA, xanthurenic acid;

REFERENCES

1. Bruno, S., et al., *Human serine racemase is allosterically modulated by NADH and reduced nicotinamide derivatives.* Biochem J, 2016. **473**(20): p. 3505-3516.
2. Suzuki, M., et al., *Glycolytic flux controls D-serine synthesis through glyceraldehyde-3-phosphate dehydrogenase in astrocytes.* Proceedings of the National Academy of Sciences of the United States of America, 2015. **112**(17): p. E2217-24.
3. Schwarcz, R., et al., *Kynurenines in the mammalian brain: when physiology meets pathology.* Nature Reviews Neuroscience, 2012. **13**(7): p. 465-77.
4. Lugo-Huitron, R., et al., *Quinolinic acid: an endogenous neurotoxin with multiple targets.* Oxid Med Cell Longev, 2013. **2013**: p. 104024.
5. Stone, T.W. and L.G. Darlington, *Endogenous kynurenines as targets for drug discovery and development.* Nature Reviews. Drug Discovery, 2002. **1**(8): p. 609-20.
6. Copeland, C.S., S.A. Neale, and T.E. Salt, *Actions of Xanthurenic acid, a putative endogenous Group II metabotropic glutamate receptor agonist, on sensory transmission in the thalamus.* Neuropharmacology, 2013. **66**: p. 133-42.
7. Di Stefano, M., et al., *A rise in NAD precursor nicotinamide mononucleotide (NMN) after injury promotes axon degeneration.* Cell Death Differ, 2015. **22**(5): p. 731-742.
8. Dixon, S.M., et al., *Slow-binding human serine racemase inhibitors from high-throughput screening of combinatorial libraries.* J Med Chem, 2006. **49**(8): p. 2388-97.
9. Marchetti, M., et al., *ATP binding to human serine racemase is cooperative and modulated by glycine.* FEBS Journal, 2013. **280**(22): p. 5853-63.
10. Blankenhorn, G. and E.G. Moore, *Sulfoxylate ion (HSO2-), the hydride donor in dithionite-dependent reduction of NAD+ analogs.* Journal of the American Chemical Society, 1980. **102**(3): p. 1092-1098.

11. Sacchi, S., et al., *Structure-function relationships in human D-amino acid oxidase.* Amino Acids, 2012. **43**(5): p. 1833-50.
12. Molla, G., et al., *Enzymatic detection of D-amino acids.* Methods in Molecular Biology, 2012. **794**: p. 273-89.
13. Foltyn, V.N., et al., *Serine racemase modulates intracellular D-serine levels through an alpha,beta-elimination activity.* Journal of Biological Chemistry, 2005. **280**(3): p. 1754-63.
14. Segel, H.I., *Enzyme Kinetics: Behavior and Analysis of Rapid Equilibrium and Steady-State Enzyme Systems* J. Chem. Educ., 1976, 53 (11), p A472.
15. Marchetti, M., et al., *ATP binding to human serine racemase is cooperative and modulated by glycine.* FEBS Journal, 2013. **280**(22): p. 5853-5863.
16. De Miranda, J., et al., *Cofactors of serine racemase that physiologically stimulate the synthesis of the N-methyl-D-aspartate (NMDA) receptor coagonist D-serine.* Proc Natl Acad Sci U S A, 2002. **99**(22): p. 14542-7.
17. Marchetti, M., et al., *Regulation of human serine racemase activity and dynamics by halides, ATP and malonate.* Amino Acids, 2015. **47**(1): p. 163-73.
18. Ying, W., *NAD+/NADH and NADP+/NADPH in cellular functions and cell death: regulation and biological consequences.* Antioxidants & Redox Signaling, 2008. **10**(2): p. 179-206.
19. Suzuki, M., et al., *Glycolytic flux controls D-serine synthesis through glyceraldehyde-3-phosphate dehydrogenase in astrocytes.* Proc Natl Acad Sci U S A, 2015. **112**(17): p. 13.

Chapter 5

Glyceraldehyde 3-phosphate dehydrogenase as target of irreversible inhibitors

Abstract

Glyceraldehyde-3-phosphate dehydrogenase (GAPDH) has recently gained attention as an anti-protozoan and an anti-cancer drug target. Protozoal GAPDHs are considered potential targets for antiparasitic drugs because, in the amastigote-phase, several pathogenic protozoa rely only on glycolysis for energy production. On the other hand, human GAPDH is a potential anti-cancer drug target because cancer cells exhibit an accelerated metabolism, particularly shifted toward glycolysis (Warburg effect). Irreversible inhibitors would be particularly suited for GAPDH inhibition, as its catalytic mechanism is based on an acidic cysteine side chain that tends to react with nucleophilic compounds. However, irreversible inhibitors are usually poorly selective. In this work, we investigated the selectivity of two groups of compounds: 2-phenoxy-1,4-naphthoquinone and its derivatives and 3-bromo isoxazolines. We showed that 2-phenoxy-1,4-naphthoquinone exhibit a kinetic preference for the *Plasmodium falciparum* homologue in comparison to others and that 3-Bromo isoxazolines – which fully inactivate the *P. falciparum* form - are only partial inhibitors of the human homolog. These studies open the possibility of designing irreversible, selective inhibitors of GAPDHs.

The work on 3-bromo isoxazolines has been published in the journal "Bioorganic and Medicinal Chemistry" [1]. The work on 2-phenoxy-1,4-naphthoquinone has been accepted for publication in the journal "Chemical Biology & Drug Design".

Candidate's contribution: Marilena Margiotta carried out the cloning, expression and purification of the human GAPDH, and performed the GAPDH activity assays and inhibition assays. The 3-bromo isoxazoline compounds were prepared and characterized by the group of Professors De Micheli and Conti of the University of Milan; 2-Phenoxy-1,4-naphthoquinone and its derivatives were prepared and characterized by the group of Professor Bolognesi of the University of Bologna.

1. Introduction

The reactivity of the catalytic cysteine of GAPDH toward G3P has been ascribed to a lower pK_a (pK_a = 6.0) [2] in comparison to free thiols, such as glutathione (pK_a = 8.6), [3] and unreactive solvent-exposed cysteine residues (pK_a = 8.4) [2, 4]. The low pK_a reflects the involvement of the catalytic cysteine in a cysteine-histidine catalytic dyad, which provides a pK_a-lowering microenvironment at the active site that stabilizes the thiolate species [2, 5]. Consistently with its distinctive pK_a, the catalytic cysteine of GAPDHs was shown to react with several, chemically diverse electrophiles, such as iodoacetic acid, [6] acrylonitrile, [7] N-acetyl-p-benzoquinone imine, [8] vinyl sulfones, [9] 9,10-phenanthrenequinone, [10] and 3-bromo-isoxazolines [1, 11].

1.1 2-phenoxy-naphthoquinone

Promising hit compounds based on the 2-phenoxy-1,4-naphthoquinone scaffold were recently proposed as drugs for the treatment of trypanosomiasis [12] and tumors [13]. Compound **1** (Fig. 5.1), was identified as a potent inhibitor of *Trypanosoma brucei* (*Tb*) growth [12] and was shown to act as *Tb*GAPDH inhibitor by means of chemical proteomic approaches. [14] A focused chemical library around compound **1** [13] was synthesized and the resulting 2-aryloxy-derivatives showed to be inhibitors of both *Tb*GAPDH [13, 15] and *h*GAPDH, [13]. In this project, we investigated the covalent inhibition mechanism of GAPDH inhibition by 2-phenoxy-naphthoquinones using four GAPDH orthologs (hGAPDH, TbGAPDH, PfGAPDH, *Arabidopsis thaliana* GAPDH, AtGAPDH).

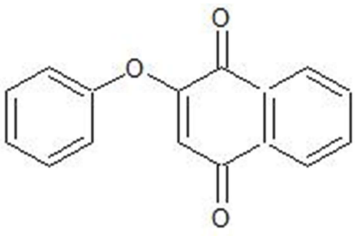

Figure 5.1 *structure of 2-phenoxy-1,4-naphtoquinone*

1.2 3-bromo isoxazoline derivatives

A new scaffold of covalent inhibitors based on the 3-Br-isoxazoline group that are active towards *Pf*GAPDH was recently identified [16-18]. Through mass spectrometry experiments on the tryptic digests of the reacted protein, it was shown that these inhibitors selectively alkylate the catalytic cysteines and that the substituents on the isoxazoline ring significantly affect their potency, mainly due to electrostatic effects. An unusual biphasicity in the inhibition time course hinted at an asymmetrical reactivity of the four active sites or at a slow conformational rearrangement upon partial alkylation [16]. In this project, we explored the reactivity of the 3-bromo-isoxazoline warhead towards hGAPDH.

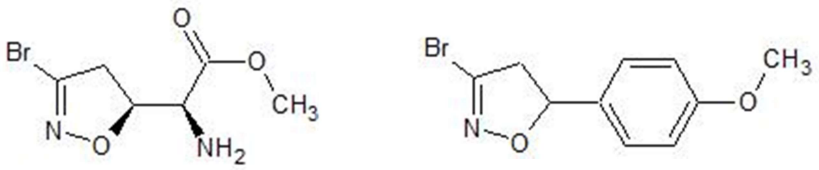

2A **2B**

Figure 5.2. *Structures of 3-Br-isoxazoline GAPDH inhibitors.*

2. Material and Methods

2.1 Materials

Chemicals were of the best commercial quality available and were purchased from Sigma-Aldrich (St. Louis, MO, USA). DL-glyceraldehyde-3-phosphate was prepared by hydrolysis of DL-glyceraldehyde-3-phosphate diethyl acetal barium salt. Stocks at 34 mM concentration were frozen in small aliquots at -80°C.

2.2 Chemical synthesis

Compound **1** (Fig. 5.1) was prepared by the group of Professor Bolognesi at the Department of Pharmacy and Biotechnology, University of Bologna. The synthesis of (S)-methyl 2-amino-2-((S)-3-bromo-4,5-dihydroisoxazol-5-yl) acetate (compound **2A,** Fig. 5.2) and of 3-bromo-5-(4-methoxyphenyl)-4,5-dihydroisoxazole (compound **2B**, Fig. 5.2) was carried out by the group of Professors De Micheli and Conti at the Department of Pharmaceutical Sciences, University of Milan.

2.3 Proteins expression and purification

The synthetic gene (GeneArt, Life Technology) encoding *Plasmodium falciparum* glyceraldehyde 3-phosphate dehydrogenase (PfGAPDH; GenBank accession number XM_001348736) codon-optimized for the expression in *E. coli* was cloned into a pMAT-derived cloning vector and then subcloned into a pET28b(+) expression vector (Novagen) using the BamHI and a SalI restriction sites. The recombinant protein contains hexa-histidine tag for protein purification followed by a thrombin cleavage site at the N-terminus. The recombinant pET28b(+)-derived plasmid was transformed into E.coli BL21 CodonPlus (DE3)-RIL cells (Merck-Millipore, Darmstadt, Germany) by electroporation. The purification is similar to human GAPDH previously described. Recombinant GAPC1 from *Arabidopsis thaliana* (*At*GAPDH) was expressed and purified as previously reported by

Bedhomme et al. [19] Recombinant *Trypanosoma brucei* GAPDH (*Tb*GAPDH) was expressed and purified as described by Pieretti et al. [14]. The molecular mass and purity of all proteins was determined by SDS-PAGE and the concentrations determined both spectrophotometrically and with the Bradford assay. [20] The specific activities measured with our standard assay (vide infra) were 15.2 U/mg, 17 U/mg, 10.6 U/mg, 23 U/mg for *h*GAPDH, *Pf*GAPDH, *Tb*GAPDH and *At*GAPDH, respectively.

2.4 Enzyme assays

GAPDH activity was evaluated using a modified version of the Ferdinand assay [21] in a buffered solution containing 10 mM TEA, 10 mM sodium arseniate, 5 mM EDTA, 1.5 mM NAD^+ and 2.2 mM DL-glyceraldehyde 3-phosphate, pH7.6. GAPDH was added at a final concentration of 30-50 nM and NADH formation was monitored at 340 nm using a Cary4000 spectrophotometer (Agilent Technologies) with the cell holder thermostated at 25°C. Arseniate was used instead of the physiological co-substrate phosphate because its product, 1-arseno 3-phosphoglycerate, unlike 1,3-bisphosphoglycerate, undergoes spontaneous hydrolysis, thus shifting the reaction towards NADH formation. The rate constant was determined by a linear fitting of the dependence of the absorption variation on time within 10% of the expected total change. The dependence of activity on G3P concentration was measured at a fixed concentration of NAD^+ (1.5 mM).

2.5 Inhibition assays

A solution containing 2 µM GAPDH, 10 mM TEA, 5 mM EDTA, 10 mM sodium arseniate, pH 7.6, was incubated at 25°C in the presence of inhibitors (compounds **1**, **2A**, **2B**) at various concentrations. Aliquots of the reaction mixtures were periodically sampled and the residual enzyme activity measured. The activity of aliquots of GAPDH maintained in the same conditions but in the absence of inhibitors was assayed in the same timeframe as control. The inactivation time courses were analysed as biexponential decays for PfGAPDH and as single exponential decays plus and offset for hGAPDH. The

observed inactivation rates of the fast and slow phases (for PfGAPDH) and that for hGAPDH were analysed in a Kitz-Wilson double reciprocal plot, performing a linear fitting with the equation:

$$\frac{1}{k_{obs}} = \frac{K_I}{k_{inact}} \frac{1}{[I]} + \frac{1}{k_{inact}}$$

The constant k_{inact} is the rate of enzyme irreversible inactivation; Ki is the dissociation constant of the initial non-covalent EI complex, [I] the concentration of the inhibitor at which the apparent rate of decay (k_{obs}) was determined. The kinact/Ki ratio is the apparent second-order rate constant for inactivation and is indicative of the inhibitor reactivity.

Protein inhibition of compound **1** was monitored also with gluconeogenic enzyme reaction, GAPDH homologs were incubated with compound **1** at indicated concentrations in solutions containing 100 mM TEA, 5 mM EDTA at pH 7.6. At different times, aliquots were sampled from the incubation mixture and assayed for enzyme activity. All inactivation experiments were monitored relative to a control sample without 1, which was set to 100% activity at each time point.

The reversibility of compound **1** inactivation was assessed by measuring GAPDH activity after 60 min treatment with 1 and after incubation for 10 minutes with 5 mM DTT. Protection assays by the glycolytic substrate G3P were determined by comparing the inactivation rates in the presence of 100 µM of compound **1** using the same conditions supplemented with 5 mM G3P. Protection by the gluconeogenic substrate BFGA was determined by adding the BPGA-generating system (3 mM 3-phosphoglycerate, 5 units/ml of 3-phosphoglycerate kinase and 2 mM ATP) to the reaction mixture where compound 1 was also present.

2.6 Mass spectrometry

The alkylation of GAPDHs by all compounds was assessed by incubating the proteins (20 µM) with a 10-fold excess of compound **1** for 1 hour. Subsequently, protein samples were analysed by MALDI TOF mass spectrometry using the instrument in linear positive mode. Briefly, GAPDH samples were loaded onto the MALDI plate with the double layer method using alpha-cyano-4-hydroxycinnamic acid (CHCA) as matrix. 1 µL of 10 mg/mL CHCA in acetone was deposited onto the MALDI plate and air dried; a second layer was obtained by diluting ten-fold the sample with 20 mg/mL CHCA in 50% acetonitrile and 0.05% TFA. Spectra of undigested GAPDH were acquired using the linear positive mode in the 10000 – 45000 m/z range.

2.7 Determination of the cysteine pKa

The pKa of the catalytic cysteine of both PfGAPDH and hGAPDH was indirectly measured using a modified version of a protocol previously reported [22], which takes advantage of the much faster reactivity of iodoacetamide (IAM) with cysteines in the thiolate form [23]. Briefly, the protein at 2 µM concentration was incubated with 20 µM IAM in citrate/Bis-Tris/TRIS buffered solutions (plus 5 mM EDTA), at pH ranging from 3.5 and 9.0. Aliquots of the reaction mixtures were sampled at fixed times and the residual enzyme activity measured. The ratio between the activity of the enzyme reacted with IAM and that of the enzyme incubated in the same buffered solution in the absence of IAM was calculated for each pH, to take into account the instability of both proteins at low pH. The pKa was determined through a fitting of the experimental points to the Henderson-Hasselbach equation. To measure the pKa of the unreacted catalytic cysteines for hGAPDH upon partial reaction with 2, the enzyme was incubated at 100 µM concentration in a solution containing 100 mM TEA, 300 µM 2, pH 7.6 for 4 hours. hGAPDH was then diluted 100-fold in the buffered solutions at different pH and the pKa was determined as described above.

2.8 Titration of the total content of cysteines

Samples of hGAPDH at 2 µM were incubated with compound **2B** for 4 hours and precipitated in cold acetone. The protein was then resuspended in a solution containing 50 mM sodium phosphate, 100 mM NaCl, 6 M guanidinium chloride pH 8.0. 5,5'-dithiobis-(2-nitrobenzoic acid) (DTNB) was then added at 20 µM concentration and the absorbance at 420 nm measured.

2.9 Gel-filtration analysis

Aliquots of 50 µL of 20 µM hGAPDH were loaded either on a Superdex 200 5/150 GL or a Superdex 200 HR 10/30 gel-filtration columns (GE Healthcare) mounted on an ÄKTA prime plus system (GE Healthcare). The columns were equilibrated with solutions containing 10 mM TEA, 150 mM NaCl, pH 7.6. The protein was detected by absorbance at 280 nm. The column was calibrated with gel-filtration standards (Sigma-Aldrich), including lysozyme (14 kDa), carbonic anhydrase (29 kDa), bovine serum albumin (66 kDa), conalbumine (75 KDa), ferredoxin (480 kDa) and alcohol dehydrogenase (150 kDa). The flow rate was 0.2 ml/min and the experiments were carried out at 4°C.

3. Results and Discussion

3.1 Inhibition assay

During the incubation of GADPH homologs with compounds **1**, **2A** or **2B**, the residual activity was measured, as described, taking aliquots at different time interval.

The activity of the enzyme is correlated to the formation of NADH, monitored at 340 nm, and is described by the linear phase of the kinetics (Fig. 5.3). Once obtained the relative activities they were normalized to the value of the control incubated in absence of inhibitors. To obtain the curve of inhibition the residual activity was plotted as function of time.

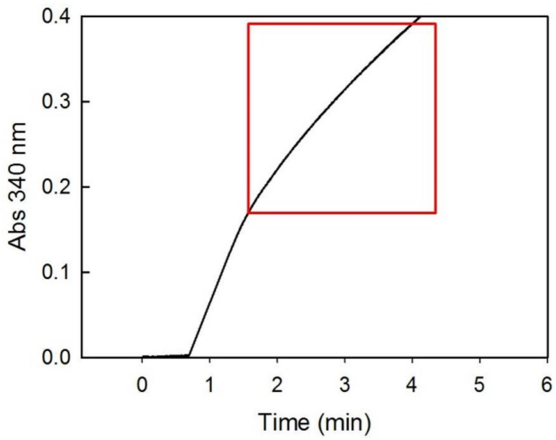

Figure 5.3. *Enzymatic kinetic of GAPDH monitored at 340 nm. In the red box the linear phase of the NADH formation.*

3.2 Inhibition studies of GAPDH orthologs by compound 1

To evaluate a possible selectivity of compound **1** toward GAPDHs, we investigated its inhibition on four orthologs: hGAPDH, TbGAPDH, PfGAPDH, and AtGAPDH. Whereas the first three have been proposed as promising drug targets, [11, 24, 25] the molecular

studies of AtGAPDH have been particularly pursued to unveil its moonlighting role in higher plants. [4] The alignment of the amino acid sequences of the four proteins (Fig. 5.3) highlights that, with the exception of the Rossmann fold of the coenzyme-binding domain and the dyad residues, no clear identities in the catalytic domains of the four enzymes are observed (Fig. 5.4). In particular, it is difficult to localize the residues involved in the stabilization of the Ps and Pi sites, responsible for the binding of the substrates (both G3P and inorganic phosphate group). [26] Thus, it is conceivable that compound **1** might exhibit slightly different inhibitory properties towards the four orthologs.

```
T.brucei          -MTIKVGINGFGRIGRMVFQALCDDGLLGNEIDVVAVVDMNTDARYFAYQMKYDSVHGKF  59
P.falcuparum      MAVTKVGINGFGRIGRLVFRAAYER----SDIEVVAINDPFMDIKHLCYLLKYDSVHGKF  56
H.sapiens         MGKVKVGVNGFGRIGRLVTRAAFNS----GKVDIVAINDPFIDLNYMVYMFQYDSTHGKF  56
A.thaliana        --KIRIGINGFGRIGRLVARVVLQR----DDVELVAVNDPFITTEYMTYMFKYDSVHGQW  54
                      ::*:********:* :.  :     ..:::**: *     .:: * ::***.**::

T.brucei          KHSVSTTKSKPSVAKDDTLVVNGHRILCVKAQRNPADLPWGKLGVEYVIESTGLFTVKSA  119
P.falcuparum      PCEVT--PG-------EGMFTVGDKKIYVHSEKDPAQIPWGKYAIDVVCESTGVFLTKEL  107
H.sapiens         HGTVK--AE-------NGKLVINGNPITIFQERDPSKIKWGDAGAEYVVESTGVFTTMEK  107
A.thaliana        KHNELKIKD-------EKTLLFGEKPVTVFGIRNPEDIPWAEAGADYVVESTGVFTDKDK  107
                                :  .  . . : :   ::* .: *.. . : * ****:*   .

T.brucei          AEGHLRGGARKVVISAPASGGAKTFVMGVNHNNYNPREQHVVSNASCTTNCLAPLVHVLV  179
P.falcuparum      AGAHLKGGAKKVIMSAPPKDDTPIYVMGINHQKYDG-KQLIVSNASCTTNCLAPIAKVL-  165
H.sapiens         AGAHLQGGAKRVIISAPSA-DAPMFVMGVNHEKYDN-SLKIISNASCTTNCLAPLAKVI-  164
A.thaliana        AAAHLKGGAKKVVISAPSK-DAPMFVVGVNEHEYKS-DLDIVSNASCTTNCLAPLAKVI-  164
                  * .**:***::*::***   .:  :*:*:*..:*.  .  ::************:.:*:

T.brucei          KEGFGISTGLMTTVHSYTATQKTVDGVS--VKDWRGGRAAALNIIPSTTGAAKAVGMVIP  237
P.falcuparum      NDNFGIVEGLMTTVHASTANQLVVDGPSKGGKDWRAGRCALQNIIPASTGAAKAVGKVLP  225
H.sapiens         HDNFGIVEGLMTTVHAITATQKTVDGPS--GKLWRDGRGALQNIIPASTGAAKAVGKVIP  222
A.thaliana        NDRFGIVEGLMTTVHSITATQKTVDGPS--MKDWRGGRAASFNIIPSSTGAAKAVGKVLP  222
                  :: ***  *******: **.* .*** *   * ** ** *  ****::******** *:*

T.brucei          STQGKLTGMAFRVPTADVSVVDLTFIATRDTSIKEIDAALKRASKTYMKNILGYTDEELV  297
P.falcuparum      ELNGKLTGVAFRVPIGTVSVVDLVCRLQKPAKYEEVAAQIKKAADGPLKGILGYTEDEVV  285
H.sapiens         ELNGKLTGMAFRVPTANVSVVDLTCRLEKPAKYDDIKKVVKQASEGPLKGILGYTEHQVV  282
A.thaliana        ALNGKLTGMSFRVPTVDVSVVDLTVRLEKAATYDEIKKAIKEESEGKLKGILGYTEDDVV  282
                    :*****::****   ******.    : :. .::   :*. :.  :*.*****:.::*

T.brucei          SADFISDSRSSIYDSKATLQNNLPNERRFFKIVSWYDNEWGYSHRVVDLVRHMAARDRAA  357
P.falcuparum      SQDFVHDNRSSIFDLKAGLA----LNDNFFKIVSWYDNEWGYSNRVLDLAVHITKN----  337
H.sapiens         SSDFNSDTHSSTFDAGAGIA----LNDHFVKLISWYDNEFGYSNRVVDLMAHMASKE---  335
A.thaliana        STDFVGDNRSSIFDAKAGIA----LSDKFVKLVSWYDNEWGYSSRVVDLIVHMSKA----  334
                  * **  *.:** :*  * :      . .*.*::******:*** **:**  *::

T.brucei          KL    359
P.falcuparum      --    337
H.sapiens         --    335
A.thaliana        --    334
```

Figure 5.3. *Sequence alignment of GAPDH orthologs of Trypanosoma brucei, Plasmodium falciparum, Homo sapiens and Arabidopsis thaliana.*

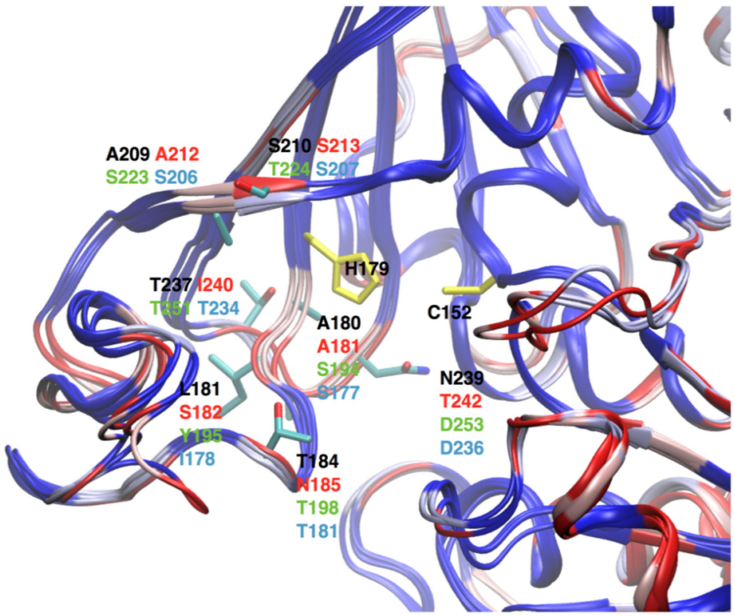

Figure 5.4. *Comparison of GAPDHs catalytic sites showed high structural conservation between the homologs. Catalytic residues are highlighted in yellow. Ribbons are colored by sequence conservation, with red color indicating less sequence conservation, and blue color corresponding to the maximum degree of sequence conservation. Licorice representation method highlighted the less conserved residues within the active sites (black, red, green and blue labels correspond to hGADPH, PfGADPH, TbGADPH, and AtGADPH, respectively).*

The inactivation kinetics of the four enzymes were determined at different concentrations of compound **1** and were time and concentration dependent. In Figure 5.5, representative inhibition time courses for hGAPDH at different concentrations of compound **1** (50-200 µM) (Panel A), and inhibition time courses for all orthologs at a fixed concentration of compound **1** (100 µM) (Panel B) are reported. An analysis of the plots clearly showed that the four orthologs exhibited different inactivation rate profiles (Fig. 5.5 B). In particular, PfGAPDH was the most reactive in the presence of 100 µM compound **1**, with a $t_{1/2}$ of around 10 minutes, whereas AtGAPDH and TbGAPDH were the

least reactive, with $t_{1/2}$ around 80 minutes. hGAPDH exhibited an intermediate reactivity, with a $t_{1/2}$ of around 40 minutes. The calculated kinact/Ki ratios (see the Table of Fig. 5.6) confirmed that 1 reacted 5-fold more efficiently with PfGAPDH (7.8 ± 1.7 M^{-1} s^{-1}) than with the Arabidopsis (1.8 ± 0.2 M^{-1} s^{-1}) and Trypanosoma (1.5 ± 0.4 M^{-1} s^{-1}) orthologs and twice as efficiently as with the human protein (3.2 ± 0.3 M^{-1} s^{-1}).

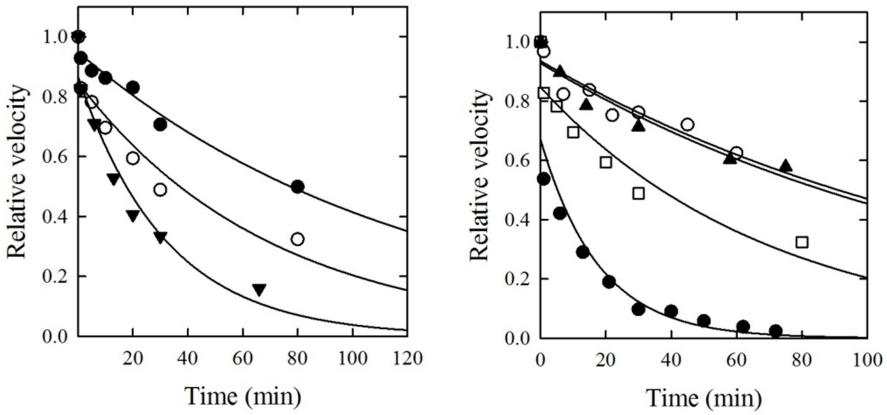

Figure 5.5. *Representative time courses of GAPDHs inactivation (forward reaction) by **1** in TEA buffer at pH 7.6.* ***A)*** *Exemplary comparison of the inhibition kinetics for one of the GAPDH orthologs, hGAPDH, at different concentrations of compound **1**: 50 µM (closed circles), 100 µM (open circles) and 200 µM (closed triangles).* ***B)*** *Exemplary comparison of inhibition kinetics at one concentration of compound **1** (100 µM) for hGAPDH (open squares), PfGAPDH (closed circles), AtGAPDH (closed triangles) and TbGAPDH (open circles). The activities were normalized to those measured in the absence of inhibitors for each ortholog. The lines are the fittings of the experimental points to an exponential decay. Both incubation and enzyme assays were carried out at 25°C.*

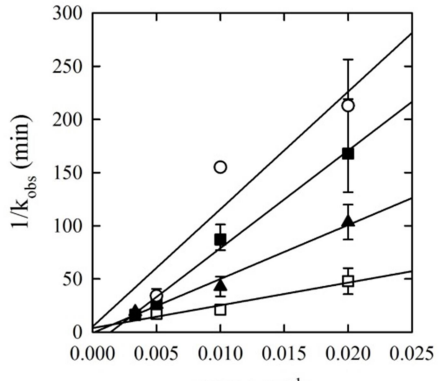

GAPDH	k_{inact}/K_i ($s^{-1}M^{-1}$)
*Pf*GAPDH	7.8 ± 1.7
*h*GAPDH	3.2± 0.3
*At*GAPDH	1.8 ± 0.2
*Tb*GAPDH	1.5 ± 0.4

Figure 5.6. *Kitz-Wilson double reciprocal plots of the inhibition of PfGAPDH (open squares), hGAPDH (closed triangles), AtGAPDH (closed squares) and TbGAPDH (open circles) by **1** in the 50-300 µM concentration range. Incubation was carried out in TEA buffer, pH 7.6. Both incubation and enzyme assays were carried out at 25°C. The solid lines represent a linear fitting to the experimental points. The error bars represent the standard error of at least two replicates.*

3.3. The binding of compound 1 with catalytic cysteine

To investigate whether inactivation of GAPDH by compound **1** occurred as a result of interactions at the active site, substrate protection experiments were carried out. G3P was added to the incubation mixtures containing compound **1**, they dramatically slowed down the inactivation of all homologs (Figure 5.7), suggesting a competition for the binding at the same residue, i.e. the catalytic cysteine. The alternative possibility that GAPDH inactivation is associated to compound **1**-mediated modification of cysteine residues other than the catalytic one, triggering an allosteric conformational change to an inactive form. The monoalkylation observed in mass spectrometry (Fig. 5.9) further suggests that the alkylated cysteine is indeed the catalytic one.

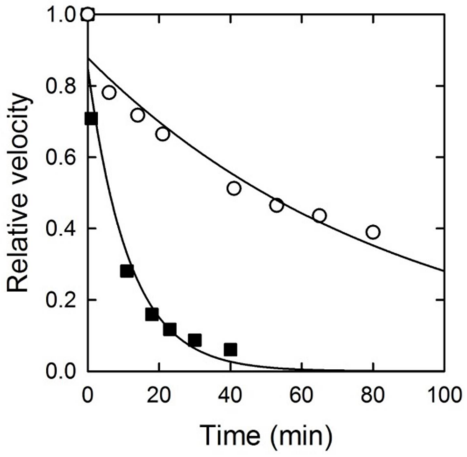

Figure 5.7. *Protection of GAPDHs towards compound **1** inactivation (forward reaction) by the substrate G3P. PfGAPDH was incubated in TEA buffer at pH 7.6 in the presence of 100 µM compound **1** (closed squares) or 100 µM compound **1** + 5 mM G3P (open circles). Both incubation and enzyme assays were carried out at 25°C. The solid lines represent a fitting of the experimental points to exponential decays.*

Inactivation by **1** was not reversed by addition of dithiothreitol (DTT) at 5 mM concentration (Figure 5.8), arguing for a non-oxidative modification of the cysteine as the underlying biochemical mechanism. Indeed, being DTT a thiol-based reductant, it could be excluded that a disulfide bond involving the cysteine thiol occurs. [27] As reported for a similar experiment performed with metalloporphyrin derivatives and apocytochrome c, this might be suggestive of a thioether bond formation between compound **1** and the protein [27].

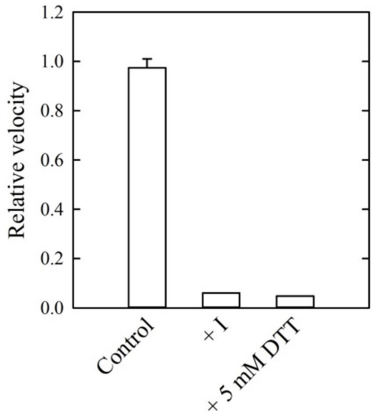

Figure 5.8. *Irreversibility of compound **1** inactivation. PfGAPDH at 5 µM concentration was incubated with **1** (200 µM) for 60 minutes at 25°C in TEA buffer at pH 7.6 until almost full inactivation was achieved (+I). DTT was then added at 5 mM concentration and the activity (forward reaction) was monitored for 70 more minutes (+5 mM DTT), with no reversal of inhibition. Both incubation and enzyme assays were carried out at 25°C. The activities were normalized to that in the absence of inhibitors (Control). The error bars represent the standard error of two replicates.*

3.4. Mass spectrometry studies of *Pf*GAPDH-1 complex

We previously failed to detect alkylation of TbGAPDH by mass spectroscopy, [14] mainly because of its instability. Therefore, MALDI-TOF analyses of undigested PfGAPDH were performed. The measured molecular mass of 39950±10 Da, was consistent with the loss of the initial methionine (expected molecular monoisotopic mass: 40081.21 Da). [11] Upon incubation of 200 µM compound **1**, a mass shift of around 145±15 Da was observed, suggesting that a single fragment of 1,4-napthquinone (157 Da) was attached (Figure 5.9). The shift was consistent with a monoalkylation of each subunit, ruling out non-selective reactivity with other solvent exposed cysteine residues. This observation suggested that compound **1** can react, as an electrophilic warhead with the catalytic thiolate nucleophilic group of the GAPD, to form a covalent bond. We also failed to detect any m/z shift upon tryptic digestion of any GAPDH upon incubation, possibly because of the limited stability of the adduct in the condition used for MALDI spectrometry. This

experiment would have allowed to conclusively identifying the catalytic cysteine as the reactive residue.

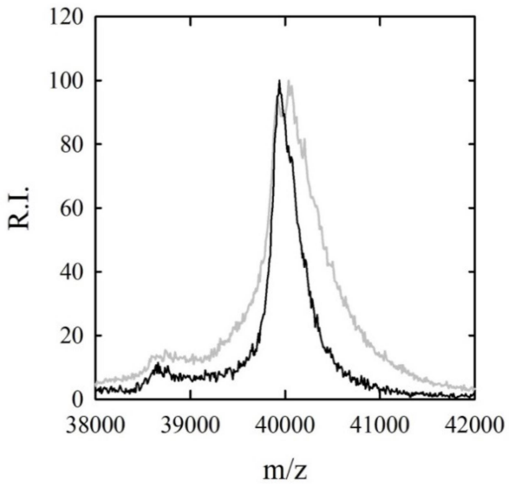

Figure 5.9. *Mass spectra of the single charged peak of undigested PfGAPDH (black line) and upon incubation for 2 hours with **1** at 200 µM concentration (gray line). A difference of 145±15 Da is consistent with a monoalkylation by **1**. The sample was diluted 1:10 with HCCA 20 mg/ml in 75% acetonitrile and 2.5% TFA. The y-axis is the percent relative intensity of the signal.*

3.5. Inhibition by compound 2A

Either hGAPDH or PfGAPDH solutions were incubated with compound **2A**, the most potent compound identified in the previous screening (Fig. 5.2) [16]. The inhibition time course was found to be remarkably different for hGAPDH and PfGAPDH (Fig. 5.10). The activity of PfGAPDH, as already observed, was rapidly abolished, whereas the activity of hGAPDH decreased sharply to about 70% of the initial activity, then remained steady for hours. Within the same time range, no change in activity for both enzymes in the absence of compound **2A** was observed (Fig. 5.10).

As already observed [16], the inhibition of PfGAPDH is a complex process that, depending on inhibitor concentration, takes place with a time course that is either monophasic or biphasic. On the contrary, the inhibition of hGAPDH appeared monophasic, with rates comparable to those of the fast phase of PfGAPDH inhibition. However, remarkably, hGAPDH activity was not abolished even when a large excess of inhibitor was present, at incubation times which were sufficient to completely quench the activity of PfGAPDH.

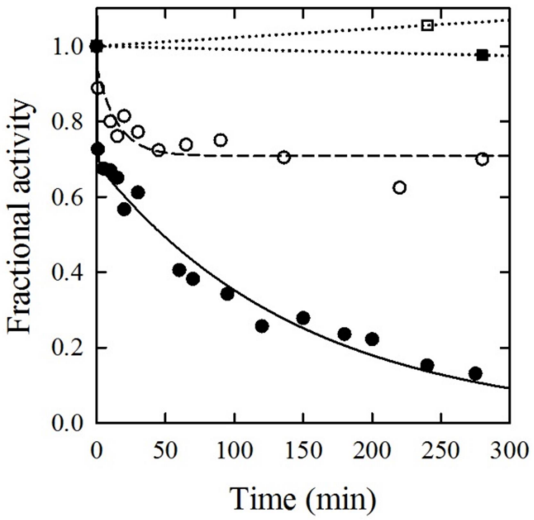

Figure 5.10. *Representative inactivation time course of PfGAPDH (closed circles) and hGAPDH (open circles) incubated with 50 µM compound* ***2A****, at 25°C. As controls, hGAPDH (open squares) and PfGAPDH (closed squares) were incubated with 0.05% methanol, equivalent to the amount added from compound* ***2A*** *stock solutions. Activities were normalized to the initial activity in the absence of compound* ***2A****. The solid line is the fitting of the time course to a sum of two exponential decays, with a resulting decay time for the slow phase of 91.7 ± 0.2 minutes. The rate constant for the fast phase could not be estimated. The dashed line is the fitting of the time course to a single exponential decay plus an offset. The decay time was 10.6 ± 3 minutes. The enzyme concentration was 2 µM.*

3.6. Inhibition by compound 2B

Considering that compound **2A** inhibited PfGAPDH too rapidly to reliably monitor the first phase [16], we designed a compound endowed with a lower reactivity. As previously reported [16], also 3-Br-5-phenyl isoxazolines are equally efficient inhibitors of PfGAPDH. Their reactivity can be modulated through the insertion of proper substituents in the para position, capable of affecting the electron density on the aromatic ring. Among a series of p-substituted derivatives, we selected compound **2B** (Fig. 5.2), which displayed a slightly lower reactivity compared to previously reported 3-Br-isoxazoline derivatives.

Compound **2B** inhibited PfGAPDH completely, albeit slower than compound **2A**, and with a similarly biphasic time course (Fig. 5.11 A). As compound **2A**, compound **2B** only partially inhibited h GPADH, with monophasic course (Fig. 5.11 B). The inactivation rate and the final fraction inactivation depended on its concentration, with higher concentration of compound **2B** producing a higher fraction of final inhibition (Fig. 5.11, inset).

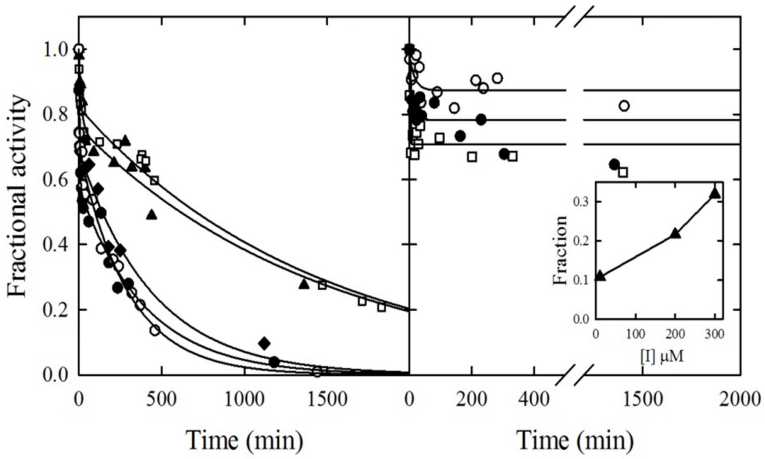

Figure 5.11. ***A)*** *Inactivation kinetics of PfGAPDH at different concentrations of* ***2B****: 20 µM (closed triangles), 50 µM (open squares), 100 µM (closed diamonds), 200 µM (closed circles), 300 µM (open circles). The lines are the best fit to a sum of two exponential decays.* ***B)*** *Inactivation kinetics of hGAPDH at different concentrations of* ***2B****: 10 µM (open circles), 200 µM (closed circles), 300 µM (open squares). The lines are the best fit to a single exponential decay with an offset. Inset: dependence of the fraction of inhibition on the concentration of compound* ***2B.***

The Kitz-Wilson analysis [28] (Fig. 5.12 A) of the slow phase of PfGAPDH inhibition confirmed that compound **2B** is significantly less efficient than compound **2A,** with a k_{inact}/K_i ratio of 0.34 $s^{-1}M^{-1}$ versus 10.7 $s^{-1}M^{-1}$ for compound **1** (Fig. 5.12 B). The near-zero intercept of the Kitz-Wilson plots for both the slow and the fast phase confirmed that the transient non-covalent binding to the active site do not contribute significantly to either phases. Therefore, both the fast phase and the slow phase are only associated to the alkylation of the catalytic cysteine, albeit with an approximately 100-fold difference in rate constants. This finding seems to confirm that a slow conformational rearrangement of the enzyme is responsible for the biphasic behaviour, rather than a different reactivity of the inhibitors at two different sites. The Kitz-Wilson analysis [29] of hGAPDH inhibition by compound **2B** yielded a k_{inact}/K_i ratio of 142 $s^{-1}M^{-1}$ (Fig. 5.12), comparable to that of the fast phase of PfGAPDH inhibition (59.9 $s^{-1}M^{-1}$).

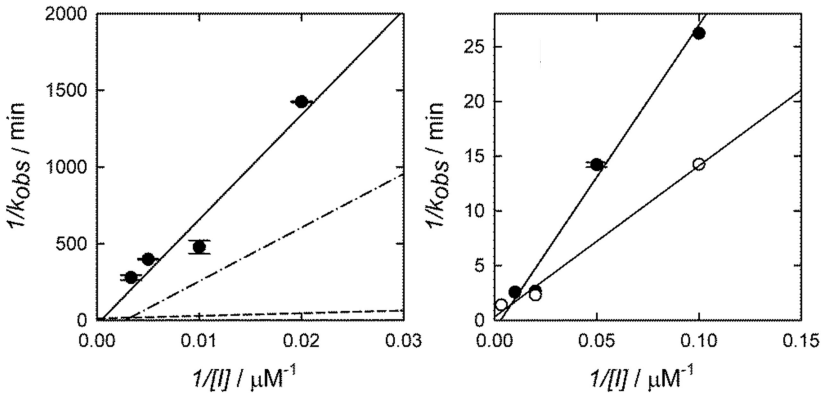

Figure 5.12. A) *Kitz-Wilson double reciprocal plots of the slow phase of PfGAPDH inhibition by* ***2B*** *(closed circles, solid line) compared to the most potent inhibitor compound* ***2A*** *(dashed line) and the least potent (dash-dot line) of the series previously reported. The k_{obs} for compound* ***2B****-mediated inactivation were determined from the fitting of the time courses reported in Fig. 3A. The calculated k_{inact}/K_i for compound 2 was 0.34 $s^{-1}M^{-1}$ versus 10.7 $s^{-1}M^{-1}$ for* ***2A. B)*** *Kitz-Wilson double reciprocal plot of the fast phase of PfGAPDH inhibition by compound* ***2B*** *compared with that for hGAPDH. The linear fitting resulted in a k_{inact}/K_i of 59.9 $s^{-1}M^{-1}$ for PfGAPDH and 142 $s^{-1}M^{-1}$ for hGAPDH.*

3.7. Cysteine titration of hGAPDH

The number of exposed cysteine residues of hGAPDH was determined by using 5,5-dithiobis-(2-nitrobenzoic acid) (DTNB) after incubation with 50 µM compound **2B**. A 7.8% decrease in reactive cysteine content was observed in comparison to the untreated control. This value is consistent with the alkylation of only one cysteine per tetramer out of the 12 present (Fig. 5.13). The alkylation stoichiometry correlates well with a 25% catalytic inactivation observed for the same sample (Fig. 5.11).

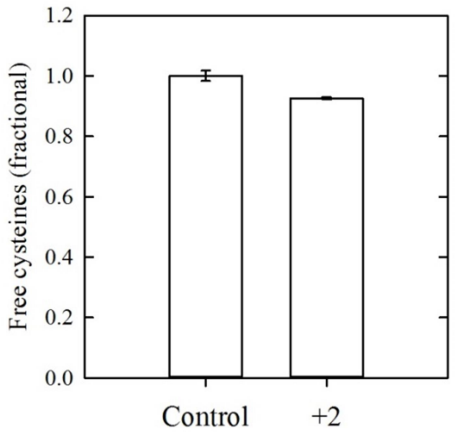

Figure 5.13. *DTNB titration of cysteine residues for denatured hGAPDH upon incubation for 4 hours with compound* ***2B*** *(+2) at 50 µM concentration compared with the unreacted protein (Control). The 7.8 % decrease in free cysteine content is consistent with the reaction of 1 catalytic cysteine out of the 4 of the tetramer. The error bars represent the standard error for three independent measurements on different samples.*

Overall, these findings suggested that the alkylation of one catalytic site of hGAPDH in a timeframe of a few minutes triggers a conformational rearrangement that completely masks the remaining three sites to further alkylation by compound **2B.**

This mechanism appears analogous to that responsible for the biphasicity of PfGAPDH inactivation, with the difference that the resulting conformation for PfGAPDH is still reactive towards compounds **2A** and **2B**, albeit with much reduced rates. Indeed, the

initial reaction rate of hGAPDH with compound **2B** is faster than that of PfGAPDH (Fig. 5.12) and only the difference in reactivity upon completion of the transition accounts for the overall selectivity of compound **2B** towards PfGAPDH. Within this model, a minimum 25% inactivation is required to produce the conformational change, but, until the transition is completed, further catalytic cysteines might react with a second order kinetics, proportionally to the concentration of the alkylating agent. This is consistent with the observation that the fractional inactivation of hGAPDH partially depends on the concentration of compound **2B** (Fig. 3B, inset). This dependence rules out the alternative possibility that the biphasic behaviour of PfGAPDH and the limited reactivity of hGAPDH are associated to a pre-existing difference in reactivity of the four active sites. In order to investigate the structural and functional consequences of the predicted conformational rearrangement, the quaternary assembly and the catalytic properties of hGAPDH were evaluated after incubation with compound **2B.**

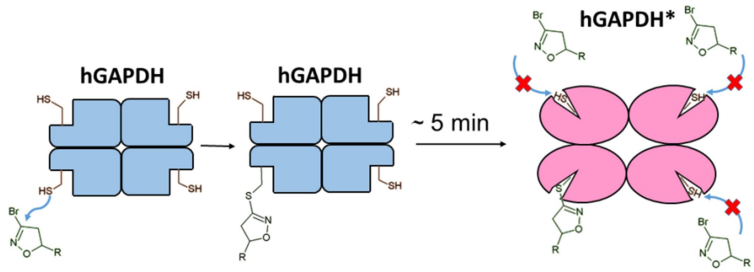

Scheme 1. *Schematic model of hGAPDH partial inactivation by 3-Br-isoxazoline inhibitors. The alkylation of the catalytic cysteine of one subunit within the tetramer triggers a conformational rearrangement in the timeframe of minutes (t) that limits further reaction at the remaining sites*

3.8. Effects of 3-Br-isoxazoline partial alkylation of hGAPDH on the reactivity of the catalytic cysteines

The deprotonation equilibrium of the catalytic cysteines is responsible for catalysis and for the reactivity with electrophilic compounds [5] The pKa of these cysteines are markedly lower than those of free thiols (around 8.3), reflecting the pKa-lowering microenvironment of the active site [2] To assess whether the alkylation of one active site cysteine within the tetramer by compound **2B** allosterically affects the microenvironment of the remaining, unreacted sites, we assessed their pKa in comparison with untreated hGAPDH and untreated PfGAPDH. The resulting pKa for hGAPDH and PfGAPDH (Fig. 5.14) were 6.0 and 6.6, respectively, in agreement with values either calculated [2] or measured [19] for GAPDHs. For hGAPDH, the pKa value after reaction with compound **2B** was 6.3 (Fig. 5.14 B), indicating that partial alkylation of the tetramer does not allosterically alter the pKa of the remaining catalytic cysteines.

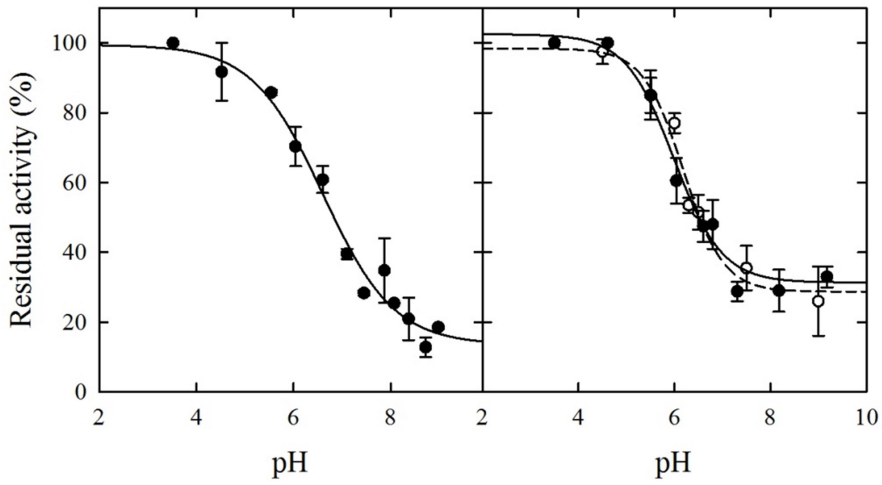

Figure 5.14. A) *Dependence of PfGAPDH residual activity on pH upon reaction with IAM. The solid line represents the fitting to the Henderson–Hasselbalch equation, yielding a pKa of 6.6 ± 0.2* ***B)*** *Dependence of hGAPDH residual activity upon reaction with IAM as a function of pH either previously incubated with compound* ***2B*** *(closed circles) or untreated (open circles). The lines represent the fitting to the Henderson–Hasselbalch equation, yielding pKa of 6.2 ±0.1 for hGAPDH pre-incubated with compound* ***2B*** *and 6.0 ±0.1 for the untreated control.*

3.9. Enzymatic parameter upon 3-Br-isoxazoline partial alkylation of hGAPDH

We investigated whether the reactivity of hGAPDH with G3P and NAD+ was affected by partial alkylation at one active site of the tetramer. The dependence of hGAPDH activity on G3P concentration was measured before and after incubation with compound **2B** and fitted to a Michaelis-Menten equation (Fig. 5.15 A). As expected, a 25% decrease in Vmax was observed, whereas the K_M did not change significantly before and after incubation (340 µM and 299 µM, respectively). Therefore, the conformational change responsible for the lack of reactivity towards compound **2B** does not affect significantly the access of G3P, as well as IAM, to the active site. This suggests that the narrowing of the access channel affects only bulkier compounds, such as 3-Br-isoaxozoline derivatives.

3.10. Effects of partial alkylation on the quaternary state of hGAPDH

GAPDH has long been recognized as a moonlighting protein, with slow-interconverting structures possibly associated with alternative functions [29, 30]. For instance, *Kluyveromyces marxianus* GAPDH crystallizes as a dimer, although it is a tetramer in solution [31]. To evaluate whether the incomplete inhibition of hGAPDH by 3-Br-isoxazoline compounds is due to an alteration of the dimer-tetramer equilibrium, gel filtration chromatography was performed. Both untreated and **2B**-treated hGAPDH exhibited retention times consistent with a tetramer, with a small shift that might be compatible with a shape modification within the tetrameric state (Fig. 5.15B).

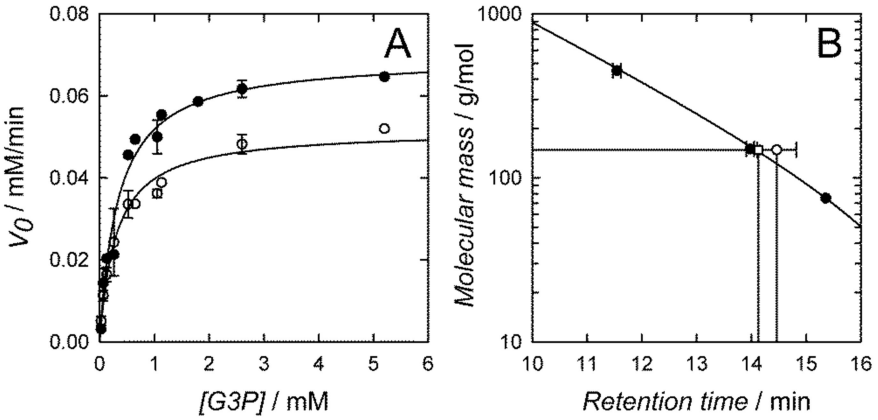

Figure 5.15. A) *Dependence of the enzyme activity of hGAPDH before (closed circles) and after (open circles) incubation with 50 µM compound* ***2B*** *for 4 hours. NAD^+ was at a fixed concentration of 1.5 mM and DL-G3P at concentrations ranging from 20 µM to 5.2 mM.* ***B)*** *Gel filtration of hGAPDH, untreated (open circle) and upon incubation for 4 hours with compound* ***2B*** *(open square) in comparison with the molecular weight standards ferredoxin (MW 480000), alcohol dehydrogenase (MW 150000) and aconitase (MW 75000) (closed circles).*

4. Conclusion

Irreversible inhibitors tend to exhibit poor selectivity. However, we showed that two groups of irreversible inhibitors of GAPDH are at least partially capable of discriminating one ortholog from the others. In the case of the 2-phenoxy-1,4-naphthoquinone compounds, the partial selectivity was demonstrated on four orthologs and was shown to depend on different rates of protein alkylation. It can be inferred that, despite a common reactivity of the catalytic cysteine residue, the active site is partially different. The selectivity observed for 3-Br-isoxazoline derivatives was shown to depend on a different mechanism. As a matter of fact, the fully and irreversibly inhibit PfGAPDH, whereas they only produce a partial inhibition of hGAPDH, consistently with a quaternary conformational change triggered by partial alkylation at a single active site within the tetramer. The conformational transition does not alter significantly neither the dimer-tetramer equilibrium, nor the intrinsic chemical properties of the active site cysteines, nor the enzymatic parameters. The selectivity of these groups of compounds could be exploited to design irreversible but selective inhibitors to be used as anti-protozoan or anti-cancer drugs.

ABBREVIATIONS:

GAPDH, glyceraldehyde-3-phosphate dehydrogenase; G3P, glyceraldehyde-3-phosphate; BPGA, 1,3-bisphosphoglyceric acid; NAD^+, nicotinamide adenine dinucleotide; *Pf, Plasmodium falciparum; h,* human; *Tb, Trypanosoma brucei*; *At, Arabidopsis thaliana;* DTT, dithiothreitol.

REFERENCES

1. Bruno, S., et al., *Selectivity of 3-bromo-isoxazoline inhibitors between human and Plasmodium falciparum glyceraldehyde-3-phosphate dehydrogenases.* Bioorg. Med. Chem., 2016. **24**(12): p. 2654-9.
2. Martyniuk, C.J., et al., *Molecular mechanism of glyceraldehyde-3-phosphate dehydrogenase inactivation by alpha,beta-unsaturated carbonyl derivatives.* Chem. Res. Toxicol., 2011. **24**(12): p. 2302-11.
3. Tummanapelli, A.K. and S. Vasudevan, *Ab Initio MD Simulations of the Bronsted Acidity of Glutathione in Aqueous Solutions: Predicting pKa Shifts of the Cysteine Residue.* J. Phys. Chem. B, 2015. **119**(49): p. 15353-8.
4. Zaffagnini, M., et al., *Plant cytoplasmic GAPDH: redox post-translational modifications and moonlighting properties.* Front. Plant Sci., 2013. **4**: p. 450.
5. Marino, S.M. and V.N. Gladyshev, *Analysis and functional prediction of reactive cysteine residues.* J. Biol. Chem., 2012. **287**(7): p. 4419-25.
6. Segal, H.L. and P.D. Boyer, *The role of sulfhydryl groups in the activity of D-glyceraldehyde 3-phosphate dehydrogenase.* J. Biol. Chem., 1953. **204**(1): p. 265-81.
7. Campian, E.C., J. Cai, and F.W. Benz, *Acrylonitrile irreversibly inactivates glyceraldehyde-3-phosphate dehydrogenase by alkylating the catalytically active cysteine 149.* Chem. Biol. Interact., 2002. **140**(3): p. 279-91.
8. Dietze, E.C., et al., *Inactivation of glyceraldehyde-3-phosphate dehydrogenase by a reactive metabolite of acetaminophen and mass spectral characterization of an arylated active site peptide.* Chem. Res. Toxicol., 1997. **10**(10): p. 1097-103.
9. Choi, D.S., et al., *Glyceraldehyde-3-phosphate dehydrogenase as a biochemical marker of cytotoxicity by vinyl sulfones in cultured murine spleen lymphocytes.* Cell Biol. Toxicol., 1995. **11**(1): p. 23-8.

10. Rodriguez, C.E., et al., *The interactions of 9,10-phenanthrenequinone with glyceraldehyde-3-phosphate dehydrogenase (GAPDH), a potential site for toxic actions.* Chem. Biol. Interact., 2005. **155**(1-2): p. 97-110.
11. Bruno, S., et al., *Discovery of covalent inhibitors of glyceraldehyde-3-phosphate dehydrogenase, a target for the treatment of malaria.* J. Med. Chem., 2014. **57**(17): p. 7465-71.
12. Bolognesi, M.L., et al., *Synthesis of a small library of 2-phenoxy-1,4-naphthoquinone and 2-phenoxy-1,4-anthraquinone derivatives bearing anti-trypanosomal and anti-leishmanial activity.* Bioorg. Med. Chem. Lett., 2008. **18**(7): p. 2272-2276.
13. Prati, F., et al., *2-Phenoxy-1,4-naphthoquinones: From a Multitarget Antitrypanosomal to a Potential Antitumor Profile.* J. Med. Chem., 2015. **58**(16): p. 6422-34.
14. Pieretti, S., et al., *Naphthoquinone Derivatives Exert Their Antitrypanosomal Activity via a Multi-Target Mechanism.* Plos Neglect. Trop. Dis., 2013. **7**(1).
15. Belluti, F., et al., *Toward the development of dual-targeted glyceraldehyde-3-phosphate dehydrogenase/trypanothione reductase inhibitors against Trypanosoma brucei and Trypanosoma cruzi.* ChemMedChem, 2014. **9**(2): p. 371-82.
16. Bruno, S., et al., *Discovery of covalent inhibitors of glyceraldehyde-3-phosphate dehydrogenase, a target for the treatment of malaria.* J Med Chem, 2014. **57**(17): p. 7465-71.
17. Tamborini, L., et al., *Synthesis and biological evaluation of CTP synthetase inhibitors as potential agents for the treatment of African trypanosomiasis.* ChemMedChem, 2012. **7**(9): p. 1623-34.
18. Conti, P., et al., *Synthesis and in vitro/in vivo evaluation of the antitrypanosomal activity of 3-bromoacivicin, a potent CTP synthetase inhibitor.* ChemMedChem, 2011. **6**(2): p. 329-33.

19. Bedhomme, M., et al., *Glutathionylation of cytosolic glyceraldehyde-3-phosphate dehydrogenase from the model plant Arabidopsis thaliana is reversed by both glutaredoxins and thioredoxins in vitro.* Biochem. J., 2012. **445**: p. 337-347.
20. Bradford, M.M., *A rapid and sensitive method for the quantitation of microgram quantities of protein utilizing the principle of protein-dye binding.* Anal. Biochem., 1976. **72**: p. 248-54.
21. Ferdinand, W., *The isolation and specific activity of rabbit-muscle glyceraldehyde phosphate dehydrogenase.* Biochemical Journal, 1964. **92**(3): p. 578-85.
22. Bedhomme, M., et al., *Glutathionylation of cytosolic glyceraldehyde-3-phosphate dehydrogenase from the model plant Arabidopsis thaliana is reversed by both glutaredoxins and thioredoxins in vitro.* Biochemical Journal, 2012. **445**(3): p. 337-47.
23. Zaffagnini, M., et al., *Glutaredoxin s12: unique properties for redox signaling.* Antioxidants & Redox Signaling, 2012. **16**(1): p. 17-32.
24. Barros-Alvarez, X., et al., *Glycosomal targets for anti-trypanosomatid drug discovery.* Curr. Med. Chem., 2014. **21**(15): p. 1679-706.
25. Ganapathy-Kanniappan, S. and J.F.H. Geschwind, *Tumor glycolysis as a target for cancer therapy: progress and prospects.* Mol. Cancer, 2013. **12**.
26. Castilho, M.S., et al., *Evidence for the two phosphate binding sites of an analogue of the thioacyl intermediate for the Trypanosoma cruzi glyceraldehyde-3-phosphate dehydrogenase-catalyzed reaction, from its crystal structure.* Biochemistry, 2003. **42**(23): p. 7143-51.
27. Daltrop, O. and S.J. Ferguson, *In vitro studies on thioether bond formation between Hydrogenobacter thermophilus apocytochrome c(552) with metalloprotoporphyrin derivatives.* J. Biol. Chem., 2004. **279**(44): p. 45347-53.
28. Kitz, R. and I.B. Wilson, *Esters of methanesulfonic acid as irreversible inhibitors of acetylcholinesterase.* Journal of Biological Chemistry, 1962. **237**: p. 3245-9.

29. Pierce, A., et al., *GAPDH is conformationally and functionally altered in association with oxidative stress in mouse models of amyotrophic lateral sclerosis.* Journal of Molecular Biology, 2008. **382**(5): p. 1195-210.

30. Naletova, I., et al., *Non-native glyceraldehyde-3-phosphate dehydrogenase can be an intrinsic component of amyloid structures.* Biochimica et Biophysica Acta, 2008. **1784**(12): p. 2052-8.

31. Ferreira-da-Silva, F., et al., *The crystal and solution structures of glyceraldehyde-3-phosphate dehydrogenase reveal different quaternary structures*. Journal of Biological Chemistry, 2006. **281**(44): p. 33433-40.